

# Iterative Methods for Image Reconstruction

Jeffrey A. Fessler

EECS Department  
The University of Michigan

ISBI Tutorial

May 14, 2008

---

These annotated slides were prepared by Jeff Fessler for attendees of the ISBI tutorial on statistical image reconstruction methods.

The purpose of the annotation is to provide supplemental details, and particularly to provide extensive literature references for further study.

For a fascinating history of tomography, see [1]. For broad coverage of image science, see [2].

For further references on image reconstruction, see review papers and chapters, *e.g.*, [3–9].

---

0.0

## Image Reconstruction Methods (Simplified View)

**Analytical**

(FBP)

(MR: iFFT)



**Iterative**

(OSEM?)

(MR: CG?)

0.1

© J. Fessler, May 12, 2008

0.0

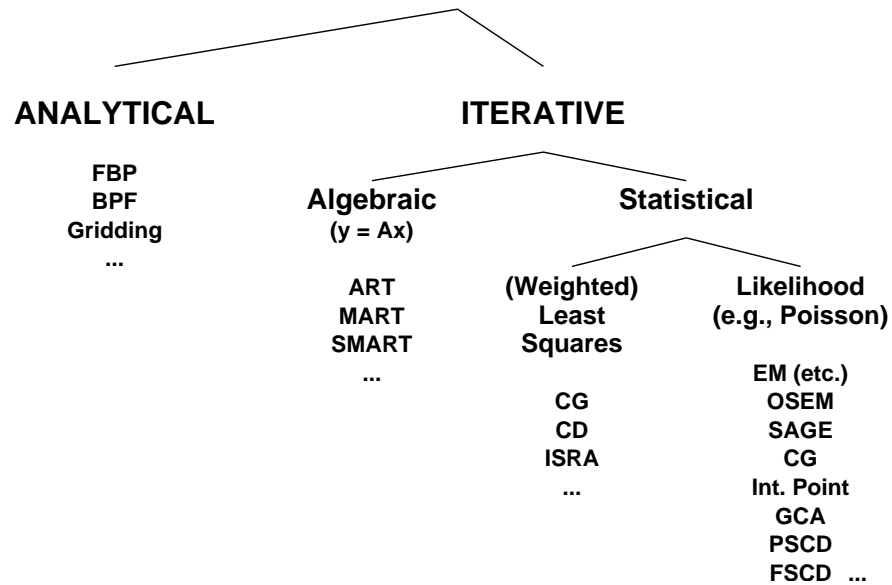
p0intro

© J. Fessler, May 12, 2008

0.1

p0intro

# Image Reconstruction Methods / Algorithms



0.2

## Outline :

### Part 0: Introduction / Overview / Examples

### Part 1: Problem Statements

- Continuous-discrete vs continuous-continuous vs discrete-discrete

### Part 2: Four of Five Choices for Statistical Image Reconstruction

- Object parameterization
- System physical modeling
- Statistical modeling of measurements
- Cost functions and regularization

### Part 3: Fifth Choice: Iterative algorithms

- Classical optimization methods
- Considerations: nonnegativity, convergence rate, ...
- Optimization transfer: EM etc.
- Ordered subsets / block iterative / incremental gradient methods

### Part 4: Performance Analysis

- Spatial resolution properties
- Noise properties
- Detection performance

0.3

---

Part of the goal is to bring order to this alphabet soup.

---

© J. Fessler, May 12, 2008

0.2

p0intro

---

Emphasis on general principles rather than specific empirical results.

The journals (and conferences like NSS/MIC!) are replete with empirical comparisons.

Although the focus of examples in this course are PET / SPECT / CT, most of the principles apply equally well to other tomography problems like MR image reconstruction, optical / diffraction tomography, etc.

---

© J. Fessler, May 12, 2008

0.3

p0intro

## History

- Successive substitution method vs direct Fourier (Bracewell, 1956)
- Iterative method for emission tomography (Kuhl, 1963)
- Iterative method for X-ray CT (Hounsfield, 1968)
- ART for tomography (Gordon, Bender, Herman, JTB, 1970)
- Weighted least squares for 3D SPECT (Goitein, NIM, 1972)
- Richardson/Lucy iteration for image restoration (1972, 1974)
- Proposals to use Poisson likelihood for emission and transmission tomography (Rockmore and Macovski, TNS, 1976, 1977)
- Expectation-maximization (EM) algorithms for Poisson model  
Emission: (Shepp and Vardi, TMI, 1982)  
Transmission: (Lange and Carson, JCAT, 1984)
- Regularized (aka Bayesian) Poisson emission reconstruction (Geman and McClure, ASA, 1985)
- Ordered-subsets EM algorithm (Hudson and Larkin, TMI, 1994)
- Commercial introduction of OSEM for PET scanners circa 1997

## Why Statistical Methods?

- Object constraints (e.g., nonnegativity, object support)
- Accurate physical models (less bias  $\implies$  improved quantitative accuracy) (e.g., nonuniform attenuation in SPECT) improved spatial resolution?
- Appropriate statistical models (less variance  $\implies$  lower image noise) (FBP treats all rays equally)
- Side information (e.g., MRI or CT boundaries)
- Nonstandard geometries (e.g., irregular sampling or “missing” data)

### Disadvantages?

- Computation time
- Model complexity
- Software complexity

### Analytical methods (a different short course!)

- Idealized mathematical model
  - Usually geometry only, greatly over-simplified physics
  - Continuum measurements (discretize/sample *after* solving)
- No statistical model
- Easier analysis of properties (due to linearity)  
e.g., Huesman (1984) FBP ROI variance for kinetic fitting

---

Bracewell's classic paper on direct Fourier reconstruction also mentions a successive substitution approach [10]  
Kuhl and Edwards [11]  
X-ray CT patent describing ART: [12]. Discussion of early EMI scanner iterative method: [13].  
Early iterative methods for SPECT by Muehllehner [14] and Kuhl [15].  
ART: [16–19]  
Richardson/Lucy iteration for image restoration was not derived from ML considerations, but turns out to be the familiar ML-EM iteration [20,21]  
Emission: [22]  
Transmission: [23]  
General expectation-maximization (EM) algorithm (Dempster *et al.*, 1977) [24]  
Emission EM algorithm: [25]  
Transmission EM algorithm: [26]  
Bayesian method for Poisson emission problem: [27]  
OSEM [28]

Prior to the proposals for Poisson likelihood models, the Lawrence Berkeley Laboratory had proposed and investigated weighted least-squares (WLS) methods for SPECT (in 3D!) using iterative algorithms; see (Goitein, 1972) [29] and (Budinger and Gullberg, 1974) [30]. These methods became widely available in 1977 through the release of the Donner RECLBL package [31].

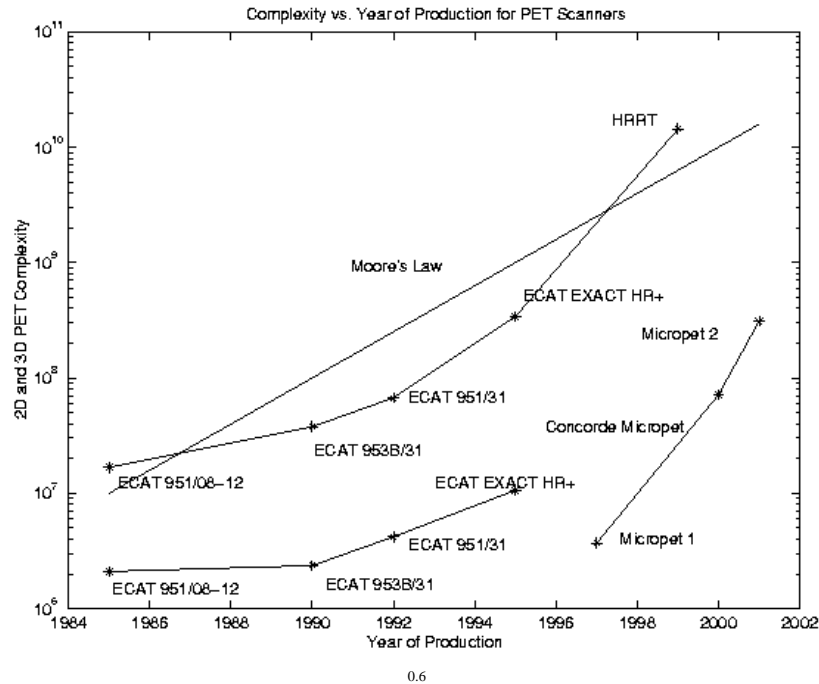
Of course there was lots of work ongoing based on “algebraic” reconstruction methods in the 1970s and before. But until WLS methods were proposed, this work was largely not “statistical.”

---

There is a continuum of physical system models that tradeoff accuracy and compute time. The “right” way to model the physics is usually too complicated, so one uses approximations. The sensitivity of statistical methods to those approximations needs more investigation.

FBP has its faults, but its properties (good and bad) are very well understood and hence predictable, due to its linearity. Spatial resolution, variance, ROI covariance (Huesman [32]), and autocorrelation have all been thoroughly analyzed (and empirical results agree with the analytical predictions). Only recently have such analyses been provided for *some* nonlinear reconstruction methods e.g., [33–44].

# What about Moore's Law?



0.6

© J. Fessler, May 12, 2008

0.6

p0intro

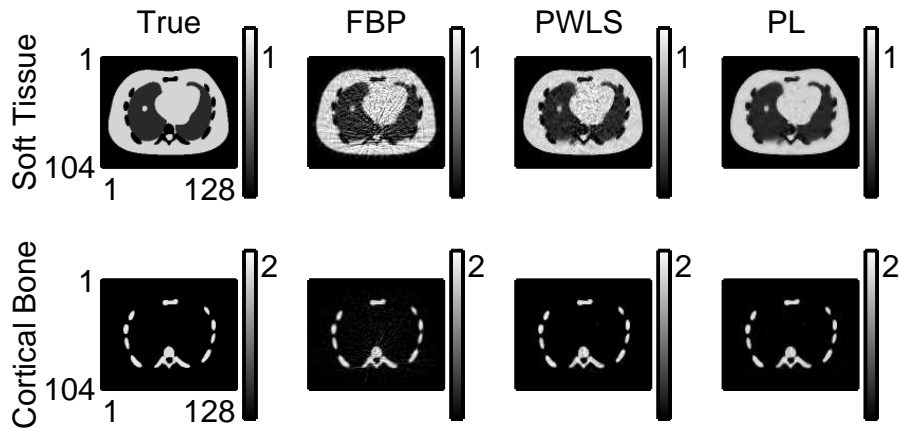
In this graph complexity is the number of lines of response (number of rays) acquired. The ECAT scanners can operate either in 2D mode (with septa in place) or 3D mode (with septa retracted) so those scanners have two points each.

I got this graph from Richard Leahy; it was made by Evren Asma. Only CTI scanners and their relatives are represented. Another such graph appeared in [45].

There is considerable ongoing effort to reduce or minimize the compute time by more efficient algorithms.

Moore's law for computing power increases will not alone solve all of the compute problems in image reconstruction. The problems increase in difficulty at nearly the same rate as the increase in compute power. (Consider the increased amount of data in 3D PET scanners relative to 2D.) (Or even the increased number of slices in 2D mode.) Or spiral CT, or fast dynamic MRI,... Therefore there is a need for further improvements in algorithms in addition to computer hardware advances.

## Benefit Example: Statistical Models



Method	NRMS Error	
	Soft Tissue	Cortical Bone
FBP	22.7%	29.6%
PWLS	13.6%	16.2%
PL	11.8%	15.8%

0.7

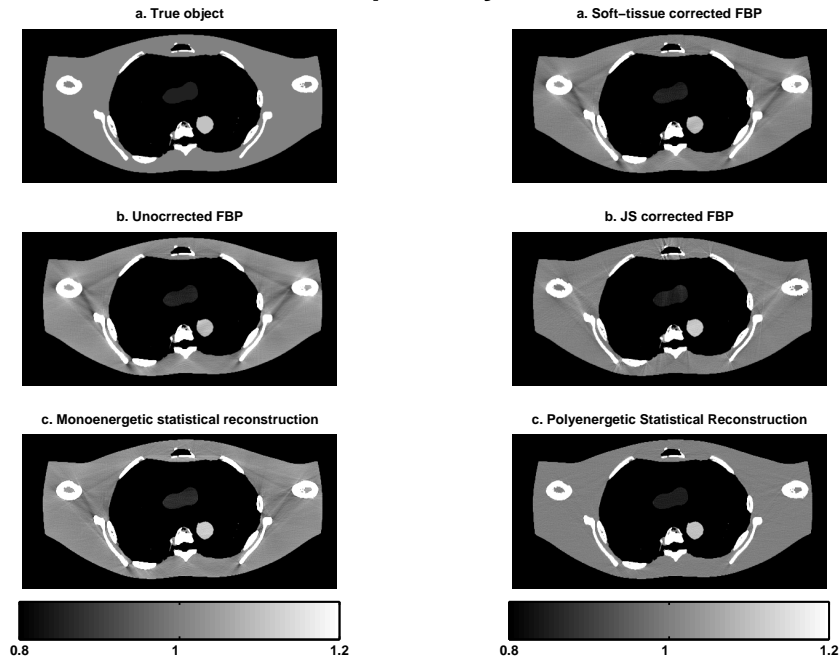
© J. Fessler, May 12, 2008

0.7

p0intro

Conventional FBP reconstruction of dual-energy X-ray CT data does not account for the noise properties of CT measurements and results in significant noise propagation into the soft tissue and cortical bone component images. Statistical reconstruction methods greatly reduces this noise, improving quantitative accuracy [46]. This is of potential importance for applications like bone density measurements.

## Benefit Example: Physical Models



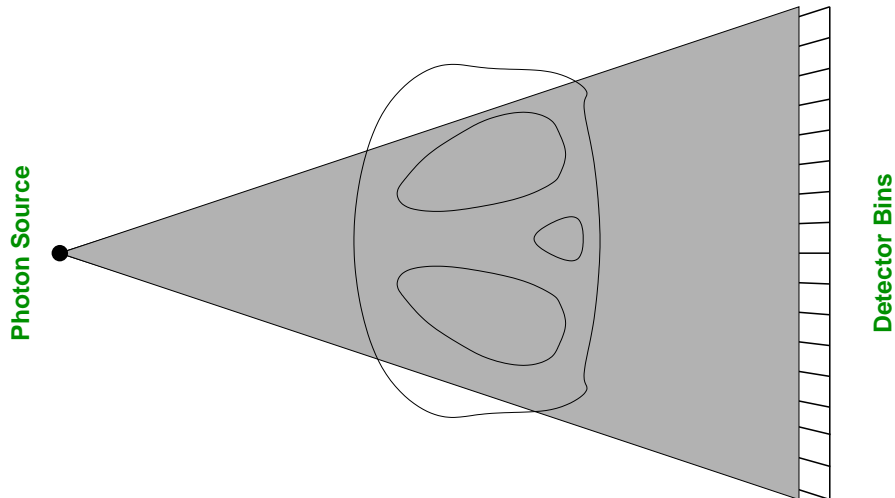
0.8

© J. Fessler, May 12, 2008

0.8

p0intro

## Benefit Example: Nonstandard Geometries



0.9

© J. Fessler, May 12, 2008

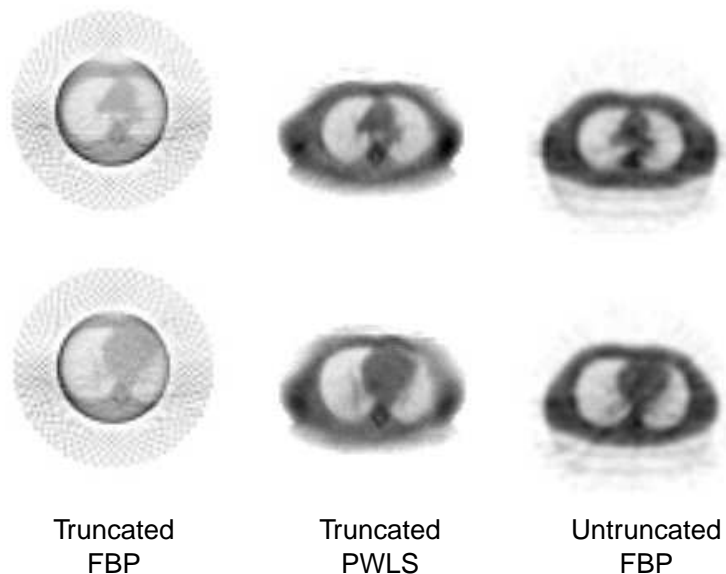
0.9

p0intro

Conventional FBP ignores the polyenergetic X-ray source spectrum. Statistical/iterative reconstruction methods can build that spectrum into the model and nearly eliminate beam-hardening artifacts [47–49].

A SPECT transmission scan with 65cm distance between line source and standard Anger camera provides partially truncated sinogram views of most patients.

## Truncated Fan-Beam SPECT Transmission Scan



0.10

The FBP reconstruction method is largely ruined by the sinogram truncation.

Despite the partial truncation, each pixel is *partly* sampled by “line integrals” at some range of angles. With the benefit of spatial regularization, nonnegativity constraints, and statistical models, a statistical reconstruction method (PWLS in this case) can recover an attenuation map that is comparable to that obtained with an untruncated scan.

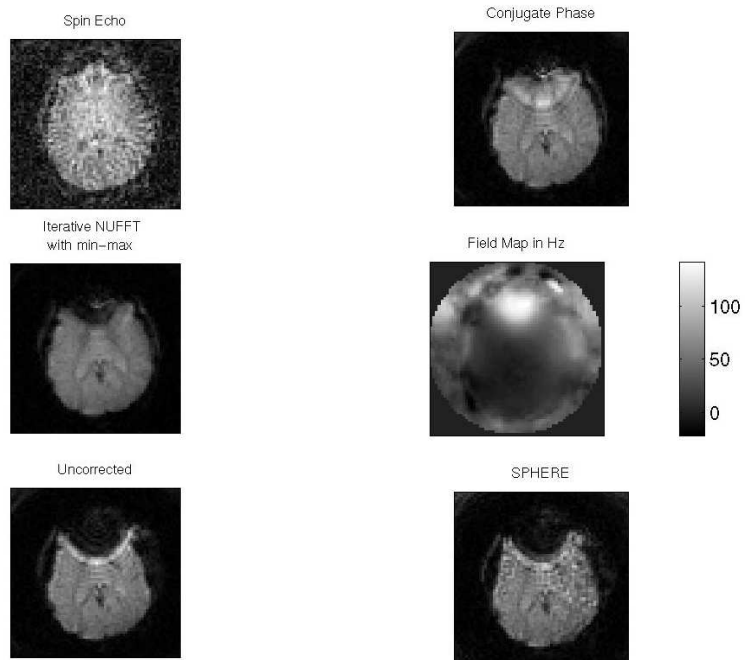
We have shown related benefits in PET with missing sinogram data due to detector gaps [50].

© J. Fessler, May 12, 2008

0.10

p0intro

## One Final Advertisement: Iterative MR Reconstruction



0.11

MR signal equation:

$$s(t) = \int f(\vec{x}) \exp(-i\omega(\vec{x})t) \exp(-i2\pi\vec{k}(\vec{x}) \cdot \vec{x}) d\vec{x}$$

- Due to field inhomogeneity, signal is *not* Fourier transform of object.
- Measure off-resonance field-map  $\omega(\vec{x})$  using two displaced echos
- Penalized WLS cost function minimized by conjugate gradient
- System matrix  $\mathbf{A}$  includes off-resonance effects
- Fast algorithm using NUFFT and time-segmentation

[51–53]

Hopefully that is enough motivation, so, on with the methodology!

© J. Fessler, May 12, 2008

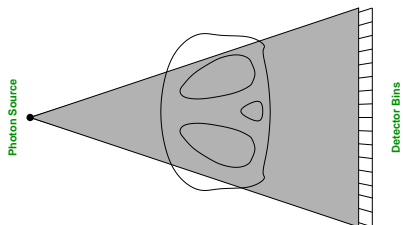
0.11

p0intro

## Part 1: Problem Statement(s)

Example:

in monoenergetic transmission tomography with photon counting detectors, the goal is to reconstruct the *attenuation map*  $\mu(\vec{x})$  from transmission measurements  $\{y_i\}_{i=1}^{n_d}$ , given the system response  $s_i(\vec{x})$ ,  $i = 1, \dots, n_d$ , for each detector element.



Statistical model:  $y_i \sim \text{Poisson}\{b_i \exp(-\int \mu(\vec{x}) s_i(\vec{x}) d\vec{x}) + r_i\}$

- $b_i$ : blank/air scan
- $s_i(\vec{x})$ : line impulse associated with line integral for  $i$ th ray, possibly including detector blur and finite source size (approximation)
- $r_i$ : background due to Compton scatter

1b.1

© J. Fessler, May 12, 2008

1b.1

p1frame

## Continuous-Discrete Models

Emission tomography:  $y_i \sim \text{Poisson}\{\int \lambda(\vec{x}) s_i(\vec{x}) d\vec{x} + r_i\}$

Transmission tomography (monoenergetic):  $y_i \sim \text{Poisson}\{b_i \exp(-\int_{L_i} \mu(\vec{x}) d\ell) + r_i\}$

Transmission (polyenergetic):  $y_i \sim \text{Poisson}\{\int I_i(\mathcal{E}) \exp(-\int_{L_i} \mu(\vec{x}, \mathcal{E}) d\ell) d\mathcal{E} + r_i\}$

Magnetic resonance imaging:  $y_i = \int f(\vec{x}) s_i(\vec{x}) d\vec{x} + \epsilon_i$

Discrete measurements  $\mathbf{y} = (y_1, \dots, y_{n_d})$

Continuous-space unknowns:  $\lambda(\vec{x})$ ,  $\mu(\vec{x})$ ,  $f(\vec{x})$

Goal: estimate  $f(\vec{x})$  given  $\mathbf{y}$

**Solution options:**

- Continuous-continuous formulations (“analytical,” *cf.* FBP for tomography)
- Continuous-discrete formulations  
Usually  $\hat{f}(\vec{x}) = \sum_{i=1}^{n_d} c_i s_i(\vec{x})$
- Discrete-discrete formulations  $f(\vec{x}) \approx \sum_{j=1}^{n_p} x_j b_j(\vec{x})$

1b.2

© J. Fessler, May 12, 2008

1b.2

p1frame

For a nice comparison of the options, see [9].

## Textbook MRI Measurement Model

---

---

Ignoring *lots* of things, the standard measurement model is:

$$y_i = s(t_i) + \text{noise}_i, \quad i = 1, \dots, n_d$$
$$s(t) = \int f(\vec{x}) e^{-i2\pi\vec{k}(t)\cdot\vec{x}} d\vec{x} = F(\vec{k}(t)).$$

$\vec{x}$ : spatial coordinates

$\vec{k}(t)$ : k-space trajectory of the MR pulse sequence

$f(\vec{x})$ : object's unknown transverse magnetization

$F(\vec{k})$ : Fourier transform of  $f(\vec{x})$ . We get noisy samples of this!

$e^{-i2\pi\vec{k}(t)\cdot\vec{x}}$  provides spatial information  $\implies$  Nobel Prize

Goal of image reconstruction: find  $f(\vec{x})$  from measurements  $\{y_i\}_{i=1}^{n_d}$ .

The unknown object  $f(\vec{x})$  is a continuous-space function, but the recorded measurements  $\mathbf{y} = (y_1, \dots, y_{n_d})$  are finite.

Under-determined (ill posed) problem  $\implies$  no canonical solution.

All MR scans provide only "partial" k-space data.

1b.3

© J. Fessler, May 12, 2008

1b.3

p1frame

## Image Reconstruction Strategies

---

---

- Continuous-continuous formulation

Pretend that a continuum of measurements are available:

$$F(\vec{k}) = \int f(\vec{x}) e^{-i2\pi\vec{k}\cdot\vec{x}} d\vec{x}.$$

The "solution" is an inverse Fourier transform:

$$f(\vec{x}) = \int F(\vec{k}) e^{i2\pi\vec{k}\cdot\vec{x}} d\vec{k}.$$

Now discretize the integral solution:

$$\hat{f}(\vec{x}) = \sum_{i=1}^{n_d} F(\vec{k}_i) e^{i2\pi\vec{k}_i\cdot\vec{x}} w_i \approx \sum_{i=1}^{n_d} y_i w_i e^{i2\pi\vec{k}_i\cdot\vec{x}},$$

where  $w_i$  values are "sampling density compensation factors." Numerous methods for choosing  $w_i$  values in the literature.

For Cartesian sampling, using  $w_i = 1/N$  suffices, and the summation is an inverse FFT.

For non-Cartesian sampling, replace summation with gridding.

1b.4

© J. Fessler, May 12, 2008

1b.4

p1frame



- Continuous-discrete formulation

Use many-to-one linear model:

$$\mathbf{y} = \mathcal{A} f + \boldsymbol{\epsilon}, \text{ where } \mathcal{A} : \mathcal{L}_2(\mathbb{R}^{\bar{d}}) \rightarrow \mathbb{C}^{n_d}.$$

Minimum norm solution (cf. “natural pixels”):

$$\min_{\hat{f}} \|\hat{f}\|_2 \text{ subject to } \mathbf{y} = \mathcal{A} \hat{f}$$

$$\hat{f} = \mathcal{A}^* (\mathcal{A} \mathcal{A}^*)^{-1} \mathbf{y} = \sum_{i=1}^{n_d} c_i e^{-i2\pi \bar{\kappa}_i \cdot \bar{\mathbf{x}}}, \text{ where } \mathcal{A} \mathcal{A}^* \mathbf{c} = \mathbf{y}.$$

- Discrete-discrete formulation

Assume parametric model for object:

$$f(\bar{\mathbf{x}}) = \sum_{j=1}^{n_p} x_j b_j(\bar{\mathbf{x}}).$$

Estimate parameter vector  $\mathbf{x} = (x_1, \dots, x_{n_p})$  from data vector  $\mathbf{y}$ .

1b.5

© J. Fessler, May 12, 2008

1b.5

p1frame

## Part 2: Five Categories of Choices

- Object parameterization: function  $f(\vec{r})$  vs finite coefficient vector  $\mathbf{x}$
- System physical model:  $\{s_i(\vec{r})\}$
- Measurement statistical model  $y_i \sim \boxed{?}$
- Cost function: data-mismatch and regularization
- Algorithm / initialization

No perfect choices - one can critique all approaches!

2.1

© J. Fessler, May 12, 2008

2.1

p2choice

---

Often these choices are made implicitly rather than explicitly. Leaving the choices implicit fortifies the common belief among non-experts that there are basically two kinds of reconstruction algorithms, FBP and “iterative.”

In fact, the choices one makes in the above five categories can affect the results significantly.

In my opinion, every paper describing iterative image reconstruction methods (or results thereof) should make as explicit as possible what choices were made in each of the above categories.

---

## Choice 1. Object Parameterization

Finite measurements:  $\{y_i\}_{i=1}^{n_d}$ . Continuous object:  $f(\vec{r})$ . Hopeless?

“All models are wrong but some models are useful.”

Linear *series expansion* approach. Replace  $f(\vec{r})$  by  $\mathbf{x} = (x_1, \dots, x_{n_p})$  where

$$f(\vec{r}) \approx \tilde{f}(\vec{r}) = \sum_{j=1}^{n_p} x_j b_j(\vec{r}) \leftarrow \text{“basis functions”}$$

Forward projection:

$$\begin{aligned} \int s_i(\vec{r}) f(\vec{r}) d\vec{r} &= \int s_i(\vec{r}) \left[ \sum_{j=1}^{n_p} x_j b_j(\vec{r}) \right] d\vec{r} = \sum_{j=1}^{n_p} \left[ \int s_i(\vec{r}) b_j(\vec{r}) d\vec{r} \right] x_j \\ &= \sum_{j=1}^{n_p} a_{ij} x_j = [\mathbf{A}\mathbf{x}]_i, \text{ where } a_{ij} \triangleq \int s_i(\vec{r}) b_j(\vec{r}) d\vec{r} \end{aligned}$$

- Projection integrals become finite summations.
- $a_{ij}$  is contribution of  $j$ th basis function (e.g., voxel) to  $i$ th measurement.
- The units of  $a_{ij}$  and  $x_j$  depend on the user-selected units of  $b_j(\vec{r})$ .
- The  $n_d \times n_p$  matrix  $\mathbf{A} = \{a_{ij}\}$  is called the *system matrix*.

2.2

## (Linear) Basis Function Choices

- Fourier series (complex / not sparse)
- Circular harmonics (complex / not sparse)
- Wavelets (negative values / not sparse)
- Kaiser-Bessel window functions (blobs)
- Overlapping circles (disks) or spheres (balls)
- Polar grids, logarithmic polar grids
- “Natural pixels”  $\{s_i(\vec{r})\}$
- B-splines (pyramids)
- Rectangular pixels / voxels (rect functions)
- Point masses / bed-of-nails / lattice of points / “comb” function
- Organ-based voxels (e.g., from CT in PET/CT systems)
- ...

2.3

---

In principle it is not entirely hopeless to reconstruction a continuous  $f(\vec{r})$  from a finite set of measurements. This is done routinely in the field of nonparametric regression [55] (the generalization of linear regression that allows for fitting smooth functions rather than just lines). But it is complicated in tomography...

Van De Walle, Barrett, *et al.* [54] have proposed pseudoinverse calculation method for MRI reconstruction from a continuous-object / discrete-data formulation, based on the general principles of Bertero *et al.* [56]. If the pseudo-inverse could truly be computed once-and-for-all then such an approach could be practically appealing. However, in practice there are object-dependent effects, such as nonuniform attenuation in SPECT and magnetic field inhomogeneity in MRI, and these preclude precomputation of the required SVDs. So pseudo-inverse approaches are impractical for typical realistic physical models.

---

© J. Fessler, May 12, 2008

2.2

p2choice

---

See [57] for an early discussion.

Many published “projector / backprojector pairs” are not based explicitly on any particular choice of basis.

Some pixel-driven backprojectors could be interpreted implicitly as point-mass object models. This model works fine for FBP, but causes artifacts for iterative methods.

Mazur *et al.* [58] approximate the shadow of each pixel by a rect function, instead of by a trapezoid. “As the shapes of pixels are artifacts of our digitisation of continuous real-world images, consideration of alternative orientation or shapes for them seems reasonable.” However, they observe slightly worse results that worsen with iteration!

Classic series-expansion reference [59]

Organ-based voxel references include [60–65]

---

© J. Fessler, May 12, 2008

2.3

p2choice

## Basis Function Considerations

### Mathematical

- Represent  $f(\vec{r})$  “well” with moderate  $n_p$  (approximation accuracy)
- *e.g.*, represent a constant (uniform) function
- Orthogonality? (not essential)
- Linear independence (ensures uniqueness of expansion)
- Insensitivity to shift of basis-function grid (approximate shift invariance)
- Rotation invariance

### Computational

- “Easy” to compute  $a_{ij}$  values and/or  $\mathbf{Ax}$
- If stored, the system matrix  $\mathbf{A}$  should be sparse (mostly zeros).
- Easy to represent nonnegative functions *e.g.*, if  $x_j \geq 0$ , then  $f(\vec{r}) \geq 0$ .  
A sufficient condition is  $b_j(\vec{r}) \geq 0$ .

2.4

## Nonlinear Object Parameterizations

Estimation of intensity *and* shape (*e.g.*, location, radius, etc.)

Surface-based (homogeneous) models

- Circles / spheres
- Ellipses / ellipsoids
- Superquadrics
- Polygons
- Bi-quadratic triangular Bezier patches, ...

Other models

- Generalized series  $f(\vec{r}) = \sum_j x_j b_j(\vec{r}; \boldsymbol{\theta})$
- Deformable templates  $f(\vec{r}) = b(\mathbf{T}_{\boldsymbol{\theta}}(\vec{r}))$
- ...

### Considerations

- Can be considerably more parsimonious
- If correct, yield greatly reduced estimation error
- Particularly compelling in limited-data problems
- Often oversimplified (all models are wrong but...)
- Nonlinear dependence on location induces non-convex cost functions, complicating optimization

2.5

---

“Well”  $\equiv$  approximation error less than estimation error

Many bases have the desirable approximation property that one can form arbitrarily accurate approximations to  $f(\vec{r})$  by taking  $n_p$  sufficiently large. (This is related to *completeness*.) Exceptions include “natural pixels” (a finite set) and the point-lattice “basis” (usually).

---

© J. Fessler, May 12, 2008

2.4

p2choice

---

Disks [66, 67]

Polygons [68]

Generalized series [69]

Bi-quadratic triangular Bezier patches [70]

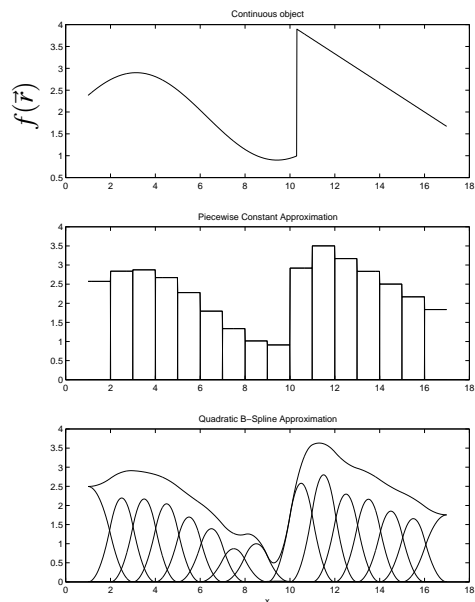
---

© J. Fessler, May 12, 2008

2.5

p2choice

## Example Basis Functions - 1D



2.6

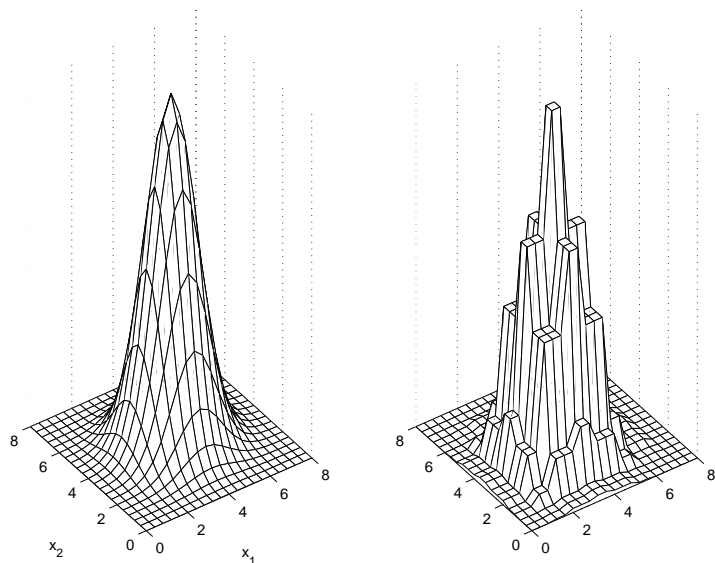
In the above example, neither the pixels nor the blobs are ideal, though both could reduce the average approximation error as low as needed by taking  $n_p$  sufficiently large.

© J. Fessler, May 12, 2008

2.6

p2choice

## Pixel Basis Functions - 2D



Continuous image  $f(\vec{r})$

Pixel basis approximation

$$\sum_{j=1}^{n_p} x_j b_j(\vec{r})$$

2.7

My tentative recommendation: use pixel / voxel basis.

- Simple
- Perfectly matched to digital displays
- Maximally sparse system matrix

Or use blobs (rotationally symmetric Kaiser-Bessel windows)

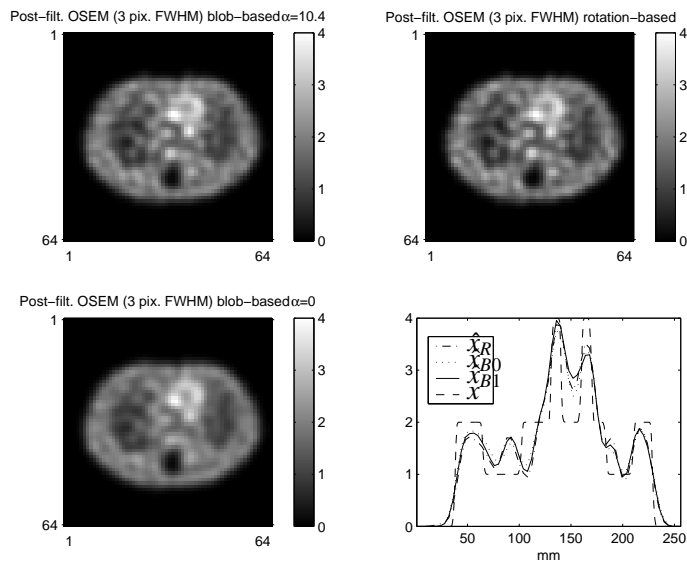
- Easy to compute projections “on the fly” due to rotational symmetry.
- Differentiable, nonnegative.
- Parsimony advantage using body-centered cubic packing

© J. Fessler, May 12, 2008

2.7

p2choice

## Blobs in SPECT: Qualitative



A slice and profiles through over-iterated and post-smoothed OSEM-reconstructed images of a single realization of noisy simulated phantom data. Superimposed on the profile of the true high-resolution phantom ( $x$ ) are those of the images reconstructed with the rotation-based model ( $\hat{x}_R$ , NMSE = 4.12%), the blob-based model with  $\alpha = 0$  ( $\hat{x}_{B0}$ , NMSE = 2.99%), and the blob-based model with  $\alpha = 10.4$  ( $\hat{x}_{B1}$ , NMSE = 3.60%).

Figure taken from [71].

Blob expositions [72, 73].

(2D SPECT thorax phantom simulations)

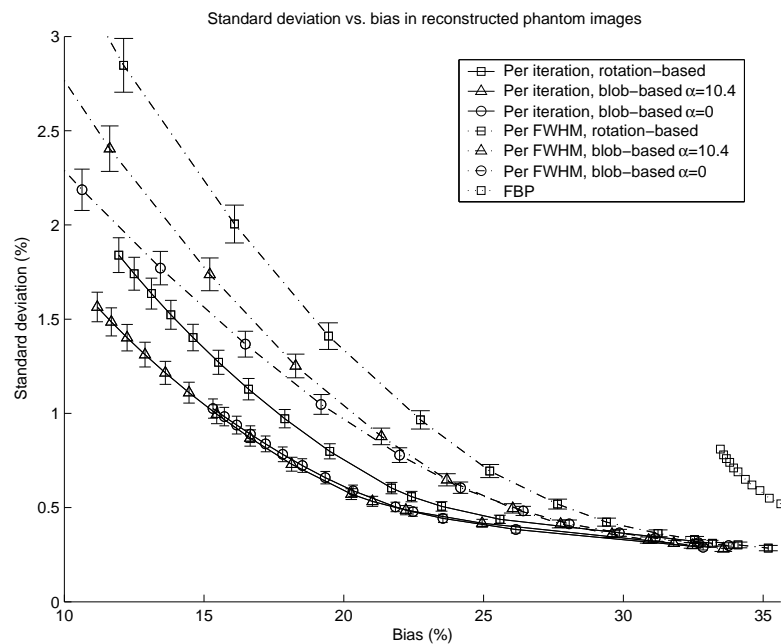
2.8

© J. Fessler, May 12, 2008

2.8

p2choice

## Blobs in SPECT: Quantitative



Bottom line: in our experience in SPECT simulations comparing bias and variance of a small ROI, iterative reconstruction improved significantly over FBP, but blobs offered only a modest improvement over a rotation-based projector/backprojector that uses square pixels implicitly. And in some cases, a "blob" with shape parameter = 0, which is a (non-smooth) circ function performed best.

2.9

© J. Fessler, May 12, 2008

2.9

p2choice

## Discrete-Discrete Emission Reconstruction Problem

Having chosen a basis and *linearly* parameterized the emission density...

Estimate the emission density coefficient vector  $\mathbf{x} = (x_1, \dots, x_{n_p})$  (aka “image”) using (something like) this statistical model:

$$y_i \sim \text{Poisson} \left\{ \sum_{j=1}^{n_p} a_{ij} x_j + r_i \right\}, \quad i = 1, \dots, n_d.$$

- $\{y_i\}_{i=1}^{n_d}$  : observed counts from each detector unit
- $\mathbf{A} = \{a_{ij}\}$  : system matrix (determined by system models)
- $r_i$  values : background contributions (determined separately)

---

Many image reconstruction problems are “find  $\mathbf{x}$  given  $\mathbf{y}$ ” where

$$y_i = g_i([\mathbf{A}\mathbf{x}]_i) + \varepsilon_i, \quad i = 1, \dots, n_d.$$

2.10

---

Called the “discrete-discrete” estimation problem since both the measurement vector and the image vector are “discretized” (finite dimensional).

In contrast, FBP is derived from the “continuous-continuous” Radon transform model.

---

2.10

© J. Fessler, May 12, 2008

p2choice

## Choice 2. System Model, aka Physics

$$\text{System matrix elements: } a_{ij} = \int s_i(\vec{r}) b_j(\vec{r}) d\vec{r}$$

- scan geometry
- collimator/detector response
- attenuation
- scatter (object, collimator, scintillator)
- duty cycle (dwell time at each angle)
- detector efficiency / dead-time losses
- positron range, noncollinearity, crystal penetration, ...
- ...

### Considerations

- Improving system model can improve
  - Quantitative accuracy
  - Spatial resolution
  - Contrast, SNR, detectability
- Computation time (and storage vs compute-on-fly)
- Model uncertainties (e.g., calculated scatter probabilities based on noisy attenuation map)
- Artifacts due to over-simplifications

2.11

---

For the pixel basis,  $a_{ij}$  is the probability that a decay in the  $j$ th pixel is recorded by the  $i$ th detector unit, or is proportional to that probability.

Attenuation enters into  $a_{ij}$  differently in PET and SPECT.

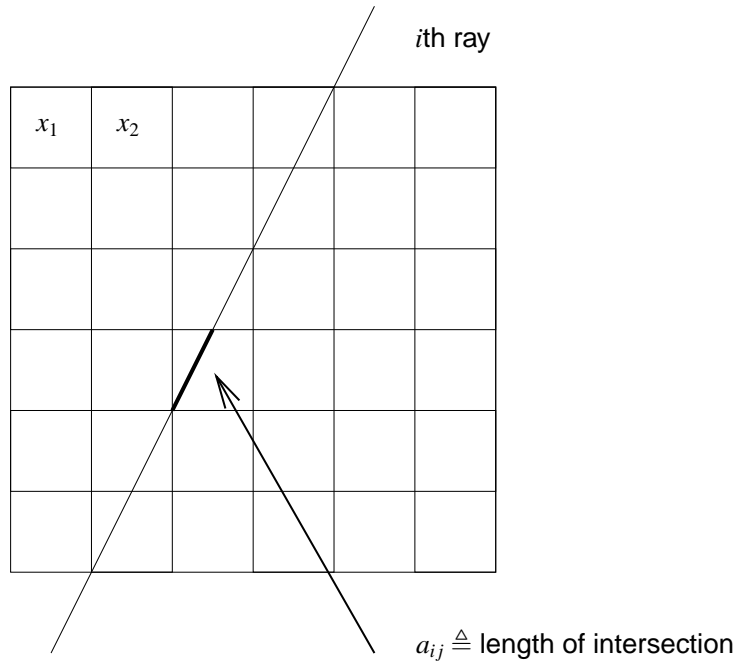
---

2.11

© J. Fessler, May 12, 2008

p2choice

## “Line Length” System Model for Tomography



2.12

Mathematically, the corresponding detector unit sensitivity pattern is

$$s_i(\vec{r}) = \delta(\vec{k}_i \cdot \vec{r} - \tau_i),$$

where  $\delta$  denotes the Dirac impulse function.

This model is usually applied with the pixel basis, but can be applied to any basis.

Does not exactly preserve counts, *i.e.*, in general

$$\int f(\vec{r}) d\vec{r} \neq \sum_{i=1}^{n_d} \sum_{j=1}^{n_p} a_{ij} x_j$$

Leads to artifacts.

Units are wrong too. (Reconstructed  $x$  will have units inverse length.)

Perhaps reasonable for X-ray CT, but unnatural for emission tomography. (Line segment length is a probability?)

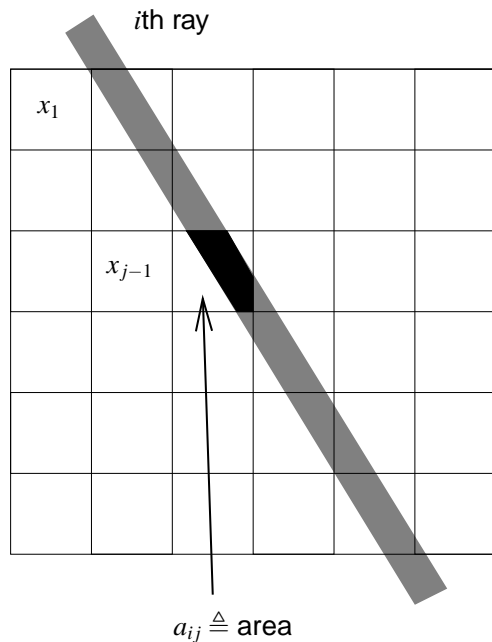
In short: I recommend using almost anything else!

© J. Fessler, May 12, 2008

2.12

p2choice

## “Strip Area” System Model for Tomography



2.13

Accounts for finite detector width.

Mathematically, the corresponding detector unit sensitivity pattern is

$$s_i(\vec{r}) = \text{rect}\left(\frac{\vec{k}_i \cdot \vec{r} - \tau_i}{w}\right),$$

where  $w$  is the detector width.

Can exactly preserve counts, since all areas are preserved, provided that the width  $w$  is an integer multiple of the center-to-center ray spacing.

Most easily applied to the pixel basis, but in principle applies to any choice.

A little more work to compute than line-lengths, but worth the extra effort (particularly when pre-computed).

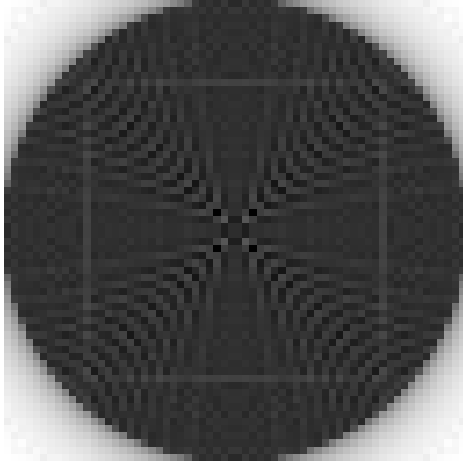
© J. Fessler, May 12, 2008

2.13

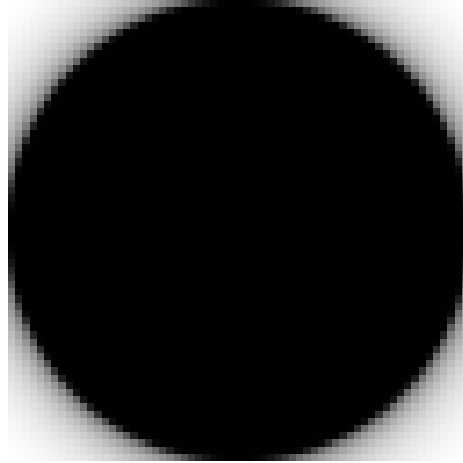
p2choice

# (Implicit) System Sensitivity Patterns

$$\sum_{i=1}^{n_d} a_{ij} \approx s(\vec{r}_j) = \sum_{i=1}^{n_d} s_i(\vec{r}_j)$$



Line Length



Strip Area

2.14

## Forward- / Back-projector “Pairs”

Forward projection (image domain to projection domain):

$$\bar{y}_i = \int s_i(\vec{r}) f(\vec{r}) d\vec{r} = \sum_{j=1}^{n_p} a_{ij} x_j = [\mathbf{Ax}]_i, \text{ or } \bar{\mathbf{y}} = \mathbf{Ax}$$

Backprojection (projection domain to image domain):

$$\mathbf{A}'\mathbf{y} = \left\{ \sum_{i=1}^{n_d} a_{ij} y_i \right\}_{j=1}^{n_p}$$

The term “forward/backprojection pair” often corresponds to an implicit choice for the object basis and the system model.

Sometimes  $\mathbf{A}'\mathbf{y}$  is implemented as  $\mathbf{By}$  for some “backprojector”  $\mathbf{B} \neq \mathbf{A}'$

Least-squares solutions (for example):

$$\hat{\mathbf{x}} = [\mathbf{A}'\mathbf{A}]^{-1} \mathbf{A}'\mathbf{y} \neq [\mathbf{BA}]^{-1} \mathbf{By}$$

2.15

---

Backprojection of a uniform sinogram.

Explicitly:

$$\sum_{i=1}^{n_d} a_{ij} = \sum_{i=1}^{n_d} \int s_i(\vec{r}) b_j(\vec{r}) d\vec{r} = \int \left[ \sum_{i=1}^{n_d} s_i(\vec{r}) \right] b_j(\vec{r}) d\vec{r} = \int s(\vec{r}) b_j(\vec{r}) d\vec{r} \approx s(\vec{r}_j)$$

where  $\vec{r}_j$  is center of  $j$ th basis function.

Shows probability for each pixel that an emission from that pixel will be detected somewhere.

These nonuniformities propagate into the reconstructed images, except when sinograms are simulated from the same model of course.

---

© J. Fessler, May 12, 2008

2.14

p2choice

---

Algorithms are generally derived using a single  $\mathbf{A}$  matrix, and usually the quantity  $\mathbf{A}'\mathbf{y}$  appears somewhere in the derivation.

If the product  $\mathbf{A}'\mathbf{y}$  is implemented by some  $\mathbf{By}$  for  $\mathbf{B} \neq \mathbf{A}'$ , then all convergence properties, statistical properties, etc. of the theoretical algorithm may be lost by the implemented algorithm.

---

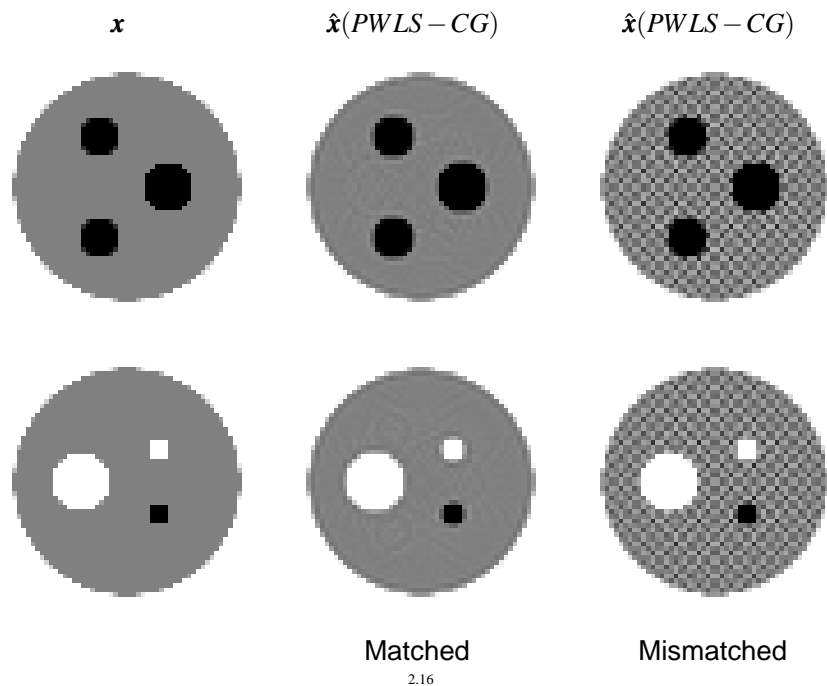
© J. Fessler, May 12, 2008

2.15

p2choice



## Mismatched Backprojector $B \neq A'$



2.16

Note: when converting from .ps to .pdf, I get JPEG image compression artifacts that may corrupt these images. If I disable compression, then the files are 8x larger...

Noiseless 3D PET data, images are  $n_x \times n_y \times n_z = 64 \times 64 \times 4$ , with  $n_u \times n_v \times n_\theta \times n_\phi = 62 \times 10 \times 60 \times 3$  projections. 15 iterations of PWLS-CG, initialized with the true image. True object values range from 0 to 2. Display windowed to [0.7, 1.3] to highlight artifacts.

In this case mismatch arises from a ray-driven forward projector but a pixel-driven back projector.

Another case where mismatch can arise is in "rotate and sum" projection / backprojection methods, if implemented carelessly.

The problem with mismatched backprojectors arises in iterative reconstruction because multiple iterations are generally needed, so discrepancies between  $B$  and  $A'$  can accumulate.

Such discrepancies may matter more for regularized methods where convergence is desired, then for unregularized methods where one stops well before convergence [74], but this is merely speculation.

The deliberate use of mismatched projectors/backprojectors has been called the "dual matrix" approach [75, 76].

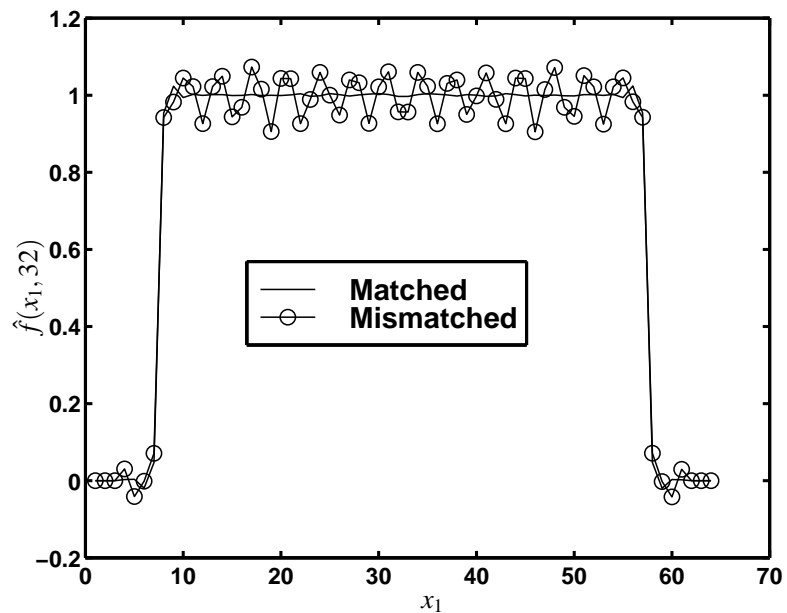
The importance of matching also arises in solving differential equations [77].

© J. Fessler, May 12, 2008

2.16

p2choice

## Horizontal Profiles



2.17

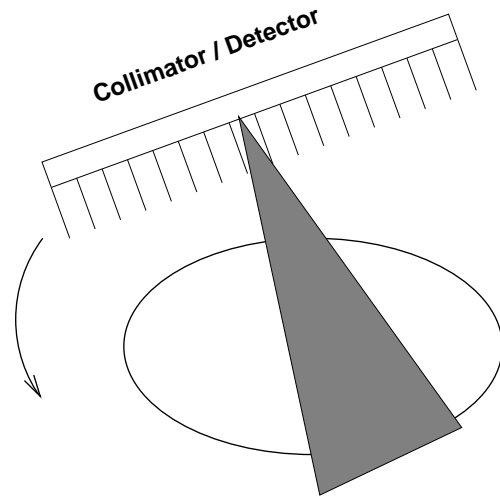
This was from noiseless simulated data!

© J. Fessler, May 12, 2008

2.17

p2choice

## SPECT System Modeling



Complications: nonuniform attenuation, depth-dependent PSF, Compton scatter

2.18

© J. Fessler, May 12, 2008

2.18

p2choice

### Choice 3. Statistical Models

After modeling the system physics, we have a deterministic “model:”

$$y_i \approx g_i([\mathbf{A}\mathbf{x}]_i)$$

for some functions  $g_i$ , e.g.,  $g_i(l) = l + r_i$  for emission tomography.

Statistical modeling is concerned with the “ $\approx$ ” aspect.

### Considerations

- More accurate models:
  - can lead to lower variance images,
  - may incur additional computation,
  - may involve additional algorithm complexity  
(e.g., proper transmission Poisson model has nonconcave log-likelihood)
- Statistical model errors (e.g., deadtime)
- Incorrect models (e.g., log-processed transmission data)

2.19

© J. Fessler, May 12, 2008

2.19

p2stat

---

Numerous papers in the literature address aspects of the system model in the context of SPECT imaging. Substantial improvements in image quality and quantitative accuracy have been demonstrated by using appropriate system models.

---

---

“Complexity” can just mean “inconvenience.” It would certainly be more convenient to precorrect the sinogram data for effects such as randoms, attenuation, scatter, detector efficiency, etc., since that would save having to store those factors for repeated use during the iterations. But such precorrections destroy the Poisson statistics and lead to suboptimal performance (higher variance).

More accurate statistical models may also yield lower bias, but bias is often dominated by approximations in the system model (neglected scatter, etc.) and by resolution effects induced by regularization.

---

## Statistical Model Choices for Emission Tomography

- “None.” Assume  $\mathbf{y} - \mathbf{r} = \mathbf{Ax}$ . “Solve algebraically” to find  $\mathbf{x}$ .
- White Gaussian noise. Ordinary least squares: minimize  $\|\mathbf{y} - \mathbf{Ax}\|^2$  (This is the appropriate statistical model for MR.)
- Non-white Gaussian noise. Weighted least squares: minimize

$$\|\mathbf{y} - \mathbf{Ax}\|_{\mathbf{w}}^2 = \sum_{i=1}^{n_d} w_i (y_i - [\mathbf{Ax}]_i)^2, \text{ where } [\mathbf{Ax}]_i \triangleq \sum_{j=1}^{n_p} a_{ij}x_j$$

(e.g., for Fourier rebinned (FORE) PET data)

- Ordinary Poisson model (ignoring or precorrecting for background)

$$y_i \sim \text{Poisson}\{[\mathbf{Ax}]_i\}$$

- Poisson model

$$y_i \sim \text{Poisson}\{[\mathbf{Ax}]_i + r_i\}$$

- Shifted Poisson model (for randoms precorrected PET)

$$y_i = y_i^{\text{prompt}} - y_i^{\text{delay}} \sim \text{Poisson}\{[\mathbf{Ax}]_i + 2r_i\} - 2r_i$$

2.20

## Shifted-Poisson Model for X-ray CT

A model that includes both photon variability and electronic readout noise:

$$y_i \sim \text{Poisson}\{\bar{y}_i(\boldsymbol{\mu})\} + \text{N}(0, \sigma^2)$$

Shifted Poisson approximation (matches first two moments):

$$[y_i + \sigma^2]_+ \sim \text{Poisson}\{\bar{y}_i(\boldsymbol{\mu}) + \sigma^2\}$$

or just use WLS...

Complications:

- Intractability of likelihood for Poisson+Gaussian
- Compound Poisson distribution due to photon-energy-dependent detector signal.

X-ray statistical modeling is a current research area in several groups!

2.21

---

These are all for the emission case.

GE uses WLS for FORE data [78].

The shifted-Poisson model for randoms-precorrected PET is described in [79–82].

Snyder *et al.* used similar models for CCD imaging [83, 84].

Missing from the above list: deadtime model [85].

My recommendations.

- If the data is uncorrected, then use Poisson model above.
- If the data was corrected for random coincidences, use shifted Poisson model.
- If the data has been corrected for other stuff, consider using WLS, e.g. [86, 87].
- Try not to correct the data so that the first choice can be used!

Classic reason for WLS over Poisson was compute time. This has been obviated by recent algorithm advances. Now the choice should be made statistically.

Preprocessing: randoms subtraction, Fourier or multislice rebinning (3d to 2d), attenuation, scatter, detector efficiency, etc.

---

© J. Fessler, May 12, 2008

2.20

p2stat

---

For Poisson+Gaussian, see [83, 84].

For compound Poisson distribution, see [88–90].

---

© J. Fessler, May 12, 2008

2.21

p2stat

## Choice 4. Cost Functions

Components:

- *Data-mismatch* term
- *Regularization* term (and regularization parameter  $\beta$ )
- Constraints (e.g., nonnegativity)

Cost function:

$$\Psi(\mathbf{x}) = \text{DataMismatch}(\mathbf{y}, \mathbf{A}\mathbf{x}) + \beta \text{Roughness}(\mathbf{x})$$

Reconstruct image  $\hat{\mathbf{x}}$  by minimization:

$$\hat{\mathbf{x}} \triangleq \arg \min_{\mathbf{x} \geq \mathbf{0}} \Psi(\mathbf{x})$$

Actually *several* sub-choices to make for Choice 4 ...

Distinguishes “statistical methods” from “algebraic methods” for “ $\mathbf{y} = \mathbf{A}\mathbf{x}$ .”

2.22

## Why Cost Functions?

(vs “procedure” e.g., adaptive neural net with wavelet denoising)

### Theoretical reasons

ML is based on minimizing a cost function: the negative log-likelihood

- ML is asymptotically consistent
- ML is asymptotically unbiased
- ML is asymptotically efficient (under true statistical model...)
- Estimation: Penalized-likelihood achieves uniform CR bound asymptotically
- Detection: Qi and Huesman showed analytically that MAP reconstruction outperforms FBP for SKE/BKE lesion detection (T-MI, Aug. 2001)

### Practical reasons

- Stability of estimates (if  $\Psi$  and algorithm chosen properly)
- Predictability of properties (despite nonlinearities)
- Empirical evidence (?)

2.23

---

$\beta$  sometimes called *hyperparameter*

---

© J. Fessler, May 12, 2008

2.22

p2stat

---

Stability means that running “too many iterations” will not compromise image quality.

Asymptotically efficient means that the variance of ML estimator approaches that given by the Cramer-Rao lower bound, which is a bound on the variance of unbiased estimators.

But nuclear imaging is not asymptotic (too few counts), and system models are always approximate, and we regularize which introduces bias anyway.

Uniform CR bound generalizes CR bound to biased case [91, 92]

Bottom line: have not found anything better, seen plenty that are worse (LS vs ML in low count)

OSEM vs MAP [93, 94]

Qi and Huesman [44]

“Iterative FBP” methods are examples of methods that are not based on any cost function, and have not shared the popularity of ML and MAP approaches e.g., [95–98].

---

2.23

© J. Fessler, May 12, 2008

p2stat

# Bayesian Framework

Given a prior distribution  $p(\mathbf{x})$  for image vectors  $\mathbf{x}$ , by Bayes' rule:

$$\text{posterior: } p(\mathbf{x}|\mathbf{y}) = p(\mathbf{y}|\mathbf{x})p(\mathbf{x}) / p(\mathbf{y})$$

SO

$$\log p(\mathbf{x}|\mathbf{y}) = \log p(\mathbf{y}|\mathbf{x}) + \log p(\mathbf{x}) - \log p(\mathbf{y})$$

- $-\log p(\mathbf{y}|\mathbf{x})$  corresponds to data mismatch term (negative log-likelihood)
- $-\log p(\mathbf{x})$  corresponds to regularizing penalty function

## Maximum a posteriori (MAP) estimator:

$$\hat{\mathbf{x}} = \arg \max_{\mathbf{x}} \log p(\mathbf{x}|\mathbf{y}) = \arg \max_{\mathbf{x}} \log p(\mathbf{y}|\mathbf{x}) + \log p(\mathbf{x})$$

- Has certain optimality properties (provided  $p(\mathbf{y}|\mathbf{x})$  and  $p(\mathbf{x})$  are correct).
- Same form as  $\Psi$

2.24

## Choice 4.1: Data-Mismatch Term

Options (for emission tomography):

- Negative log-likelihood of statistical model. Poisson *emission* case:

$$-L(\mathbf{x}; \mathbf{y}) = -\log p(\mathbf{y}|\mathbf{x}) = \sum_{i=1}^{n_d} ([\mathbf{A}\mathbf{x}]_i + r_i) - y_i \log([\mathbf{A}\mathbf{x}]_i + r_i) + \log y_i!$$

- Ordinary (unweighted) least squares:  $\sum_{i=1}^{n_d} \frac{1}{2}(y_i - \hat{r}_i - [\mathbf{A}\mathbf{x}]_i)^2$
- Data-weighted least squares:  $\sum_{i=1}^{n_d} \frac{1}{2}(y_i - \hat{r}_i - [\mathbf{A}\mathbf{x}]_i)^2 / \hat{\sigma}_i^2$ ,  $\hat{\sigma}_i^2 = \max(y_i + \hat{r}_i, \sigma_{\min}^2)$ , (causes bias due to data-weighting).
- Reweighted least-squares:  $\hat{\sigma}_i^2 = [\mathbf{A}\hat{\mathbf{x}}]_i + \hat{r}_i$
- Model-weighted least-squares (nonquadratic, but convex!)

$$\sum_{i=1}^{n_d} \frac{1}{2}(y_i - \hat{r}_i - [\mathbf{A}\mathbf{x}]_i)^2 / ([\mathbf{A}\mathbf{x}]_i + \hat{r}_i)$$

- Nonquadratic cost-functions that are robust to outliers
- ...

## Considerations

- Faithfulness to statistical model vs computation
- Ease of optimization (convex?, quadratic?)
- Effect of statistical modeling errors

2.25

I avoid the Bayesian terminology because

- Images drawn from the "prior" distributions almost never look like real objects
- The risk function associated with MAP estimation seems less natural to me than a quadratic risk function. The quadratic choice corresponds to conditional mean estimation  $\hat{\mathbf{x}} = E[\mathbf{x}|\mathbf{y}]$  which is used very rarely by those who describe Bayesian methods for image formation.
- I often use penalty functions  $R(\mathbf{x})$  that depend on the data  $\mathbf{y}$ , which can hardly be called "priors," e.g., [38].

2.24

© J. Fessler, May 12, 2008

p2stat

Poisson probability mass function (PMF):

$$p(\mathbf{y}|\mathbf{x}) = \prod_{i=1}^{n_d} e^{-\bar{y}_i} \bar{y}_i^{y_i} / y_i! \quad \text{where } \bar{\mathbf{y}} \triangleq \mathbf{A}\mathbf{x} + \mathbf{r}$$

Reweighted least-squares [99]

Model-weighted least-squares [100, 101]

$$f(l) = \frac{1}{2}(y - r - l)^2 / (l + r) \quad \check{f}(l) = y^2 / (l + r)^3 > 0$$

Robust norms [102, 103]

Generally the data-mismatch term and the statistical model go hand-in-hand.

2.25

© J. Fessler, May 12, 2008

p2stat

## Choice 4.2: Regularization

Forcing too much “data fit” gives noisy images

Ill-conditioned problems: small data noise causes large image noise

### Solutions:

- Noise-reduction methods
- True regularization methods

### Noise-reduction methods

- Modify the *data*
  - Prefilter or “denoise” the sinogram measurements
  - Extrapolate missing (e.g., truncated) data
- Modify an *algorithm* derived for an ill-conditioned problem
  - Stop algorithm before convergence
  - Run to convergence, post-filter
  - Toss in a filtering step every iteration or couple iterations
  - Modify update to “dampen” high-spatial frequencies

2.26

## Noise-Reduction vs True Regularization

Advantages of noise-reduction methods

- Simplicity (?)
- Familiarity
- Appear less subjective than using penalty functions or priors
- Only fiddle factors are # of iterations, or amount of smoothing
- Resolution/noise tradeoff usually varies with iteration (stop when image looks good - in principle)
- Changing post-smoothing does not require re-iterating

Advantages of true regularization methods

- Stability (unique minimizer & convergence  $\implies$  initialization independence)
- Faster convergence
- Predictability
- Resolution can be made object independent
- Controlled resolution (e.g., spatially uniform, edge preserving)
- Start with reasonable image (e.g., FBP)  $\implies$  reach solution faster.

2.27

---

Dampen high-frequencies in EM [104]

FBP with an apodized ramp filter belongs in the “modify the algorithm” category. The FBP method is derived based on a highly idealized system model. The solution so derived includes a ramp filter, which causes noise amplification if used unmodified. Throwing in apodization of the ramp filter attempts to “fix” this problem with the FBP “algorithm.”

The fault is not with the *algorithm* but with the problem definition and cost function. Thus the fix should be to the latter, not to the algorithm.

The estimate-maximize smooth (EMS) method [105] uses filtering every iteration.

The continuous image  $f(\vec{r})$ - discrete data problem is *ill-posed*.

If the discrete-discrete problem has a full column rank system matrix  $\mathbf{A}$ , then that problem is well-posed, but still probably ill-conditioned.

---

© J. Fessler, May 12, 2008

---

Running many iterations followed by post-filtering seems preferable to aborting early by stopping rules [106, 107].

Lalush *et al.* reported small differences between post-filtering and MAP reconstructions with an entropy prior [108].

Slijpen and Beekman conclude that post-filtering slightly more accurate than “oracle” filtering between iterations for SPECT reconstruction [109].

---

© J. Fessler, May 12, 2008

2.26

p2reg

2.27

p2reg

## True Regularization Methods

Redefine the *problem* to eliminate ill-conditioning, rather than patching the data or algorithm!

### Options

- Use bigger pixels (fewer basis functions)
  - Visually unappealing
  - Can only preserve edges coincident with pixel edges
  - Results become even less invariant to translations
- Method of sieves (constrain image roughness)
  - Condition number for “pre-emission space” can be even worse
  - Lots of iterations
  - Commutability condition rarely holds exactly in practice
  - Degenerates to post-filtering in some cases

- Change cost function by adding a roughness penalty / prior

$$\hat{\mathbf{x}} = \arg \min_{\mathbf{x}} \Psi(\mathbf{x}), \quad \Psi(\mathbf{x}) = \mathcal{L}(\mathbf{x}) + \beta R(\mathbf{x})$$

- Disadvantage: apparently subjective choice of penalty
- Apparent difficulty in choosing penalty parameter(s), e.g.,  $\beta$  (cf. apodizing filter / cutoff frequency in FBP)

2.28

## Penalty Function Considerations

- Computation
- Algorithm complexity
- Uniqueness of minimizer of  $\Psi(\mathbf{x})$
- Resolution properties (edge preserving?)
- # of adjustable parameters
- Predictability of properties (resolution and noise)

### Choices

- separable vs nonseparable
- quadratic vs nonquadratic
- convex vs nonconvex

2.29

---

Big pixels [110]

Sieves [111, 112]

Lots of iterations for convergence [106, 113]

---

© J. Fessler, May 12, 2008

2.28

p2reg

---

There is a huge literature on different regularization methods. Of the many proposed methods, and many anecdotal results illustrating properties of such methods, only the “lowly” quadratic regularization method has been shown *analytically* to yield detection results that are superior to FBP [44].

---

© J. Fessler, May 12, 2008

2.29

p2reg

## Penalty Functions: Separable vs Nonseparable

### Separable

- Identity norm:  $R(\mathbf{x}) = \frac{1}{2} \mathbf{x}' \mathbf{I} \mathbf{x} = \sum_{j=1}^{n_p} x_j^2 / 2$   
penalizes large values of  $\mathbf{x}$ , but causes “squashing bias”
- Entropy:  $R(\mathbf{x}) = \sum_{j=1}^{n_p} x_j \log x_j$
- Gaussian prior with mean  $\mu_j$ , variance  $\sigma_j^2$ :  $R(\mathbf{x}) = \sum_{j=1}^{n_p} \frac{(x_j - \mu_j)^2}{2\sigma_j^2}$
- Gamma prior  $R(\mathbf{x}) = \sum_{j=1}^{n_p} p(x_j, \mu_j, \sigma_j)$  where  $p(x, \mu, \sigma)$  is Gamma pdf

The first two basically keep pixel values from “blowing up.”  
The last two encourage pixels values to be close to prior means  $\mu_j$ .

$$\text{General separable form: } R(\mathbf{x}) = \sum_{j=1}^{n_p} f_j(x_j)$$

Slightly simpler for minimization, but these do not explicitly enforce smoothness.  
The simplicity advantage has been overcome in newer algorithms.

2.30

## Penalty Functions: Separable vs Nonseparable

**Nonseparable** (partially couple pixel values) to penalize *roughness*

$x_1$	$x_2$	$x_3$
$x_4$	$x_5$	

Example

$$R(\mathbf{x}) = (x_2 - x_1)^2 + (x_3 - x_2)^2 + (x_5 - x_4)^2 + (x_4 - x_1)^2 + (x_5 - x_2)^2$$

2	2	2
2	1	

$$R(\mathbf{x}) = 1$$

3	3	1
2	2	

$$R(\mathbf{x}) = 6$$

1	3	1
2	2	

$$R(\mathbf{x}) = 10$$

Rougher images  $\implies$  larger  $R(\mathbf{x})$  values

2.31

The identity norm penalty is a form of Tikhonov-Miller regularization [114].

The Gaussian and Gamma bias the results towards the prior image. This can be good or bad depending on whether the prior image is correct or not! If the prior image comes from a normal database, but the patient is abnormal, such biases would be undesirable.

For arguments favoring maximum entropy, see [115]. For critiques of maximum entropy regularization, see [116–118].

A key development in overcoming the “difficulty” with nonseparable regularization was a 1995 paper by De Pierro: [119].

© J. Fessler, May 12, 2008

2.30

p2reg

If diagonal neighbors were included there would be 3 more terms in this example.

© J. Fessler, May 12, 2008

2.31

p2reg



# Roughness Penalty Functions

First-order neighborhood and pairwise pixel differences:

$$R(\mathbf{x}) = \sum_{j=1}^{n_p} \frac{1}{2} \sum_{k \in \mathcal{N}_j} \psi(x_j - x_k)$$

$\mathcal{N}_j \triangleq$  neighborhood of  $j$ th pixel (e.g., left, right, up, down)  
 $\psi$  called the potential function

Finite-difference approximation to continuous roughness measure:

$$R(f(\cdot)) = \int \|\nabla f(\vec{r})\|^2 d\vec{r} = \int \left| \frac{\partial}{\partial x} f(\vec{r}) \right|^2 + \left| \frac{\partial}{\partial y} f(\vec{r}) \right|^2 + \left| \frac{\partial}{\partial z} f(\vec{r}) \right|^2 d\vec{r}.$$

Second derivatives also useful:  
 (More choices!)

$$\left. \frac{\partial^2}{\partial x^2} f(\vec{r}) \right|_{\vec{r}=\vec{r}_j} \approx f(\vec{r}_{j+1}) - 2f(\vec{r}_j) + f(\vec{r}_{j-1})$$

$$R(\mathbf{x}) = \sum_{j=1}^{n_p} \psi(x_{j+1} - 2x_j + x_{j-1}) + \dots$$

2.32

For differentiable basis functions (e.g., B-splines), one can find  $\int \|\nabla f(\vec{r})\|^2 d\vec{r}$  exactly in terms of coefficients, e.g., [120].

See Gindi *et al.* [121, 122] for comparisons of first and second order penalties.

2.32

© J. Fessler, May 12, 2008

p2reg

## Penalty Functions: General Form

$$R(\mathbf{x}) = \sum_k \psi_k([\mathbf{C}\mathbf{x}]_k) \quad \text{where} \quad [\mathbf{C}\mathbf{x}]_k = \sum_{j=1}^{n_p} c_{kj} x_j$$

Example:

$x_1$	$x_2$	$x_3$
$x_4$	$x_5$	

$$\mathbf{C}\mathbf{x} = \begin{bmatrix} -1 & 1 & 0 & 0 & 0 \\ 0 & -1 & 1 & 0 & 0 \\ 0 & 0 & 0 & -1 & 1 \\ -1 & 0 & 0 & 1 & 0 \\ 0 & -1 & 0 & 0 & 1 \end{bmatrix} \begin{bmatrix} x_1 \\ x_2 \\ x_3 \\ x_4 \\ x_5 \end{bmatrix} = \begin{bmatrix} x_2 - x_1 \\ x_3 - x_2 \\ x_5 - x_4 \\ x_4 - x_1 \\ x_5 - x_2 \end{bmatrix}$$

$$R(\mathbf{x}) = \sum_{k=1}^5 \psi_k([\mathbf{C}\mathbf{x}]_k) = \psi_1(x_2 - x_1) + \psi_2(x_3 - x_2) + \psi_3(x_5 - x_4) + \psi_4(x_4 - x_1) + \psi_5(x_5 - x_2)$$

2.33

This form is general enough to cover nearly all the penalty functions that have been used in tomography. Exceptions include priors based on nonseparable line-site models [123–126], and the median root “prior” [127, 128], both of which are nonconvex.

It is just coincidence that  $\mathbf{C}$  is square in this example. In general, for a  $n_x \times n_y$  image, there are  $n_x(n_y - 1)$  horizontal pairs and  $n_y(n_x - 1)$  vertical pairs, so  $\mathbf{C}$  will be a  $(2n_x n_y - n_x - n_y) \times (n_x n_x)$  very sparse matrix (for a first-order neighborhood consisting of horizontal and vertical cliques).

Concretely, for a  $n_x \times n_y$  image ordered lexicographically, for a first-order neighborhood we use

$$\mathbf{C} = \begin{bmatrix} \mathbf{I}_{n_y} \otimes \mathbf{D}_{n_x} \\ \mathbf{D}_{n_y} \otimes \mathbf{I}_{n_x} \end{bmatrix}$$

where  $\otimes$  denotes the Kronecker product and  $\mathbf{D}_n$  denotes the following  $(n - 1) \times n$  matrix:

$$\mathbf{D}_n \triangleq \begin{bmatrix} -1 & 1 & 0 & 0 & 0 \\ 0 & -1 & 1 & 0 & 0 \\ 0 & 0 & \ddots & \ddots & 0 \\ 0 & 0 & 0 & -1 & 1 \end{bmatrix}.$$

2.33

© J. Fessler, May 12, 2008

p2reg

## Penalty Functions: Quadratic vs Nonquadratic

$$R(\mathbf{x}) = \sum_k \psi_k([\mathbf{C}\mathbf{x}]_k)$$

### Quadratic $\psi_k$

If  $\psi_k(t) = t^2/2$ , then  $R(\mathbf{x}) = \frac{1}{2}\mathbf{x}'\mathbf{C}'\mathbf{C}\mathbf{x}$ , a quadratic form.

- Simpler optimization
- Global smoothing

### Nonquadratic $\psi_k$

- Edge preserving
- More complicated optimization. (This is essentially solved in convex case.)
- Unusual noise properties
- Analysis/prediction of resolution and noise properties is difficult
- More adjustable parameters (e.g.,  $\delta$ )

Example: Huber function.  $\psi(t) \triangleq \begin{cases} t^2/2, & |t| \leq \delta \\ \delta|t| - \delta^2/2, & |t| > \delta \end{cases}$

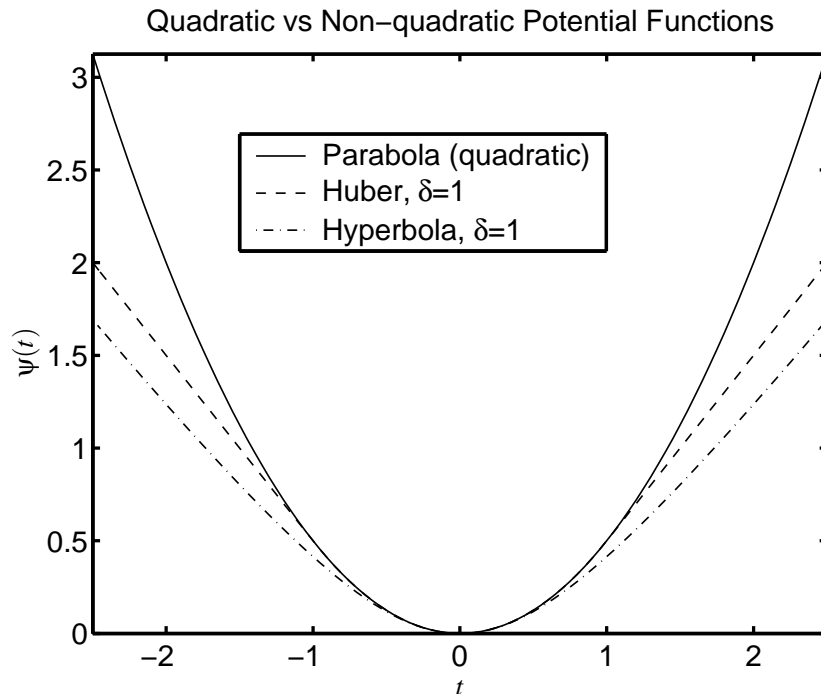
Example: Hyperbola function.  $\psi(t) \triangleq \delta^2 \left( \sqrt{1 + (t/\delta)^2} - 1 \right)$

2.34

© J. Fessler, May 12, 2008

2.34

p2reg



Lower cost for large differences  $\implies$  edge preservation

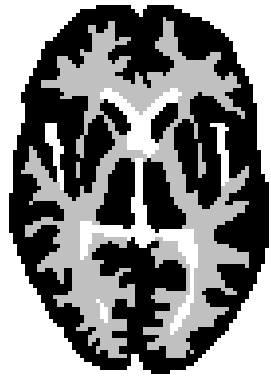
2.35

© J. Fessler, May 12, 2008

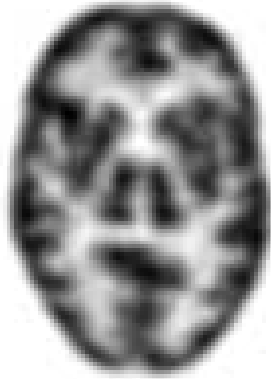
2.35

p2reg

## Edge-Preserving Reconstruction Example



Phantom



Quadratic Penalty



Huber Penalty

2.36

---

In terms of ROI quantification, a nonquadratic penalty may outperform quadratic penalties for certain types of objects (especially phantom-like piecewise smooth objects). But the benefits of nonquadratic penalties for visual tasks is largely unknown.

The smaller  $\delta$  is in the Huber penalty, the stronger the degree of edge preservation, and the more unusual the noise effects. In this case I used  $\delta = 0.4$ , for a phantom that is 0 in background, 1 in white matter, 4 in graymatter. Thus  $\delta$  is one tenth the maximum value, as has been recommended by some authors.

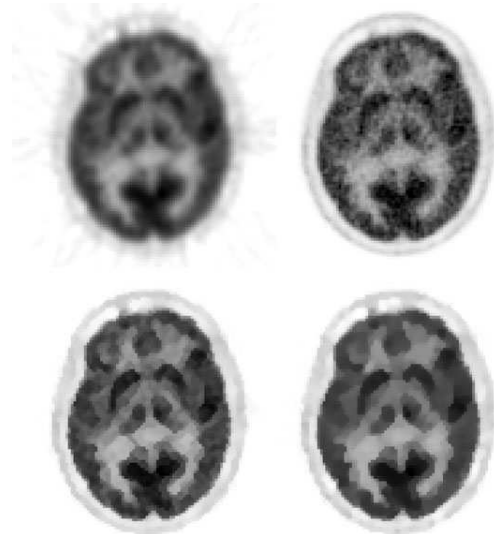
---

© J. Fessler, May 12, 2008

2.36

p2reg

## More “Edge Preserving” Regularization



Chlewicki *et al.*, PMB, Oct. 2004: “Noise reduction and convergence of Bayesian algorithms with blobs based on the Huber function and median root prior”

2.37

---

Figure taken from [129].

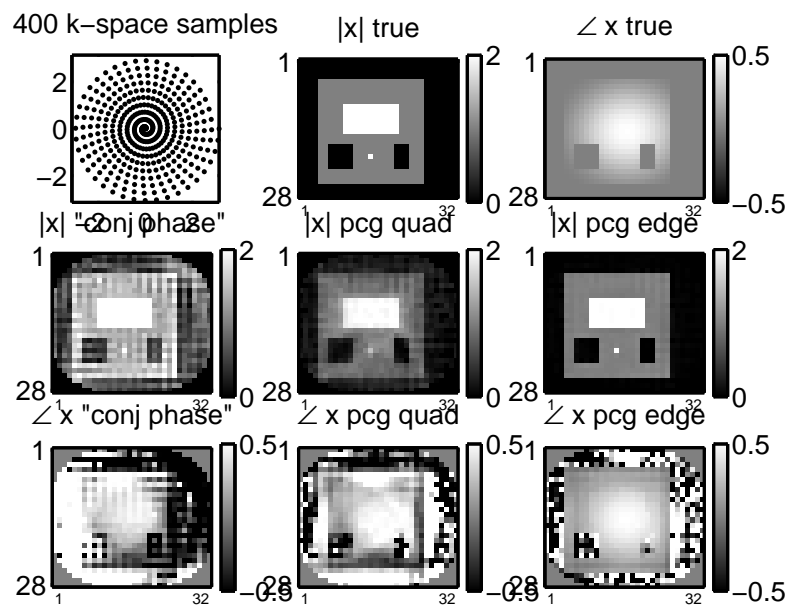
---

© J. Fessler, May 12, 2008

2.37

p2reg

# Piecewise Constant "Cartoon" Objects



2.38

© J. Fessler, May 12, 2008

2.38

p2reg

## Total Variation Regularization

Non-quadratic roughness penalty:

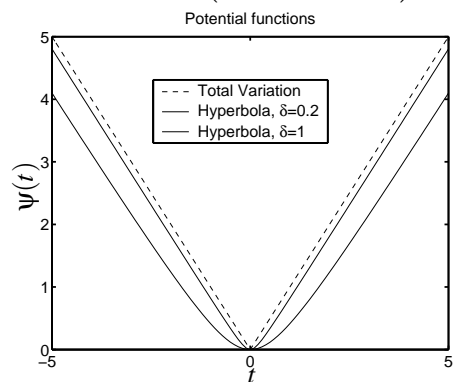
$$\int \|\nabla f(\vec{r})\| d\vec{r} \approx \sum_k \|[C\mathbf{x}]_k\|$$

Uses *magnitude* instead of *squared magnitude* of gradient.

Problem:  $|\cdot|$  is not differentiable.

Practical solution:

$$|t| \approx \delta \left( \sqrt{1 + (t/\delta)^2} - 1 \right) \quad (\text{hyperbola!})$$



2.39

To be more precise, in 2D:  $\|\nabla f(x,y)\| = \sqrt{\left|\frac{\partial f}{\partial x}\right|^2 + \left|\frac{\partial f}{\partial y}\right|^2}$  so the *total variation* is

$$\iint \|\nabla f(x,y)\| dx dy \approx \sum_n \sum_m \sqrt{|f(n,m) - f(n-1,m)|^2 + |f(n,m) - f(n,m-1)|^2}$$

Total variation in image reconstruction [130–132]. A critique [133].

© J. Fessler, May 12, 2008

2.39

p2reg

# Total Variation Example

todo: example showing blocky reconstruction with TV

2.40

© J. Fessler, May 12, 2008

2.40

p2reg

## Compressed Sensing

aka compressive sampling or sparsity regularization

Idea: find a basis  $\mathbf{B}$  for representing  $\mathbf{x}$  in terms of coefficients  $\boldsymbol{\theta}$ :  
 $\mathbf{x} = \mathbf{B}\boldsymbol{\theta}$ , where only a “small number” of  $\theta_j$  values are nonzero.

Previous cost function:  $\Psi(\mathbf{x}) = \text{DataMismatch}(\mathbf{y}, \mathbf{A}\mathbf{x}) + \beta \text{Roughness}(\mathbf{x})$

New cost function with sparsity regularization:

$$\Psi(\boldsymbol{\theta}) = \text{DataMismatch}(\mathbf{y}, \mathbf{A}\mathbf{B}\boldsymbol{\theta}) + \beta \|\boldsymbol{\theta}\|_0$$

Recall:  $\|\boldsymbol{\theta}\|_p \triangleq (\sum_j |\theta_j|^p)^{1/p}$   
 $\|\boldsymbol{\theta}\|_\infty \triangleq \lim_{p \rightarrow \infty} \|\boldsymbol{\theta}\|_p = \max_j |\theta_j|$   
 $\|\boldsymbol{\theta}\|_0 \triangleq \lim_{p \rightarrow 0} \|\boldsymbol{\theta}\|_p^p = \sum_j 1_{\{\theta_j \neq 0\}}$  (not a norm in the Banach sense)

Because  $\|\boldsymbol{\theta}\|_0$  is nonconvex, it usually is replaced with  $\|\boldsymbol{\theta}\|_1$ .  
Because  $\|\boldsymbol{\theta}\|_1$  is nondifferentiable, the corner is often rounded (hyperbola).  
If  $\mathbf{B}$  is the Harr wavelet basis, then  $\|\boldsymbol{\theta}\|_1 = \|\mathbf{B}^{-1}\mathbf{x}\|_1$  is similar to TV regularization.

For certain types of under-sampled measurements  $\mathbf{A}$ , “good” reconstructions are possible!  
Example: radial k-space sampling for Shepp-Logan.

2.41

© J. Fessler, May 12, 2008

2.41

p2reg

See [134–143].

# Penalty Functions: Convex vs Nonconvex

## Convex

- Easier to optimize
- Guaranteed unique minimizer of  $\Psi$  (for convex negative log-likelihood)

## Nonconvex

- Greater degree of edge preservation
- Nice images for piecewise-constant phantoms!
- Even more unusual noise properties
- Multiple extrema
- More complicated optimization (simulated / deterministic annealing)
- Estimator  $\hat{\mathbf{x}}$  becomes a discontinuous function of data  $\mathbf{Y}$

## Nonconvex examples

- “broken parabola”

$$\psi(t) = \min(t^2, t_{\max}^2)$$

- true median root prior:

$$R(\mathbf{x}) = \sum_{j=1}^{n_p} \frac{(x_j - \text{median}_j(\mathbf{x}))^2}{\text{median}_j(\mathbf{x})} \text{ where } \text{median}_j(\mathbf{x}) \text{ is local median}$$

Exception: orthonormal wavelet threshold *denoising* via nonconvex potentials!

The above form is not exactly what has been called the median root prior by Alenius *et al.* [128]. They have used  $\text{median}_j(\mathbf{x}^{(n)})$  which is not a true prior since it depends on the previous iteration. Hsiao, Rangarajan, and Ginda have developed a very interesting prior that is similar to the “medial root prior” but is convex [144].

For nice analysis of nonconvex problems, see the papers by Mila Nikolova [145].

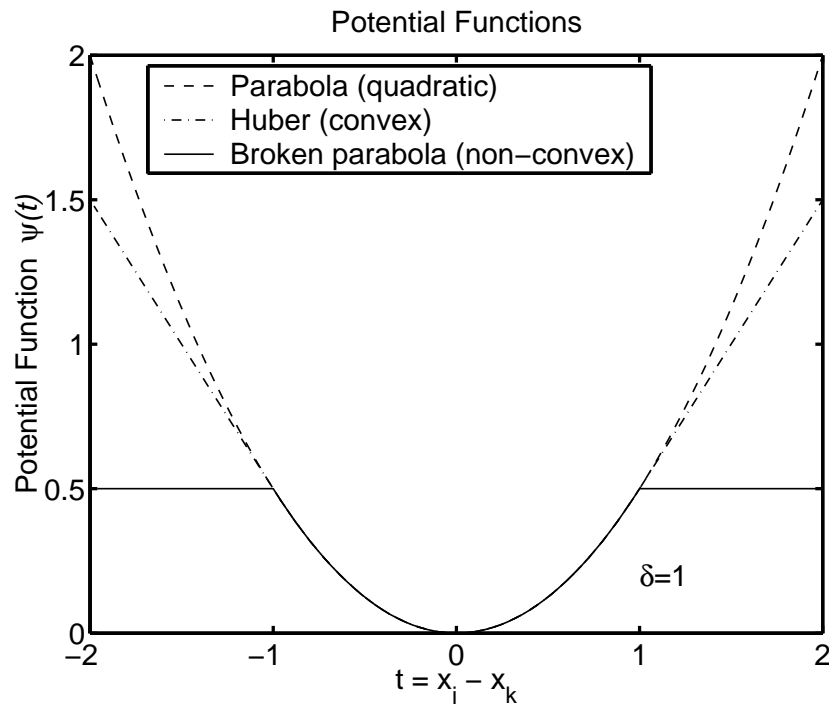
For orthonormal wavelet denoising, the cost functions [146] usually have the form

$$\Psi(\mathbf{x}) = \|\mathbf{y} - \mathbf{A}\mathbf{x}\|^2 + \sum_{j=1}^{n_p} \psi(x_j)$$

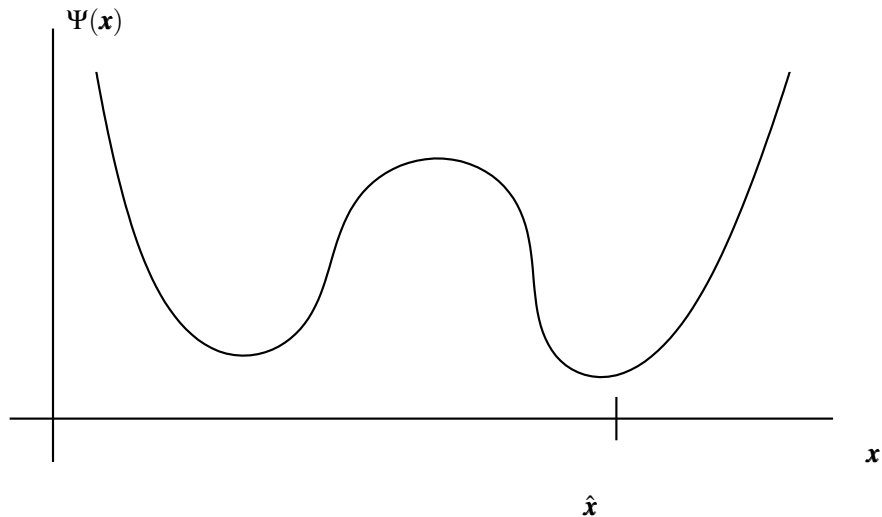
where  $\mathbf{A}$  is an orthonormal. When  $\mathbf{A}$  is orthonormal we can write:  $\|\mathbf{y} - \mathbf{A}\mathbf{x}\|^2 = \|\mathbf{A}'\mathbf{y} - \mathbf{x}\|^2$ , so

$$\Psi(\mathbf{x}) = \sum_{j=1}^{n_p} (x_j - [\mathbf{A}'\mathbf{y}]_j)^2 + \psi(x_j)$$

which separates completely into  $n_p$  1-D minimization problems, each of which has a *unique* minimizer for all useful potential functions.



# Local Extrema and Discontinuous Estimators



Small change in data  $\implies$  large change in minimizer  $\hat{x}$ .  
Using convex penalty functions obviates this problem.

2.44

## Augmented Regularization Functions

Replace roughness penalty  $R(\mathbf{x})$  with  $R(\mathbf{x}|\mathbf{b}) + \alpha R(\mathbf{b})$ ,  
where the elements of  $\mathbf{b}$  (often binary) indicate boundary locations.

- Line-site methods
- Level-set methods

Joint estimation problem:

$$(\hat{\mathbf{x}}, \hat{\mathbf{b}}) = \arg \min_{\mathbf{x}, \mathbf{b}} \Psi(\mathbf{x}, \mathbf{b}), \quad \Psi(\mathbf{x}, \mathbf{b}) = \mathcal{L}(\mathbf{x}; \mathbf{y}) + \beta R(\mathbf{x}|\mathbf{b}) + \alpha R(\mathbf{b}).$$

Example:  $b_{jk}$  indicates the presence of edge between pixels  $j$  and  $k$ :

$$R(\mathbf{x}|\mathbf{b}) = \sum_{j=1}^{n_p} \sum_{k \in \mathcal{N}_j} (1 - b_{jk}) \frac{1}{2} (x_j - x_k)^2$$

Penalty to discourage too many edges (e.g.):

$$R(\mathbf{b}) = \sum_{jk} b_{jk}.$$

- Can encourage local edge continuity
- May require annealing methods for minimization

2.45

[103] discuss discontinuity

© J. Fessler, May 12, 2008

2.44

p2reg

Line-site methods: [123–126].  
Level-set methods: [147–149].

For the simple *non-interacting* line-site penalty function  $R(\mathbf{b})$  given above, one can perform the minimization over  $\mathbf{b}$  analytically, yielding an equivalent regularization method of the form  $R(\mathbf{x})$  with a broken parabola potential function [150].

More sophisticated line-site methods use neighborhoods of line-site variables to encourage local boundary continuity [123–126].

The convex median prior of Hsiao *et al.* uses augmented regularization but does not require annealing [144].

© J. Fessler, May 12, 2008

2.45

p2reg

## Modified Penalty Functions

$$R(\mathbf{x}) = \sum_{j=1}^{n_p} \frac{1}{2} \sum_{k \in \mathcal{N}_j} w_{jk} \Psi(x_j - x_k)$$

Adjust weights  $\{w_{jk}\}$  to

- Control resolution properties
- Incorporate anatomical side information (MR/CT)  
(avoid smoothing across anatomical boundaries)

### Recommendations

- Emission tomography:
  - Begin with quadratic (nonseparable) penalty functions
  - Consider modified penalty for resolution control and choice of  $\beta$
  - Use modest regularization and post-filter more if desired
- Transmission tomography (attenuation maps), X-ray CT
  - consider convex nonquadratic (e.g., Huber) penalty functions
  - choose  $\delta$  based on attenuation map units (water, bone, etc.)
  - choice of regularization parameter  $\beta$  remains nontrivial,  
learn appropriate values by experience for given study type

2.46

---

Resolution properties [38, 151–153].

Side information (a very incomplete list) [154–165].

---

## Choice 4.3: Constraints

- Nonnegativity
- Known support
- Count preserving
- Upper bounds on values  
e.g., maximum  $\mu$  of attenuation map in transmission case

### Considerations

- Algorithm complexity
- Computation
- Convergence rate
- Bias (in low-count regions)
- ...

2.47

© J. Fessler, May 12, 2008

2.46

p2reg

---

Sometimes it is stated that the ML-EM algorithm “preserves counts.” This only holds when  $r_i = 0$  in the statistical model. The count-preserving property originates from the likelihood, not the algorithm. The ML estimate, under the Poisson model, happens to preserve counts. It is fine that ML-EM does so every iteration, but that does not mean that it is superior to other algorithms that get to the optimum  $\hat{\mathbf{x}}$  faster without necessarily preserving counts along the way.

I do not recommend artificially renormalizing each iteration to try to “preserve counts.”

---

© J. Fessler, May 12, 2008

2.47

p2reg



## Open Problems

- Performance prediction for nonquadratic regularization
- Effect of nonquadratic regularization on detection tasks
- Choice of regularization parameters for nonquadratic regularization

---

Deadtime statistics are analyzed in [166, 167]. Bottom line: in most SPECT and PET systems with paralyzable deadtime, the measurements are non-Poisson, but the mean and variance are nearly identical. So presumably the Poisson statistical model is adequate, provided the deadtime losses are included in the system matrix  $\mathbf{A}$ .

Some of these types of questions are being addressed, *e.g.*, effects of sensitivity map errors (a type of system model mismatch) in list-mode reconstruction [168]. Qi's bound on system model error relative to data error: [169].

---

2.48

© J. Fessler, May 12, 2008

2.48

p2reg

## Summary

- 1. Object parameterization: function  $f(\vec{r})$  vs vector  $\mathbf{x}$
- 2. System physical model:  $s_i(\vec{r})$
- 3. Measurement statistical model  $Y_i \sim \boxed{?}$
- 4. Cost function: data-mismatch / regularization / constraints

**Reconstruction Method  $\triangleq$  Cost Function + Algorithm**

Naming convention: “criterion”-“algorithm”:

- ML-EM, MAP-OSL, PL-SAGE, PWLS+SOR, PWLS-CG, ...

2.49

© J. Fessler, May 12, 2008

2.49

p2reg

## Part 3. Algorithms

Method = Cost Function + Algorithm

### Outline

- Ideal algorithm
- Classical general-purpose algorithms
- Considerations:
  - nonnegativity
  - parallelization
  - convergence rate
  - monotonicity
- Algorithms tailored to cost functions for imaging
  - Optimization transfer
  - EM-type methods
  - Poisson emission problem
  - Poisson transmission problem
- Ordered-subsets / block-iterative algorithms
  - Recent convergent versions (relaxation, incrementalism)

3.1

### Why iterative algorithms?

- For nonquadratic  $\Psi$ , no closed-form solution for minimizer.
- For quadratic  $\Psi$  with nonnegativity constraints, no closed-form solution.
- For quadratic  $\Psi$  without constraints, closed-form solutions:

$$\text{PWLS: } \hat{\mathbf{x}} = \arg \min_x \|\mathbf{y} - \mathbf{Ax}\|_{\mathbf{W}^{1/2}}^2 + \mathbf{x}'\mathbf{Rx} = [\mathbf{A}'\mathbf{WA} + \mathbf{R}]^{-1}\mathbf{A}'\mathbf{Wy}$$

$$\text{OLS: } \hat{\mathbf{x}} = \arg \min_x \|\mathbf{y} - \mathbf{Ax}\|^2 = [\mathbf{A}'\mathbf{A}]^{-1}\mathbf{A}'\mathbf{y}$$

Impractical (memory and computation) for realistic problem sizes.  
 $\mathbf{A}$  is sparse, but  $\mathbf{A}'\mathbf{A}$  is not.

All algorithms are imperfect. No single best solution.

3.2

---

Choosing a cost function is an important part of imaging science.

Choosing an algorithm should be mostly a matter of computer science (numerical methods).

Nevertheless, it gets a lot of attention by imaging scientists since our cost functions have forms that can be exploited to get faster convergence than general-purpose methods.

---

© J. Fessler, May 12, 2008

3.1

p3alg

---

Singular value decomposition (SVD) techniques have been proposed for the OLS cost function as a method for reducing the computation problem, e.g., [170–179].

The idea is that one could precompute the pseudo-inverse of  $\mathbf{A}$  “once and for all.” However  $\mathbf{A}$  includes physical effects like attenuation, which change for every patient. And for data-weighted least squares,  $\mathbf{W}$  changes for each scan too.

Image reconstruction never requires the matrix inverse  $[\mathbf{A}'\mathbf{A}]^{-1}$ ; all that is required is a solution to the normal equations  $[\mathbf{A}'\mathbf{A}]\hat{\mathbf{x}} = \mathbf{A}'\mathbf{y}$  which is easier, but still nontrivial.

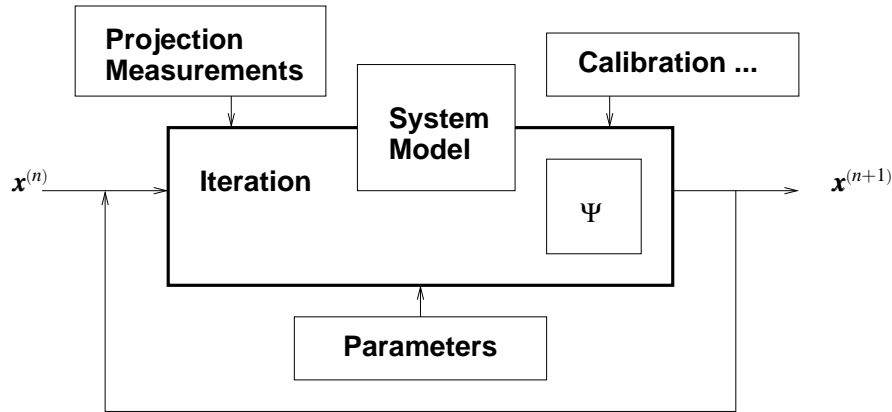
---

© J. Fessler, May 12, 2008

3.2

p3alg

## General Iteration



Deterministic iterative mapping:  $\mathbf{x}^{(n+1)} = \mathcal{M}(\mathbf{x}^{(n)})$

3.3

© J. Fessler, May 12, 2008

3.3

p3alg

## Ideal Algorithm

$$\mathbf{x}^* \triangleq \arg \min_{\mathbf{x} \geq 0} \Psi(\mathbf{x}) \quad (\text{global minimizer})$$

### Properties

stable and convergent  
converges quickly  
globally convergent  
fast  
robust  
user friendly

$\{\mathbf{x}^{(n)}\}$  converges to  $\mathbf{x}^*$  if run indefinitely  
 $\{\mathbf{x}^{(n)}\}$  gets “close” to  $\mathbf{x}^*$  in just a few iterations  
 $\lim_n \mathbf{x}^{(n)}$  independent of starting image  $\mathbf{x}^{(0)}$   
requires minimal computation per iteration  
insensitive to finite numerical precision  
nothing to adjust (e.g., acceleration factors)

parallelizable  
simple  
flexible  
(matrix stored by row or column, or factored, or projector/backprojector)

(when necessary)  
easy to program and debug  
accommodates any type of system model

Choices: forgo one or more of the above

3.4

© J. Fessler, May 12, 2008

3.4

p3alg

There are also stochastic iterative algorithms, such as simulated annealing [123] and the stochastic EM algorithm [180].

One might argue that the “ideal algorithm” would be the algorithm that produces  $\mathbf{x}^{\text{true}}$ . In the framework presented here, it is the job of the cost function to try to make  $\mathbf{x}^* \approx \mathbf{x}^{\text{true}}$ , and the job of the algorithm to find  $\mathbf{x}^*$  by minimizing  $\Psi$ .

In fact, *nothing* in the above list really has to do with image quality. In the statistical framework, image quality is determined by  $\Psi$ , not by the algorithm.

Note on terminology: “algorithms” do not really converge, it is the *sequence* of estimates  $\{\mathbf{x}^{(n)}\}$  that converges, but everyone abuses this all the time, so I will too.

# Classic Algorithms

## Non-gradient based

- Exhaustive search
- Nelder-Mead simplex (amoeba)

Converge very slowly, but work with nondifferentiable cost functions.

## Gradient based

- Gradient descent

$$\mathbf{x}^{(n+1)} \triangleq \mathbf{x}^{(n)} - \alpha \nabla \Psi(\mathbf{x}^{(n)})$$

Choosing  $\alpha$  to ensure convergence is nontrivial.

- Steepest descent

$$\mathbf{x}^{(n+1)} \triangleq \mathbf{x}^{(n)} - \alpha_n \nabla \Psi(\mathbf{x}^{(n)}) \quad \text{where } \alpha_n \triangleq \arg \min_{\alpha} \Psi(\mathbf{x}^{(n)} - \alpha \nabla \Psi(\mathbf{x}^{(n)}))$$

Computing stepsize  $\alpha_n$  can be expensive or inconvenient.

## Limitations

- Converge slowly.
- Do not easily accommodate nonnegativity constraint.

3.5

## Gradients & Nonnegativity - A Mixed Blessing

**Unconstrained optimization** of differentiable cost functions:

$$\nabla \Psi(\mathbf{x}) = \mathbf{0} \quad \text{when } \mathbf{x} = \mathbf{x}^*$$

- A necessary condition always.
- A sufficient condition for strictly convex cost functions.
- Iterations search for zero of gradient.

**Nonnegativity-constrained minimization:**

Karush-Kuhn-Tucker conditions

$$\left. \frac{\partial}{\partial x_j} \Psi(\mathbf{x}) \right|_{\mathbf{x}=\mathbf{x}^*} \quad \text{is} \quad \begin{cases} = 0, & x_j^* > 0 \\ \geq 0, & x_j^* = 0 \end{cases}$$

- A necessary condition always.
- A sufficient condition for strictly convex cost functions.
- Iterations search for ???
- $0 = x_j^* \frac{\partial}{\partial x_j} \Psi(\mathbf{x}^*)$  is a necessary condition, but never sufficient condition.

3.6

---

Nice discussion of optimization algorithms in [181].

Row and column gradients:

$$\nabla \Psi(\mathbf{x}) = \left[ \frac{\partial}{\partial x_1} \Psi, \frac{\partial}{\partial x_2} \Psi, \dots, \frac{\partial}{\partial x_{n_p}} \Psi \right], \quad \nabla = \nabla'$$

Using gradients excludes nondifferentiable penalty functions such as the Laplacian prior which involves  $|x_j - x_k|$ . See [182–184] for solutions to this problem.

---

© J. Fessler, May 12, 2008

3.5

p3alg

---



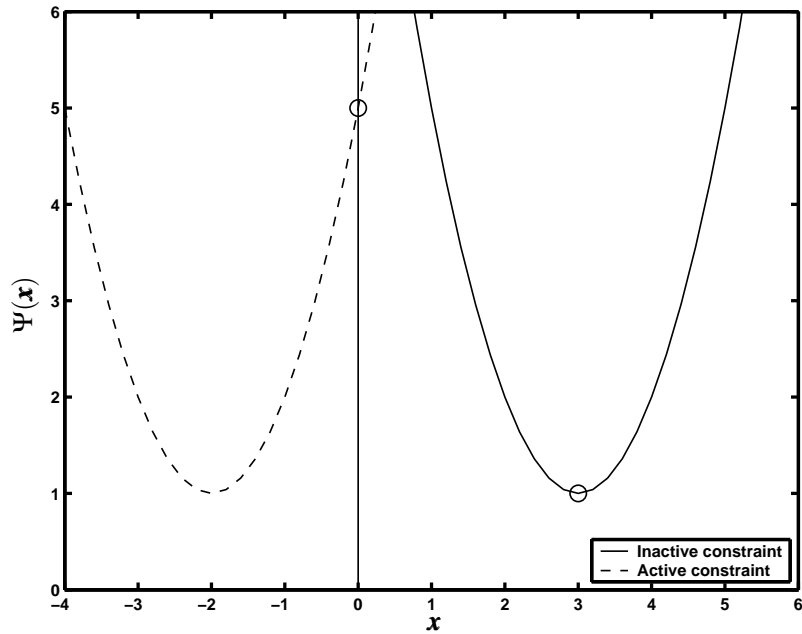
---

© J. Fessler, May 12, 2008

3.6

p3alg

# Karush-Kuhn-Tucker Illustrated



3.7

The usual condition  $\frac{\partial}{\partial x_j} \Psi(\mathbf{x}) = 0$  only applies for pixels where the nonnegativity constraint is inactive.

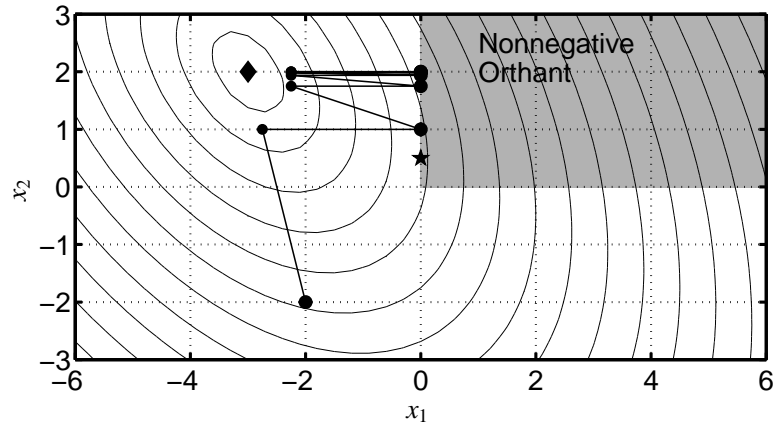
© J. Fessler, May 12, 2008

3.7

p3alg

## Why Not Clip Negatives?

WLS with Clipped Newton-Raphson



Newton-Raphson with negatives set to zero each iteration.  
Fixed-point of iteration is not the constrained minimizer!

3.8

By clipped negatives, I mean you start with some nominal algorithm  $\mathcal{M}_0(\mathbf{x})$  and modify it to be:  $\mathbf{x}^{(n+1)} = \mathcal{M}(\mathbf{x}^{(n)})$  where  $\mathcal{M}(\mathbf{x}) = [\mathcal{M}_0(\mathbf{x})]_+$  and the  $j$ th element of  $[\mathbf{x}]_+$  is  $x_j$  if  $x_j > 0$  or 0 if  $x_j \leq 0$ . Basically, you run your favorite iteration and then set any negatives to zero before proceeding to the next iteration.

Simple 2D quadratic problem. Curves show contours of equal value of the cost function  $\Psi$ .

Same problem arises with upper bounds too.

The above problem applies to many simultaneous update iterative methods. For sequential update methods, such as coordinate descent, clipping works fine.

There are some simultaneous update iterative methods where it will work though; projected gradient descent with a positive-definite diagonal preconditioner, for example.

© J. Fessler, May 12, 2008

3.8

p3alg

## Newton-Raphson Algorithm

$$\mathbf{x}^{(n+1)} = \mathbf{x}^{(n)} - [\nabla^2 \Psi(\mathbf{x}^{(n)})]^{-1} \nabla \Psi(\mathbf{x}^{(n)})$$

### Advantage:

- Super-linear convergence rate (if convergent)

### Disadvantages:

- Requires twice-differentiable  $\Psi$
- Not guaranteed to converge
- Not guaranteed to monotonically decrease  $\Psi$
- Does not enforce nonnegativity constraint
- Computing Hessian  $\nabla^2 \Psi$  often expensive
- Impractical for image recovery due to matrix inverse

General purpose remedy: bound-constrained Quasi-Newton algorithms

3.9

## Newton's Quadratic Approximation

2nd-order Taylor series:

$$\Psi(\mathbf{x}) \approx \phi(\mathbf{x}; \mathbf{x}^{(n)}) \triangleq \Psi(\mathbf{x}^{(n)}) + \nabla \Psi(\mathbf{x}^{(n)}) (\mathbf{x} - \mathbf{x}^{(n)}) + \frac{1}{2} (\mathbf{x} - \mathbf{x}^{(n)})^T \nabla^2 \Psi(\mathbf{x}^{(n)}) (\mathbf{x} - \mathbf{x}^{(n)})$$

Set  $\mathbf{x}^{(n+1)}$  to the ("easily" found) minimizer of this quadratic approximation:

$$\begin{aligned} \mathbf{x}^{(n+1)} &\triangleq \arg \min_{\mathbf{x}} \phi(\mathbf{x}; \mathbf{x}^{(n)}) \\ &= \mathbf{x}^{(n)} - [\nabla^2 \Psi(\mathbf{x}^{(n)})]^{-1} \nabla \Psi(\mathbf{x}^{(n)}) \end{aligned}$$

Can be nonmonotone for Poisson emission tomography log-likelihood, even for a single pixel and single ray:

$$\Psi(x) = (x + r) - y \log(x + r).$$

3.10

---

$\nabla^2 \Psi(\mathbf{x})$  is called the *Hessian matrix*. It is a  $n_p \times n_p$  matrix (where  $n_p$  is the dimension of  $\mathbf{x}$ ). The  $j, k$ th element of it is  $\frac{\partial^2}{\partial x_j \partial x_k} \Psi(\mathbf{x})$ .

A "matrix inverse" actually is not necessary. One can rewrite the above iteration as  $\mathbf{x}^{(n+1)} = \mathbf{x}^{(n)} - \mathbf{d}^{(n)}$  where  $\mathbf{d}^{(n)}$  is the solution to the system of equations:  $\nabla^2 \Psi(\mathbf{x}^{(n)}) \mathbf{d}^{(n)} = \nabla \Psi(\mathbf{x}^{(n)})$ . Unfortunately, this is a non-sparse  $n_p \times n_p$  system of equations, requiring  $O(n_p^3)$  flops to solve, which is expensive. Instead of solving the system exactly one could use approximate iterative techniques, but then it should probably be considered a preconditioned gradient method rather than Newton-Raphson.

Quasi-Newton algorithms [185–188] [189, p. 136] [190, p. 77] [191, p. 63].

bound-constrained Quasi-Newton algorithms (LBFGS) [187, 192–195].

---

© J. Fessler, May 12, 2008

3.9

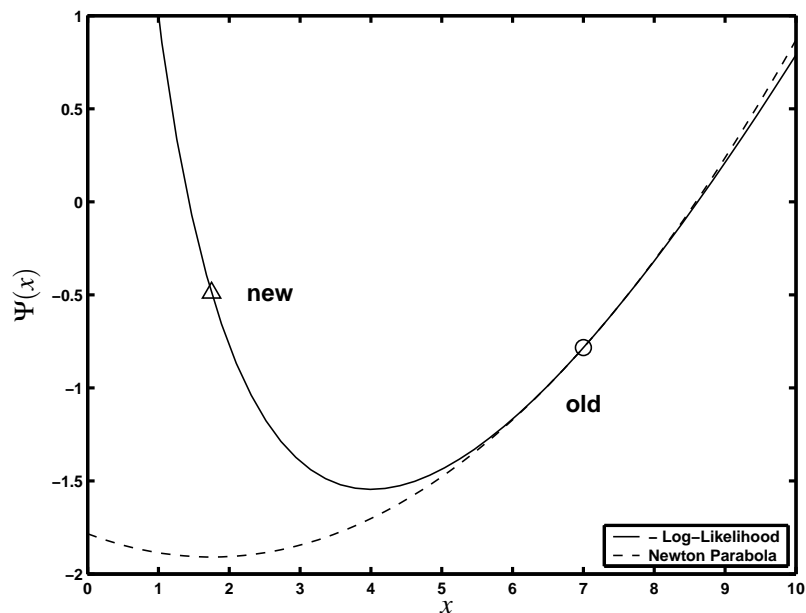
p3alg

© J. Fessler, May 12, 2008

3.10

p3alg

## Nonmonotonicity of Newton-Raphson



3.11

© J. Fessler, May 12, 2008

3.11

p3alg

## Consideration: Monotonicity

An algorithm is monotonic if

$$\Psi(\mathbf{x}^{(n+1)}) \leq \Psi(\mathbf{x}^{(n)}), \quad \forall \mathbf{x}^{(n)}.$$

Three categories of algorithms:

- Nonmonotonic (or unknown)
- Forced monotonic (e.g., by line search)
- Intrinsically monotonic (by design, simplest to implement)

### Forced monotonicity

Most nonmonotonic algorithms can be converted to forced monotonic algorithms by adding a line-search step:

$$\mathbf{x}^{\text{temp}} \triangleq \mathcal{M}(\mathbf{x}^{(n)}), \quad \mathbf{d} = \mathbf{x}^{\text{temp}} - \mathbf{x}^{(n)}$$

$$\mathbf{x}^{(n+1)} \triangleq \mathbf{x}^{(n)} - \alpha_n \mathbf{d}^{(n)} \quad \text{where} \quad \alpha_n \triangleq \arg \min_{\alpha} \Psi(\mathbf{x}^{(n)} - \alpha \mathbf{d}^{(n)})$$

Inconvenient, sometimes expensive, nonnegativity problematic.

3.12

© J. Fessler, May 12, 2008

3.12

p3alg

Although monotonicity is not a necessary condition for an algorithm to converge globally to  $\mathbf{x}^*$ , it is often the case that global convergence and monotonicity go hand in hand. In fact, for strictly convex  $\Psi$ , algorithms that monotonically decrease  $\Psi$  each iteration are guaranteed to converge under reasonable regularity conditions [196].

Any algorithm containing a line search step will have difficulties with nonnegativity. In principle one can address these problems using a “bent-line” search [197], but this can add considerable computation per iteration.

# Conjugate Gradient (CG) Algorithm

## Advantages:

- Fast converging (if suitably preconditioned) (in unconstrained case)
- Monotonic (forced by line search in nonquadratic case)
- Global convergence (unconstrained case)
- Flexible use of system matrix  $A$  and tricks
- Easy to implement in unconstrained quadratic case
- Highly parallelizable

## Disadvantages:

- Nonnegativity constraint awkward (slows convergence?)
- Line-search somewhat awkward in nonquadratic cases
- Possible need to “restart” after many iterations

Highly recommended for unconstrained quadratic problems (e.g., PWLS without nonnegativity). Useful (but perhaps not ideal) for Poisson case too.

3.13

## Consideration: Parallelization

### Simultaneous (fully parallelizable)

update all pixels simultaneously using all data  
EM, Conjugate gradient, ISRA, OSL, SIRT, MART, ...

### Block iterative (ordered subsets)

update (nearly) all pixels using one subset of the data at a time  
OSEM, RBBI, ...

### Row action

update many pixels using a single ray at a time  
ART, RAMLA

### Pixel grouped (multiple column action)

update some (but not all) pixels simultaneously a time, using all data  
Grouped coordinate descent, multi-pixel SAGE  
(Perhaps the most nontrivial to implement)

### Sequential (column action)

update one pixel at a time, using all (relevant) data  
Coordinate descent, SAGE

3.14

---

CG is like steepest descent, but the search direction is modified each iteration to be conjugate to the previous search direction.

Preconditioners [198, 199]

Poisson case [93, 200, 201].

Efficient line-search for (nonquadratic) edge-preserving regularization described in [199].

---

© J. Fessler, May 12, 2008

3.13

p3alg

---

Sequential algorithms are the least parallelizable since one cannot update the second pixel until the first pixel has been updated (to preserve monotonicity and convergence properties).

SAGE [202, 203]  
Grouped coordinate descent [204]  
Multi-pixel SAGE [205]  
RAMLA [206]  
OSEM [28]  
RBBI [207–209]  
ISRA [210–212]  
OSL [213, 214]

---

© J. Fessler, May 12, 2008

3.14

p3alg



# Coordinate Descent Algorithm

aka Gauss-Siedel, successive over-relaxation (SOR), iterated conditional modes (ICM)

Update one pixel at a time, holding others fixed to their most recent values:

$$x_j^{\text{new}} = \arg \min_{x_j \geq 0} \Psi(x_1^{\text{new}}, \dots, x_{j-1}^{\text{new}}, x_j, x_{j+1}^{\text{old}}, \dots, x_{n_p}^{\text{old}}), \quad j = 1, \dots, n_p$$

## Advantages:

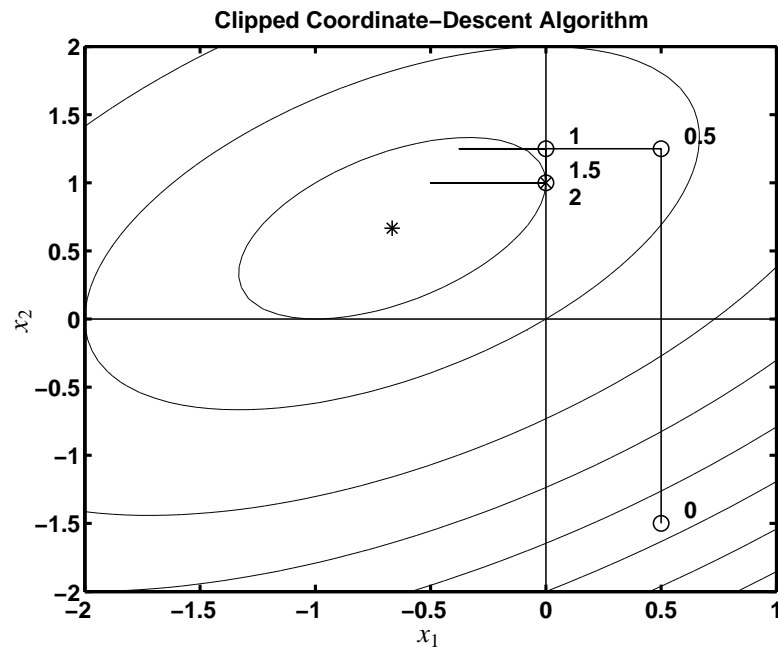
- Intrinsically monotonic
- Fast converging (from good initial image)
- Global convergence
- Nonnegativity constraint trivial

## Disadvantages:

- Requires column access of system matrix  $A$
- Cannot exploit some “tricks” for  $A$ , e.g., factorizations
- Expensive “arg min” for nonquadratic problems
- Poorly parallelizable

3.15

## Constrained Coordinate Descent Illustrated



3.16

Fast convergence shown by Sauer and Bouman with clever frequency-domain analysis [215].

Any ordering can be used. Convergence rate may vary with ordering.

Global convergence even with negatives clipped [216].

One can replace the “arg min” with a one-dimensional Newton-Raphson step [204, 217–219]. However, this change then loses the guarantee of monotonicity for nonquadratic  $\Psi$ . Also, evaluating the second partial derivatives of  $\Psi$  with respect to  $x_j$  is expensive (costs an extra modified backprojection per iteration) [204].

The paraboloidal surrogates coordinate descent (PSCD) algorithm circumvents these problems [220].

© J. Fessler, May 12, 2008

3.15

p3alg

In this particular case, the nonnegativity constraint led to exact convergence in 1.5 iterations.

© J. Fessler, May 12, 2008

3.16

p3alg

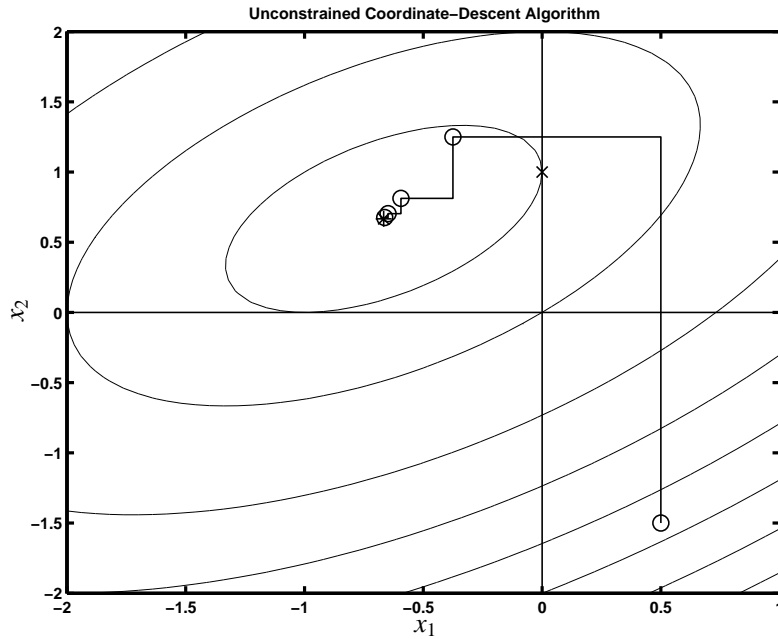
# Coordinate Descent - Unconstrained

---

In general coordinate descent converges at a linear rate [86, 215].

Interestingly, for this particular problem the nonnegativity constraint accelerated convergence.

---



3.17

© J. Fessler, May 12, 2008

3.17

p3alg

## Coordinate-Descent Algorithm Summary

Recommended when all of the following apply:

- quadratic or nearly-quadratic convex cost function
- nonnegativity constraint desired
- precomputed and stored system matrix  $\mathbf{A}$  with column access
- parallelization not needed (standard workstation)

Cautions:

- Good initialization (e.g., properly scaled FBP) essential.  
(Uniform image or zero image cause slow initial convergence.)
- Must be programmed carefully to be efficient.  
(Standard Gauss-Siedel implementation is suboptimal.)
- Updates high-frequencies fastest  $\implies$  poorly suited to unregularized case

Used daily in UM clinic for 2D SPECT / PWLS / nonuniform attenuation

Under investigation for 3D helical CT reconstruction by Thibault *et al.*

---

In saying “not good for the unregularized case” I am assuming one does not really wish to find the minimizer of  $\Psi$  in that case. If you really want the minimizer of  $\Psi$  in the unregularized case, then coordinate descent may still be useful.

CD in practice: [221–223].

---

3.18

© J. Fessler, May 12, 2008

3.18

p3alg

# Summary of General-Purpose Algorithms

## Gradient-based

- Fully parallelizable
- Inconvenient line-searches for nonquadratic cost functions
- Fast converging in unconstrained case
- Nonnegativity constraint inconvenient

## Coordinate-descent

- Very fast converging
- Nonnegativity constraint trivial
- Poorly parallelizable
- Requires precomputed/stored system matrix

CD is well-suited to moderate-sized 2D problem (e.g., 2D PET), but challenging for large 2D problems (X-ray CT) and fully 3D problems

Neither is ideal.

∴ need *special-purpose algorithms* for image reconstruction!

3.19

---

Interior-point methods for general-purpose constrained optimization have recently been applied to image reconstruction [224] and deserve further examination.

---

## Data-Mismatch Functions Revisited

For fast converging, intrinsically monotone algorithms, consider the form of  $\Psi$ .

**WLS:**

$$\ell(\mathbf{x}) = \sum_{i=1}^{n_d} \frac{1}{2} w_i (y_i - [\mathbf{Ax}]_i)^2 = \sum_{i=1}^{n_d} h_i([\mathbf{Ax}]_i), \quad \text{where } h_i(l) \triangleq \frac{1}{2} w_i (y_i - l)^2.$$

**Emission Poisson (negative) log-likelihood:**

$$\ell(\mathbf{x}) = \sum_{i=1}^{n_d} ([\mathbf{Ax}]_i + r_i) - y_i \log([\mathbf{Ax}]_i + r_i) = \sum_{i=1}^{n_d} h_i([\mathbf{Ax}]_i)$$

where  $h_i(l) \triangleq (l + r_i) - y_i \log(l + r_i)$ .

**Transmission Poisson log-likelihood:**

$$\ell(\mathbf{x}) = \sum_{i=1}^{n_d} (b_i e^{-[\mathbf{Ax}]_i} + r_i) - y_i \log(b_i e^{-[\mathbf{Ax}]_i} + r_i) = \sum_{i=1}^{n_d} h_i([\mathbf{Ax}]_i)$$

where  $h_i(l) \triangleq (b_i e^{-l} + r_i) - y_i \log(b_i e^{-l} + r_i)$ .

MRI, polyenergetic X-ray CT, confocal microscopy, image restoration, ...  
All have same *partially separable* form.

3.20

© J. Fessler, May 12, 2008

3.19

p3alg

---

All the algorithms discussed this far are generic; they can be applied to any differentiable  $\Psi$ .

---

© J. Fessler, May 12, 2008

3.20

p3x

# General Imaging Cost Function

General form for data-mismatch function:

$$\ell(\mathbf{x}) = \sum_{i=1}^{n_d} h_i([\mathbf{A}\mathbf{x}]_i)$$

General form for regularizing penalty function:

$$R(\mathbf{x}) = \sum_k \psi_k([\mathbf{C}\mathbf{x}]_k)$$

General form for cost function:

$$\Psi(\mathbf{x}) = \ell(\mathbf{x}) + \beta R(\mathbf{x}) = \sum_{i=1}^{n_d} h_i([\mathbf{A}\mathbf{x}]_i) + \beta \sum_k \psi_k([\mathbf{C}\mathbf{x}]_k)$$

Properties of  $\Psi$  we can exploit:

- summation form (due to independence of measurements)
- convexity of  $h_i$  functions (usually)
- summation argument (inner product of  $\mathbf{x}$  with  $i$ th row of  $\mathbf{A}$ )

Most methods that use these properties are forms of *optimization transfer*.

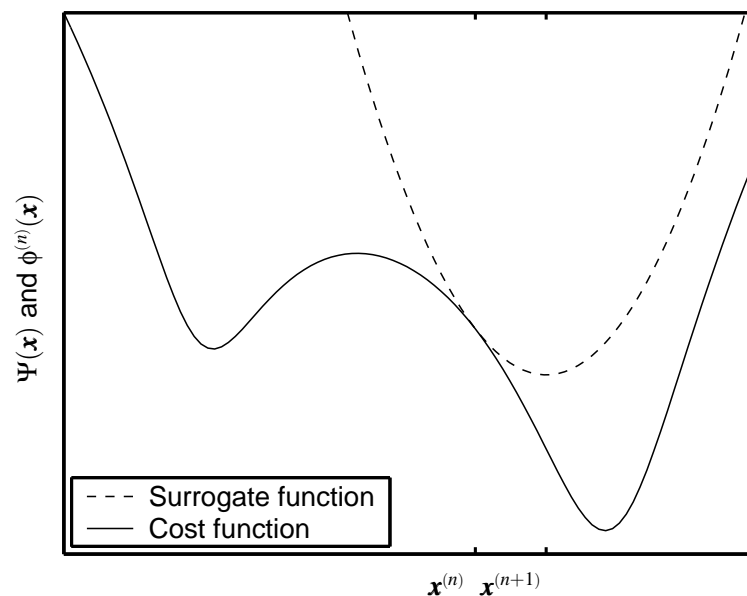
3.21

© J. Fessler, May 12, 2008

3.21

p3x

## Optimization Transfer Illustrated



3.22

© J. Fessler, May 12, 2008

3.22

p3x

This figure does not do justice to the problem. A one-dimensional  $\Psi$  is usually easy to minimize. The problem is in multiple dimensions.

## Optimization Transfer

General iteration:

$$\mathbf{x}^{(n+1)} = \arg \min_{\mathbf{x} \geq \mathbf{0}} \phi(\mathbf{x}; \mathbf{x}^{(n)})$$

Monotonicity conditions (cost function  $\Psi$  decreases provided these hold):

- $\phi(\mathbf{x}^{(n)}; \mathbf{x}^{(n)}) = \Psi(\mathbf{x}^{(n)})$  (matched current value)
- $\nabla_{\mathbf{x}} \phi(\mathbf{x}; \mathbf{x}^{(n)}) \Big|_{\mathbf{x}=\mathbf{x}^{(n)}} = \nabla \Psi(\mathbf{x}) \Big|_{\mathbf{x}=\mathbf{x}^{(n)}}$  (matched gradient)
- $\phi(\mathbf{x}; \mathbf{x}^{(n)}) \geq \Psi(\mathbf{x}) \quad \forall \mathbf{x} \geq \mathbf{0}$  (lies above)

These 3 (sufficient) conditions are satisfied by the  $Q$  function of the EM algorithm (and its relatives like SAGE).

The 3rd condition is *not* satisfied by the Newton-Raphson quadratic approximation, which leads to its nonmonotonicity.

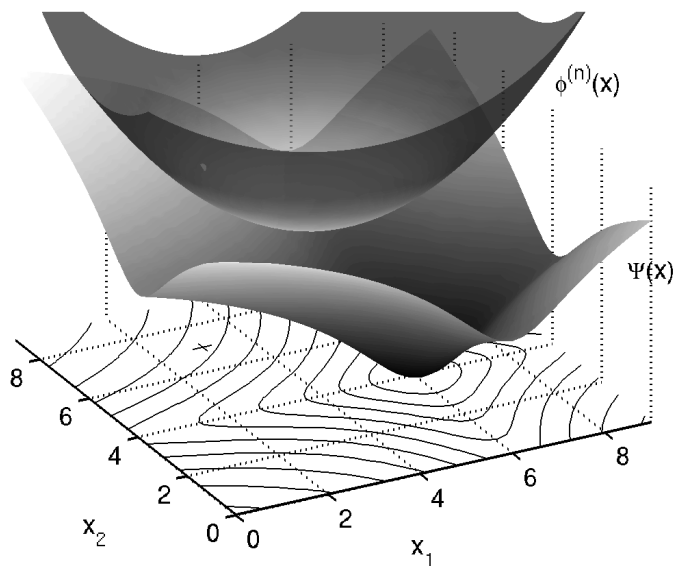
3.23

© J. Fessler, May 12, 2008

3.23

p3x

## Optimization Transfer in 2d



3.24

© J. Fessler, May 12, 2008

3.24

p3x

# Optimization Transfer of EM Algorithm

E-step: choose surrogate function  $\phi(\mathbf{x}; \mathbf{x}^{(n)})$

M-step: minimize surrogate function

$$\mathbf{x}^{(n+1)} = \arg \min_{\mathbf{x} \geq \mathbf{0}} \phi(\mathbf{x}; \mathbf{x}^{(n)})$$

Designing surrogate functions

- Easy to “compute”
- Easy to minimize
- Fast convergence rate

Often mutually incompatible goals  $\therefore$  compromises

---

From the point of view of “per iteration convergence rate,” the optimal “surrogate function” would be just  $\Psi$  itself. However, then the M-step is very difficult (in fact it is the original optimization problem). Such an “algorithm” would converge in one very expensive “iteration.”

---

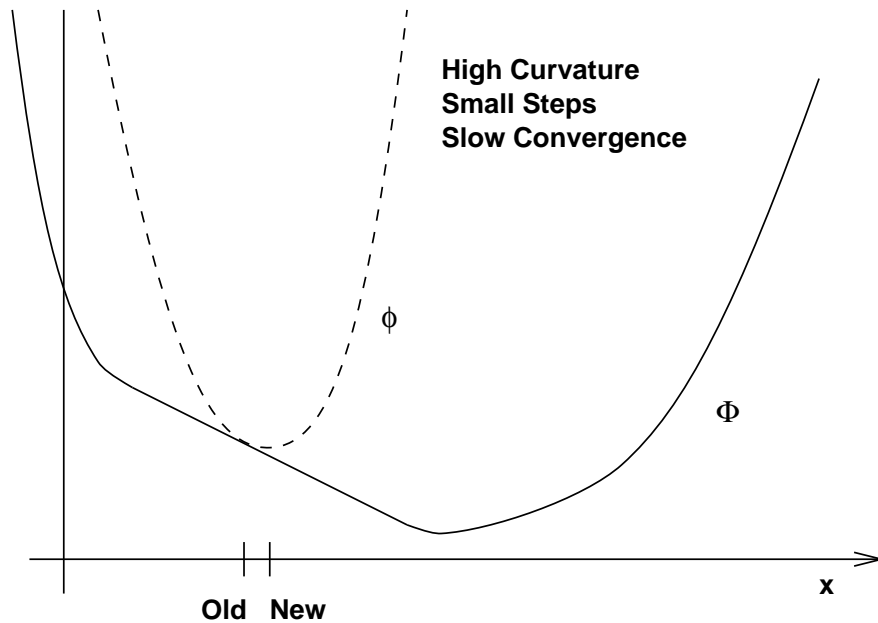
3.25

© J. Fessler, May 12, 2008

3.25

p3x

## Convergence Rate: Slow



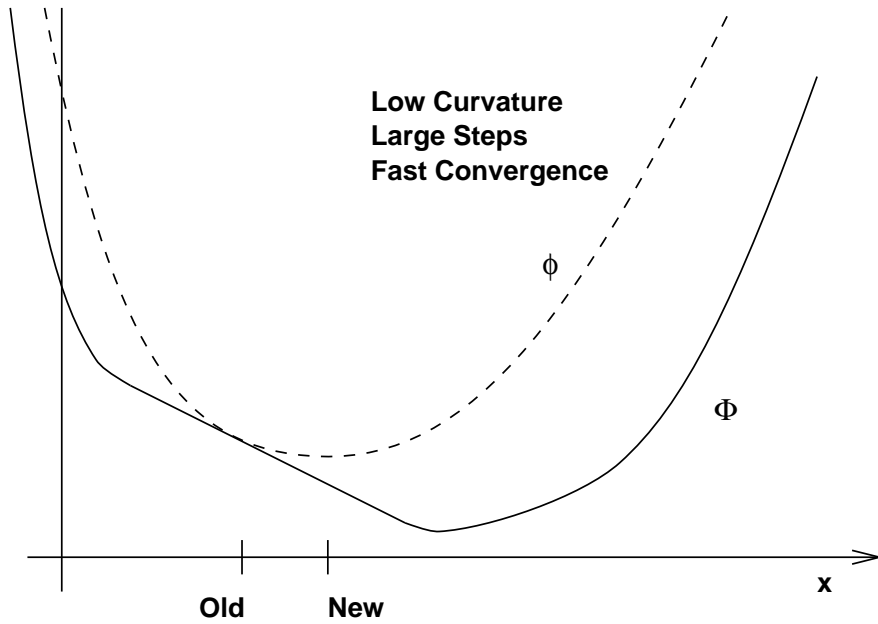
3.26

© J. Fessler, May 12, 2008

3.26

p3x

## Convergence Rate: Fast



3.27

---

Tradeoff between curvature and ease of M-step... Can we beat this tradeoff?

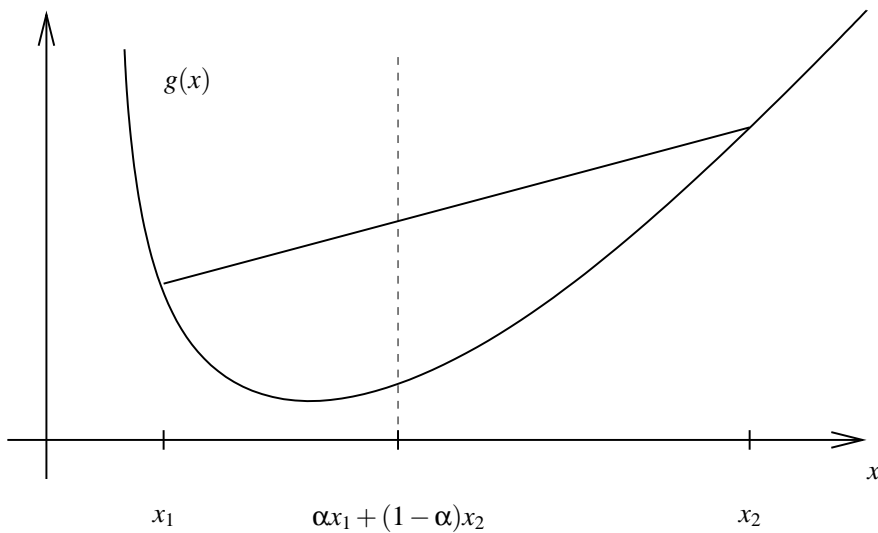
---

© J. Fessler, May 12, 2008

3.27

p3x

## Tool: Convexity Inequality



$g$  convex  $\implies g(\alpha x_1 + (1 - \alpha)x_2) \leq \alpha g(x_1) + (1 - \alpha)g(x_2)$  for  $\alpha \in [0, 1]$

More generally:  $\alpha_k \geq 0$  and  $\sum_k \alpha_k = 1 \implies g(\sum_k \alpha_k x_k) \leq \sum_k \alpha_k g(x_k)$ . Sum outside!

3.28

---

The emission Poisson ray log-likelihood  $h_i$  is strictly convex on  $(-r_i, \infty)$ . This turns out to be adequate for the derivation.

---

© J. Fessler, May 12, 2008

3.28

p3x

## Example 1: Classical ML-EM Algorithm

Negative Poisson log-likelihood cost function (unregularized):

$$\Psi(\mathbf{x}) = \sum_{i=1}^{n_d} h_i([\mathbf{Ax}]_i), \quad h_i(l) = (l + r_i) - y_i \log(l + r_i).$$

Intractable to minimize directly due to summation within logarithm.

Clever trick due to De Pierro (let  $\bar{y}_i^{(n)} = [\mathbf{Ax}^{(n)}]_i + r_i$ ):

$$[\mathbf{Ax}]_i = \sum_{j=1}^{n_p} a_{ij} x_j = \sum_{j=1}^{n_p} \left[ \frac{a_{ij} x_j^{(n)}}{\bar{y}_i^{(n)}} \right] \left( \frac{x_j}{x_j^{(n)}} \bar{y}_i^{(n)} \right).$$

Since the  $h_i$ 's are *convex* in Poisson emission model:

$$h_i([\mathbf{Ax}]_i) = h_i \left( \sum_{j=1}^{n_p} \left[ \frac{a_{ij} x_j^{(n)}}{\bar{y}_i^{(n)}} \right] \left( \frac{x_j}{x_j^{(n)}} \bar{y}_i^{(n)} \right) \right) \leq \sum_{j=1}^{n_p} \left[ \frac{a_{ij} x_j^{(n)}}{\bar{y}_i^{(n)}} \right] h_i \left( \frac{x_j}{x_j^{(n)}} \bar{y}_i^{(n)} \right)$$

$$\Psi(\mathbf{x}) = \sum_{i=1}^{n_d} h_i([\mathbf{Ax}]_i) \leq \phi(\mathbf{x}; \mathbf{x}^{(n)}) \triangleq \sum_{i=1}^{n_d} \sum_{j=1}^{n_p} \left[ \frac{a_{ij} x_j^{(n)}}{\bar{y}_i^{(n)}} \right] h_i \left( \frac{x_j}{x_j^{(n)}} \bar{y}_i^{(n)} \right)$$

Replace convex cost function  $\Psi(\mathbf{x})$  with *separable* surrogate function  $\phi(\mathbf{x}; \mathbf{x}^{(n)})$ .

3.29

### “ML-EM Algorithm” M-step

E-step gave separable surrogate function:

$$\phi(\mathbf{x}; \mathbf{x}^{(n)}) = \sum_{j=1}^{n_p} \phi_j(x_j; \mathbf{x}^{(n)}), \quad \text{where } \phi_j(x_j; \mathbf{x}^{(n)}) \triangleq \sum_{i=1}^{n_d} \left[ \frac{a_{ij} x_j^{(n)}}{\bar{y}_i^{(n)}} \right] h_i \left( \frac{x_j}{x_j^{(n)}} \bar{y}_i^{(n)} \right).$$

M-step separates:

$$\mathbf{x}^{(n+1)} = \arg \min_{\mathbf{x} \geq \mathbf{0}} \phi(\mathbf{x}; \mathbf{x}^{(n)}) \implies x_j^{(n+1)} = \arg \min_{x_j \geq 0} \phi_j(x_j; \mathbf{x}^{(n)}), \quad j = 1, \dots, n_p$$

Minimizing:

$$\frac{\partial}{\partial x_j} \phi_j(x_j; \mathbf{x}^{(n)}) = \sum_{i=1}^{n_d} a_{ij} h_i' \left( \frac{\bar{y}_i^{(n)}}{x_j} \right) = \sum_{i=1}^{n_d} a_{ij} \left[ 1 - \frac{y_i}{\bar{y}_i^{(n)}} \frac{x_j}{x_j^{(n)}} \right] \Big|_{x_j=x_j^{(n+1)}} = 0.$$

Solving (in case  $r_i = 0$ ):

$$x_j^{(n+1)} = x_j^{(n)} \frac{\left[ \sum_{i=1}^{n_d} a_{ij} \frac{y_i}{[\mathbf{Ax}^{(n)}]_i} \right]}{\left( \sum_{i=1}^{n_d} a_{ij} \right)}, \quad j = 1, \dots, n_p$$

- Derived without any statistical considerations, unlike classical EM formulation.
- Uses only convexity and algebra.
- Guaranteed monotonic: surrogate function  $\phi$  satisfies the 3 required properties.
- M-step trivial due to *separable surrogate*.

3.30

The clever (multiplicative) trick in the first equation is due to Alvaro De Pierro [212].

Note that the bracketed terms sum over  $j$  to unity.

I believe that this is the shortest and simplest possible derivation of the ML-EM algorithm, out of five distinct derivations I have seen.

This derivation is complete only for the case  $r_i = 0$ . It is easily generalized to  $r_i \neq 0$ .

© J. Fessler, May 12, 2008

3.29

p3x

When  $r_i = 0$ ,  $h_i(l) \triangleq \frac{d}{dl} h_i(l) = 1 - y_i/l$ .

Case where  $r_i \neq 0$  can also be handled with more algebra. Just replace final  $[\mathbf{Ax}^{(n)}]_i$  with  $\bar{y}_i^{(n)} = [\mathbf{Ax}^{(n)}]_i + r_i$ .

To be rigorous, we should check that the Karush-Kuhn-Tucker condition holds for our minimizer of  $\phi_j(\cdot; \mathbf{x}^{(n)})$ . It does, provided  $\mathbf{x}^{(n)} \geq \mathbf{0}$ .

I prefer this derivation over the statistical EM derivation, even though we are doing statistical image reconstruction. Statistics greatly affect the design of  $\Psi$ , but minimizing  $\Psi$  is really just a numerical problem, and statistics need not have any role in that.

© J. Fessler, May 12, 2008

3.30

p3x



# ML-EM is Scaled Gradient Descent

$$\begin{aligned}
 x_j^{(n+1)} &= x_j^{(n)} \left[ \frac{\sum_{i=1}^{n_d} a_{ij} \frac{y_i}{\hat{y}_i^{(n)}}}{\sum_{i=1}^{n_d} a_{ij}} \right] \\
 &= x_j^{(n)} + x_j^{(n)} \left[ \frac{\sum_{i=1}^{n_d} a_{ij} \left( \frac{y_i}{\hat{y}_i^{(n)}} - 1 \right)}{\sum_{i=1}^{n_d} a_{ij}} \right] \\
 &= \boxed{x_j^{(n)} - \left( \frac{x_j^{(n)}}{\sum_{i=1}^{n_d} a_{ij}} \right) \frac{\partial}{\partial x_j} \Psi(\mathbf{x}^{(n)})}, \quad j = 1, \dots, n_p
 \end{aligned}$$

$$\mathbf{x}^{(n+1)} = \mathbf{x}^{(n)} + \mathbf{D}(\mathbf{x}^{(n)}) \nabla \Psi(\mathbf{x}^{(n)})$$

This particular diagonal scaling matrix remarkably

- ensures monotonicity,
- ensures nonnegativity.

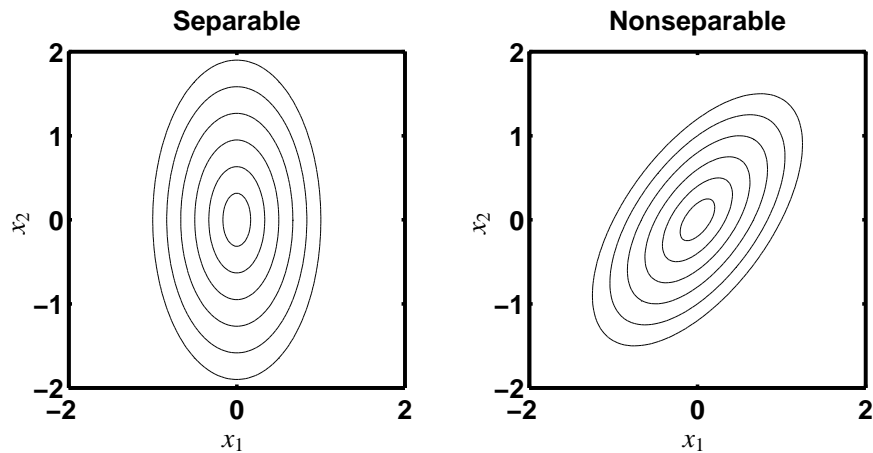
3.31

© J. Fessler, May 12, 2008

3.31

p3x

## Consideration: Separable vs Nonseparable



Contour plots: loci of equal function values.

Uncoupled vs coupled minimization.

3.32

© J. Fessler, May 12, 2008

3.32

p3x

---

To find the minimizer of a separable function, one can minimize separately with respect to each argument. To find the minimizer of a nonseparable function, one must consider the variables together. In this sense the minimization problem “couples” together the unknown parameters.

---

## Separable Surrogate Functions (Easy M-step)

The preceding EM derivation structure applies to *any* cost function of the form

$$\Psi(\mathbf{x}) = \sum_{i=1}^{n_d} h_i([\mathbf{A}\mathbf{x}]_i).$$

cf ISRA (for nonnegative LS), “convex algorithm” for transmission reconstruction

Derivation yields a separable surrogate function

$$\Psi(\mathbf{x}) \leq \phi(\mathbf{x}; \mathbf{x}^{(n)}), \text{ where } \phi(\mathbf{x}; \mathbf{x}^{(n)}) = \sum_{j=1}^{n_p} \phi_j(x_j; \mathbf{x}^{(n)})$$

M-step separates into 1D minimization problems (fully parallelizable):

$$\mathbf{x}^{(n+1)} = \arg \min_{\mathbf{x} \geq \mathbf{0}} \phi(\mathbf{x}; \mathbf{x}^{(n)}) \implies x_j^{(n+1)} = \arg \min_{x_j \geq 0} \phi_j(x_j; \mathbf{x}^{(n)}), \quad j = 1, \dots, n_p$$

Why do EM / ISRA / convex-algorithm / etc. converge so slowly?

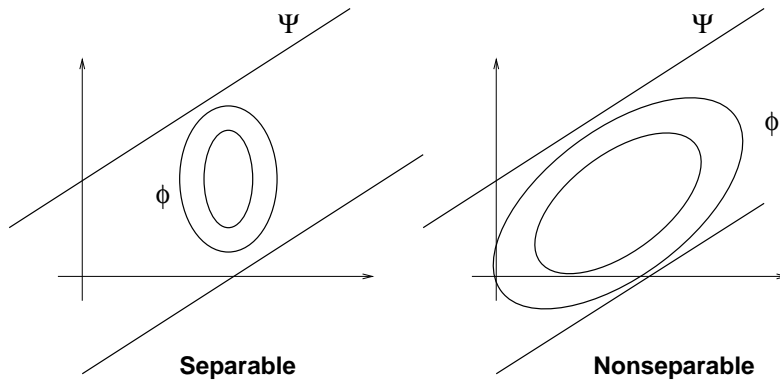
3.33

© J. Fessler, May 12, 2008

3.33

p3x

### Separable vs Nonseparable



Separable surrogates (e.g., EM) have high curvature  $\therefore$  slow convergence.  
 Nonseparable surrogates can have lower curvature  $\therefore$  faster convergence.  
 Harder to minimize? Use paraboloids (quadratic surrogates).

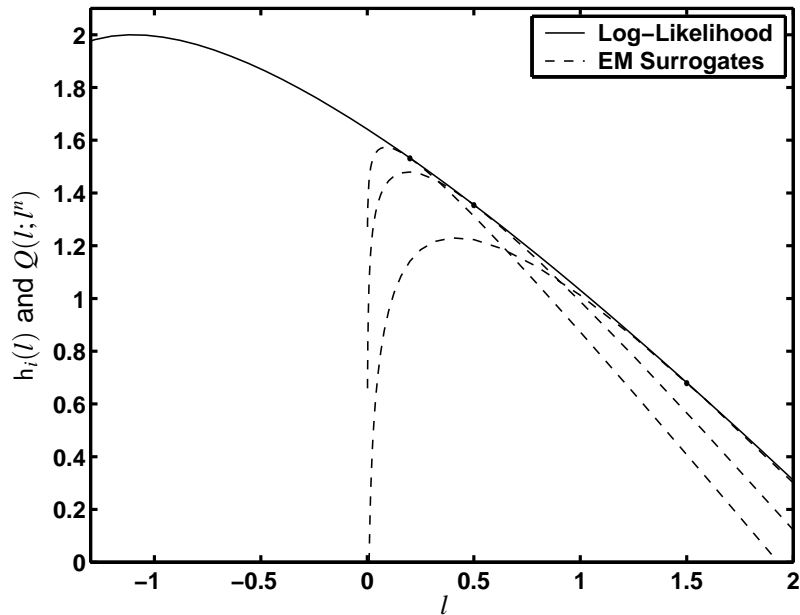
3.34

© J. Fessler, May 12, 2008

3.34

p3x

# High Curvature of EM Surrogate



3.35

Sublinear convergence rate of EM shown in [226].

3.35

p3x

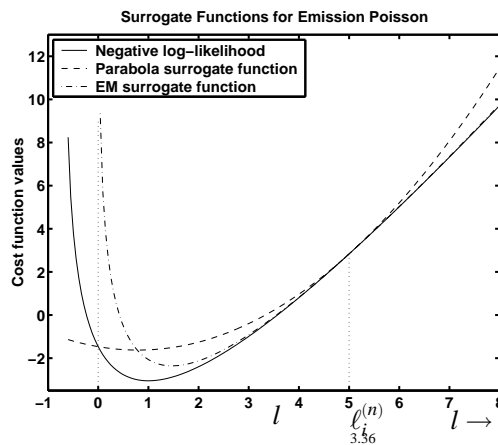
# 1D Parabola Surrogate Function

Find parabola  $q_i^{(n)}(l)$  of the form:

$$q_i^{(n)}(l) = h_i(\ell_i^{(n)}) + \dot{h}_i(\ell_i^{(n)})(l - \ell_i^{(n)}) + c_i^{(n)} \frac{1}{2}(l - \ell_i^{(n)})^2, \text{ where } \ell_i^{(n)} \triangleq [\mathbf{A}\mathbf{x}^{(n)}]_i$$

Satisfies tangent condition. Choose curvature to ensure “lies above” condition:

$$c_i^{(n)} \triangleq \min \left\{ c \geq 0 : q_i^{(n)}(l) \geq h_i(l), \quad \forall l \geq 0 \right\}.$$



Lower curvature!

3.36

© J. Fessler, May 12, 2008

3.36

p3x

## Paraboloidal Surrogate

Combining 1D parabola surrogates yields *paraboloidal surrogate*:

$$\Psi(\mathbf{x}) = \sum_{i=1}^{n_d} h_i([\mathbf{A}\mathbf{x}]_i) \leq \phi(\mathbf{x}; \mathbf{x}^{(n)}) = \sum_{i=1}^{n_d} q_i^{(n)}([\mathbf{A}\mathbf{x}]_i)$$

$$\text{Rewriting: } \phi(\boldsymbol{\delta} + \mathbf{x}^{(n)}; \mathbf{x}^{(n)}) = \Psi(\mathbf{x}^{(n)}) + \nabla \Psi(\mathbf{x}^{(n)}) \boldsymbol{\delta} + \frac{1}{2} \boldsymbol{\delta}' \mathbf{A}' \text{diag}\{c_i^{(n)}\} \mathbf{A} \boldsymbol{\delta}$$

### Advantages

- Surrogate  $\phi(\mathbf{x}; \mathbf{x}^{(n)})$  is *quadratic*, unlike Poisson log-likelihood  
 $\implies$  easier to minimize
- Not separable (unlike EM surrogate)
- Not self-similar (unlike EM surrogate)
- Small curvatures  $\implies$  fast convergence
- Intrinsically monotone global convergence
- Fairly simple to derive / implement

### Quadratic minimization

- Coordinate descent
  - + fast converging
  - + Nonnegativity easy
  - precomputed column-stored system matrix
- Gradient-based quadratic minimization methods<sup>3.37</sup>
  - Nonnegativity inconvenient

---

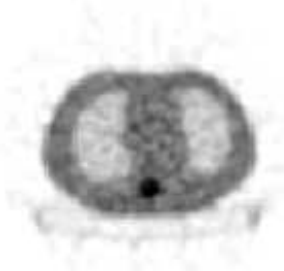
Instead of coordinate descent, one could also apply nonnegativity-constrained conjugate gradient.

PSCD recommended for 2D emission Poisson likelihood when system matrix precomputed and stored by columns.

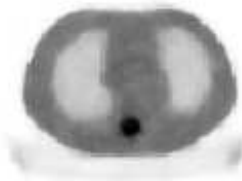
---

## Example: PSCD for PET Transmission Scans

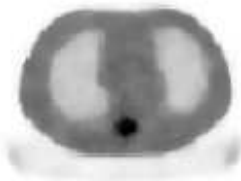
FBP



PL-OSTR-16  
4 iterations



PL-PSCD  
10 iterations



- square-pixel basis
- strip-integral system model
- shifted-Poisson statistical model
- edge-preserving convex regularization (Huber)
- nonnegativity constraint
- inscribed circle support constraint
- paraboloidal surrogate coordinate descent (PSCD) algorithm

## Separable Paraboloidal Surrogate

To derive a parallelizable algorithm apply another De Pierro trick:

$$[\mathbf{Ax}]_i = \sum_{j=1}^{n_p} \pi_{ij} \left[ \frac{a_{ij}}{\pi_{ij}} (x_j - x_j^{(n)}) + \ell_i^{(n)} \right], \quad \ell_i^{(n)} = [\mathbf{Ax}^{(n)}]_i.$$

Provided  $\pi_{ij} \geq 0$  and  $\sum_{j=1}^{n_p} \pi_{ij} = 1$ , since parabola  $q_i$  is convex:

$$q_i^{(n)}([\mathbf{Ax}]_i) = q_i^{(n)} \left( \sum_{j=1}^{n_p} \pi_{ij} \left[ \frac{a_{ij}}{\pi_{ij}} (x_j - x_j^{(n)}) + \ell_i^{(n)} \right] \right) \leq \sum_{j=1}^{n_p} \pi_{ij} q_i^{(n)} \left( \frac{a_{ij}}{\pi_{ij}} (x_j - x_j^{(n)}) + \ell_i^{(n)} \right)$$

$$\therefore \phi(\mathbf{x}; \mathbf{x}^{(n)}) = \sum_{i=1}^{n_d} q_i^{(n)}([\mathbf{Ax}]_i) \leq \tilde{\phi}(\mathbf{x}; \mathbf{x}^{(n)}) \triangleq \sum_{i=1}^{n_d} \sum_{j=1}^{n_p} \pi_{ij} q_i^{(n)} \left( \frac{a_{ij}}{\pi_{ij}} (x_j - x_j^{(n)}) + \ell_i^{(n)} \right)$$

Separable Paraboloidal Surrogate:

$$\tilde{\phi}(\mathbf{x}; \mathbf{x}^{(n)}) = \sum_{j=1}^{n_p} \phi_j(x_j; \mathbf{x}^{(n)}), \quad \phi_j(x_j; \mathbf{x}^{(n)}) \triangleq \sum_{i=1}^{n_d} \pi_{ij} q_i^{(n)} \left( \frac{a_{ij}}{\pi_{ij}} (x_j - x_j^{(n)}) + \ell_i^{(n)} \right)$$

Parallelizable M-step (cf gradient descent!):

$$x_j^{(n+1)} = \arg \min_{x_j \geq 0} \phi_j(x_j; \mathbf{x}^{(n)}) = \left[ x_j^{(n)} - \frac{1}{d_j^{(n)}} \frac{\partial}{\partial x_j} \Psi(\mathbf{x}^{(n)}) \right]_+, \quad d_j^{(n)} = \sum_{i=1}^{n_d} \frac{a_{ij}^2}{\pi_{ij}} c_i^{(n)}$$

Natural choice is  $\pi_{ij} = |a_{ij}|/|a|_i$ ,  $|a|_i = \sum_{j=1}^{n_p} |a_{ij}|$

---

De Pierro's "additive trick" in [119].

For the natural choice  $\pi_{ij} = |a_{ij}|/|a|_i$ , we have

$$d_j^{(n)} = \sum_{i=1}^{n_d} |a_{ij}| |a|_i c_i^{(n)}$$


---

## Example: Poisson ML Transmission Problem

Transmission negative log-likelihood (for  $i$ th ray):

$$h_i(l) = (b_i e^{-l} + r_i) - y_i \log(b_i e^{-l} + r_i).$$

Optimal (smallest) parabola surrogate curvature (Erdođan, T-MI, Sep. 1999):

$$c_i^{(n)} = c(\ell_i^{(n)}, h_i), \quad c(l, h) = \begin{cases} \left[ 2 \frac{h(0) - h(l) + \dot{h}(l)l}{l^2} \right]_+, & l > 0 \\ [\ddot{h}(l)]_+, & l = 0. \end{cases}$$

**Separable Paraboloidal Surrogate (SPS) Algorithm:**

Precompute  $|a|_i = \sum_{j=1}^{n_p} a_{ij}$ ,  $i = 1, \dots, n_d$

$$\begin{aligned} \ell_i^{(n)} &= [\mathbf{Ax}^{(n)}]_i && \text{(forward projection)} \\ \bar{y}_i^{(n)} &= b_i e^{-\ell_i^{(n)}} + r_i && \text{(predicted means)} \\ \dot{h}_i^{(n)} &= 1 - y_i / \bar{y}_i^{(n)} && \text{(slopes)} \\ c_i^{(n)} &= c(\ell_i^{(n)}, h_i) && \text{(curvatures)} \end{aligned}$$

$$x_j^{(n+1)} = \left[ x_j^{(n)} - \frac{1}{d_j^{(n)}} \frac{\partial}{\partial x_j} \Psi(\mathbf{x}^{(n)}) \right]_+ = \left[ x_j^{(n)} - \frac{\sum_{i=1}^{n_d} a_{ij} \dot{h}_i^{(n)}}{\sum_{i=1}^{n_d} |a_{ij}| |a|_i c_i^{(n)}} \right]_+, \quad j = 1, \dots, n_p$$

Monotonically decreases cost function each iteration.

No logarithm!

---

Note that this algorithm never takes the logarithm of the transmission data, since it is based directly on a statistical model for the raw measurements. This is a significant part of the reason why it works well for low-count measurements.

Optimal parabola surrogate curvature for transmission problem [220]. Emission problem [227].

A Matlab m-file for this algorithm is available from  
<http://www.eecs.umich.edu/~fessler/code>  
as `transmission/tml_sps.m`

Related m-files also of interest include `transmission/tpl_osps.m`

---

## The MAP-EM M-step “Problem”

Add a penalty function to our surrogate for the negative log-likelihood:

$$\Psi(\mathbf{x}) = \ell(\mathbf{x}) + \beta R(\mathbf{x})$$

$$\phi(\mathbf{x}; \mathbf{x}^{(n)}) = \sum_{j=1}^{n_p} \phi_j(x_j; \mathbf{x}^{(n)}) + \beta R(\mathbf{x})$$

$$\text{M-step: } \mathbf{x}^{(n+1)} = \arg \min_{\mathbf{x} \geq \mathbf{0}} \phi(\mathbf{x}; \mathbf{x}^{(n)}) = \arg \min_{\mathbf{x} \geq \mathbf{0}} \sum_{j=1}^{n_p} \phi_j(x_j; \mathbf{x}^{(n)}) + \beta R(\mathbf{x}) = ?$$

For nonseparable penalty functions, the M-step is coupled  $\therefore$  difficult.

### Suboptimal solutions

- Generalized EM (GEM) algorithm (coordinate descent on  $\phi$ )  
Monotonic, but inherits slow convergence of EM.
- One-step late (OSL) algorithm (use outdated gradients) (Green, T-MI, 1990)

$$\frac{\partial}{\partial x_j} \phi(\mathbf{x}; \mathbf{x}^{(n)}) = \frac{\partial}{\partial x_j} \phi_j(x_j; \mathbf{x}^{(n)}) + \beta \frac{\partial}{\partial x_j} R(\mathbf{x}) \stackrel{?}{\approx} \frac{\partial}{\partial x_j} \phi_j(x_j; \mathbf{x}^{(n)}) + \beta \frac{\partial}{\partial x_j} R(\mathbf{x}^{(n)})$$

Nonmonotonic. Known to diverge, depending on  $\beta$ .

Temptingly simple, but *avoid!*

### Contemporary solution

- Use separable surrogate for penalty function too (De Pierro, T-MI, Dec. 1995)  
Ensures monotonicity. Obviates all reasons for using OSL!

3.41

## De Pierro’s MAP-EM Algorithm

Apply separable paraboloidal surrogates to penalty function:

$$R(\mathbf{x}) \leq R_{\text{SPS}}(\mathbf{x}; \mathbf{x}^{(n)}) = \sum_{j=1}^{n_p} R_j(x_j; \mathbf{x}^{(n)})$$

$$\text{Overall separable surrogate: } \phi(\mathbf{x}; \mathbf{x}^{(n)}) = \sum_{j=1}^{n_p} \phi_j(x_j; \mathbf{x}^{(n)}) + \beta \sum_{j=1}^{n_p} R_j(x_j; \mathbf{x}^{(n)})$$

The M-step becomes fully parallelizable:

$$x_j^{(n+1)} = \arg \min_{x_j \geq 0} \phi_j(x_j; \mathbf{x}^{(n)}) - \beta R_j(x_j; \mathbf{x}^{(n)}), \quad j = 1, \dots, n_p.$$

Consider quadratic penalty  $R(\mathbf{x}) = \sum_k \psi([\mathbf{C}\mathbf{x}]_k)$ , where  $\psi(t) = t^2/2$ .

If  $\gamma_{kj} \geq 0$  and  $\sum_{j=1}^{n_p} \gamma_{kj} = 1$  then

$$[\mathbf{C}\mathbf{x}]_k = \sum_{j=1}^{n_p} \gamma_{kj} \left[ \frac{c_{kj}}{\gamma_{kj}} (x_j - x_j^{(n)}) + [\mathbf{C}\mathbf{x}^{(n)}]_k \right].$$

Since  $\psi$  is convex:

$$\begin{aligned} \psi([\mathbf{C}\mathbf{x}]_k) &= \psi \left( \sum_{j=1}^{n_p} \gamma_{kj} \left[ \frac{c_{kj}}{\gamma_{kj}} (x_j - x_j^{(n)}) + [\mathbf{C}\mathbf{x}^{(n)}]_k \right] \right) \\ &\leq \sum_{j=1}^{n_p} \gamma_{kj} \psi \left( \frac{c_{kj}}{\gamma_{kj}} (x_j - x_j^{(n)}) + [\mathbf{C}\mathbf{x}^{(n)}]_k \right) \end{aligned}$$

3.42

OSL [213, 214]  
GEM [228–230]

De Pierro’s separable penalty derived in [119].

© J. Fessler, May 12, 2008

3.41

p3x

Often we just choose

$$\gamma_{kj} = \begin{cases} \frac{1}{\text{number of nonzero } c_{kj}'\text{s in } k\text{th row of } \mathbf{C}}, & c_{kj} \neq 0 \\ 0, & \text{otherwise,} \end{cases}$$

which satisfies the two conditions  $\gamma_{kj} \geq 0$  and  $\sum_{j=1}^{n_p} \gamma_{kj} = 1$ , e.g.

$$\mathbf{C} = \begin{bmatrix} -1 & 1 & 0 & 0 & 0 \\ 0 & -1 & 1 & 0 & 0 \\ 0 & 0 & 0 & -1 & 1 \\ -1 & 0 & 0 & 1 & 0 \\ 0 & -1 & 0 & 0 & 1 \end{bmatrix}, \quad \{\gamma_{kj}\} = \begin{bmatrix} \frac{1}{2} & \frac{1}{2} & 0 & 0 & 0 \\ 0 & \frac{1}{2} & \frac{1}{2} & 0 & 0 \\ 0 & 0 & 0 & \frac{1}{2} & \frac{1}{2} \\ \frac{1}{2} & 0 & 0 & \frac{1}{2} & 0 \\ 0 & \frac{1}{2} & 0 & 0 & \frac{1}{2} \end{bmatrix}.$$

Alternatively we use the choice

$$\gamma_{kj} = \frac{|c_{kj}|}{\sum_{j'=1}^{n_p} |c_{kj'}|},$$

which happens to yield the same result when the elements of  $\mathbf{C}$  are just  $\pm 1$  as in the above example. For non-unity  $c_{kj}$ ’s, the latter ratio seems to be preferable in terms of convergence rate.

© J. Fessler, May 12, 2008

3.42

p3x

## De Pierro's Algorithm Continued

So  $R(\mathbf{x}) \leq R(\mathbf{x}; \mathbf{x}^{(n)}) \triangleq \sum_{j=1}^{n_p} R_j(x_j; \mathbf{x}^{(n)})$  where

$$R_j(x_j; \mathbf{x}^{(n)}) \triangleq \sum_k \gamma_{kj} \Psi \left( \frac{c_{kj}}{\gamma_{kj}} (x_j - x_j^{(n)}) + [\mathbf{C}\mathbf{x}^{(n)}]_k \right)$$

M-step: Minimizing  $\phi_j(x_j; \mathbf{x}^{(n)}) + \beta R_j(x_j; \mathbf{x}^{(n)})$  yields the iteration:

$$x_j^{(n+1)} = \frac{x_j^{(n)} \sum_{i=1}^{n_d} a_{ij} y_i / \bar{y}_i^{(n)}}{B_j + \sqrt{B_j^2 + \left( x_j^{(n)} \sum_{i=1}^{n_d} a_{ij} y_i / \bar{y}_i^{(n)} \right) \left( \beta \sum_k c_{kj}^2 / \gamma_{kj} \right)}}$$

$$\text{where } B_j \triangleq \frac{1}{2} \left[ \sum_{i=1}^{n_d} a_{ij} + \beta \sum_k \left( c_{kj} [\mathbf{C}\mathbf{x}^{(n)}]_k - \frac{c_{kj}^2}{\gamma_{kj}} x_j^{(n)} \right) \right], \quad j = 1, \dots, n_p$$

and  $\bar{y}_i^{(n)} = [\mathbf{A}\mathbf{x}^{(n)}]_i + r_i$ .

Advantages: Intrinsically monotone, nonnegativity, fully parallelizable. Requires only a couple % more computation per iteration than ML-EM

Disadvantages: Slow convergence (like EM) due to separable surrogate

3.43

## Ordered Subsets Algorithms

aka *block iterative* or *incremental gradient* algorithms

The gradient appears in essentially every algorithm:

$$\boldsymbol{\ell}(\mathbf{x}) = \sum_{i=1}^{n_d} h_i([\mathbf{A}\mathbf{x}]_i) \implies \frac{\partial}{\partial x_j} \boldsymbol{\ell}(\mathbf{x}) = \sum_{i=1}^{n_d} a_{ij} \dot{h}_i([\mathbf{A}\mathbf{x}]_i).$$

This is a *backprojection* of a sinogram of the derivatives  $\{\dot{h}_i([\mathbf{A}\mathbf{x}]_i)\}$ .

Intuition: with half the angular sampling, this backprojection would be fairly similar

$$\frac{1}{n_d} \sum_{i=1}^{n_d} a_{ij} \dot{h}_i(\cdot) \approx \frac{1}{|S|} \sum_{i \in S} a_{ij} \dot{h}_i(\cdot),$$

where  $S$  is a subset of the rays.

To "OS-ize" an algorithm, replace all backprojections with partial sums.

Recall typical iteration:

$$\mathbf{x}^{(n+1)} = \mathbf{x}^{(n)} - \mathbf{D}(\mathbf{x}^{(n)}) \nabla \Psi(\mathbf{x}^{(n)}).$$

3.44

As a concrete example, consider  $R(\mathbf{x}) = \sum_{j=1}^{n_p} \frac{1}{2} \sum_{k \in \mathcal{N}_j} \frac{1}{2} (x_j - x_k)^2$  with  $\mathcal{N}_j$  corresponding to the  $|\mathcal{N}_j|$  nearest neighbors to the  $j$ th pixel. For this penalty with the choice  $\gamma_{kj} = |c_{kj}|/c_k$  where  $c_k = \sum_{j=1}^{n_p} |c_{kj}| = |\mathcal{N}_j|$ , the separable surrogate is [119]:

$$R_j(x_j; \mathbf{x}^{(n)}) = \sum_{k \in \mathcal{N}_j} \frac{1}{2} \frac{1}{|\mathcal{N}_j|} \left( |\mathcal{N}_j| (x_j - x_j^{(n)}) + x_j^{(n)} - x_j^{(k)} \right)^2.$$

Matlab m-file available from [http://www.eecs.umich.edu/~fessler/code/as emission/eql\\_empt.m](http://www.eecs.umich.edu/~fessler/code/as%20emission/eql_empt.m)

Caution: use stable quadratic roots [181] (slightly more complicated than above).

One can make an ordered-subsets version of De Pierro's MAP-EM easily. Such an approach is preferable to the OSL version of OS-EM mentioned by Hudson and Larkin [28].

One can do multiple M-step subiterations for minimal additional computation with some improvement in convergence rate.

For a tomography problem with a  $64 \times 64$  image,  $64 \times 80$  sinogram, and strip-area system matrix, De Pierro's MAP-EM algorithm requires 4% more flops per iteration than classic ML-EM.

© J. Fessler, May 12, 2008

3.43

p3x

The dramatic improvements in apparent "convergence rate" of OSEM over classic ML-EM are due largely to the fact that the latter converges so slowly.

Modern, faster converging algorithms may benefit much less from OS modifications.

Richard Larkin (personal communication) has described the development of OSEM as something of a fortuitous programming "accident." In the course of developing software to implement the E-ML-EM algorithm, he first implemented a version that updated the image immediately after the reprojection of each view. Later he implemented the classical E-ML-EM algorithm but found it to give worse images (in the early iterations). (Due of course to its slow convergence.) The "immediate update" version turns out to be OSEM with 1 view per subset.

Several publications hinted at the use of subsets of projection views for acceleration, e.g., [231–234], and D. Polite's 1983 dissertation. But it was the paper by Larkin and Hudson that incited widespread use of OSEM [28].

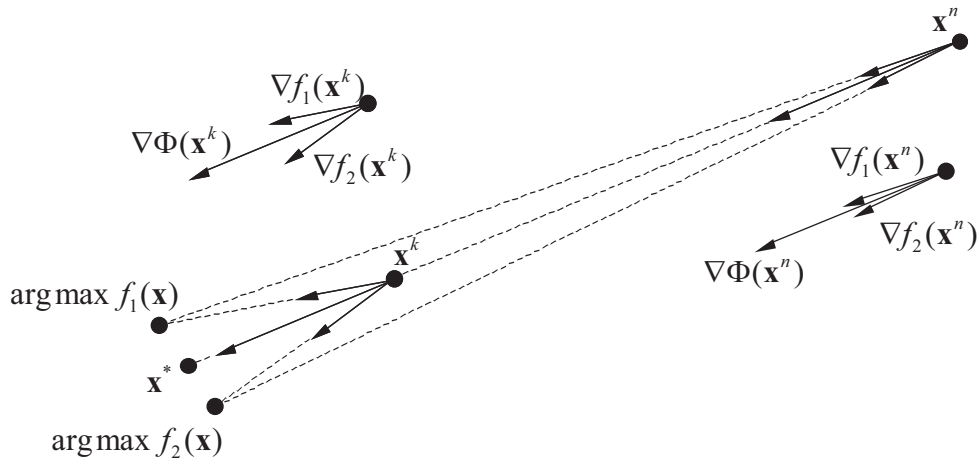
In the general optimization literature, such algorithms are called *incremental gradient* methods [235–239], and they date back to the 1970's [240].

3.44

© J. Fessler, May 12, 2008

p3x

# Geometric View of Ordered Subsets



Two subset case:  $\Psi(x) = f_1(x) + f_2(x)$  (e.g., odd and even projection views).

For  $x^{(n)}$  far from  $x^*$ , even partial gradients should point roughly towards  $x^*$ .  
 For  $x^{(n)}$  near  $x^*$ , however,  $\nabla\Psi(x) \approx \mathbf{0}$ , so  $\nabla f_1(x) \approx -\nabla f_2(x) \implies$  cycles!  
 Issues. "Subset gradient balance":  $\nabla\Psi(x) \approx M\nabla f_k(x)$ . Choice of ordering.

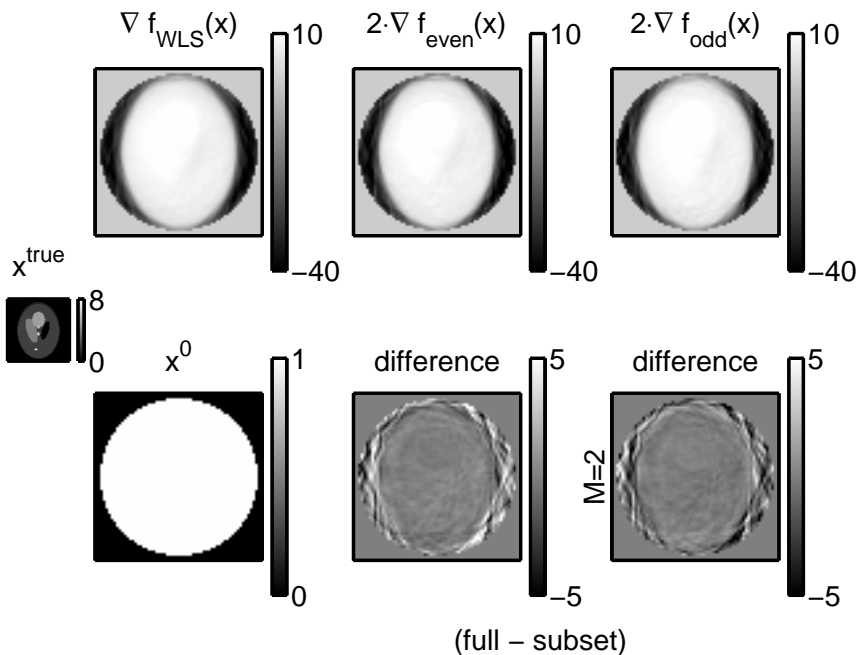
3.45

© J. Fessler, May 12, 2008

3.45

p3x

## Incremental Gradients (WLS, 2 Subsets)



3.46

Here the initial image  $x^{(0)}$  is far from the solution so the incremental gradients, i.e., the gradients computed from just the even or odd angles, agree well with the full gradient.

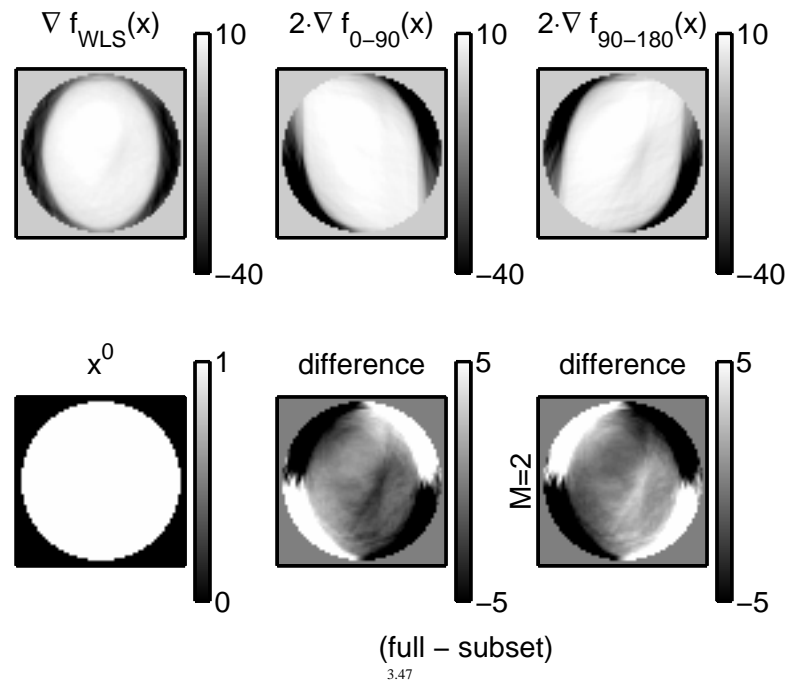
© J. Fessler, May 12, 2008

3.46

p3x



## Subset Gradient Imbalance



3.47

Here the first subset was angles 0-90°, and the second subset was angles 90-180°, roughly speaking. Now the incremental gradients do not agree as well with the full gradient. (Of course the *sum* of the two incremental gradients would still equal the full gradient.) This imbalance is expected to slow “convergence.”

© J. Fessler, May 12, 2008

3.47

p3x

## Problems with OS-EM

- Non-monotone
- Does not converge (may cycle)
- Byrne’s “rescaled block iterative” (RBI) approach converges only for consistent (noiseless) data
- ∴ unpredictable
  - What resolution after  $n$  iterations?  
Object-dependent, spatially nonuniform
  - What variance after  $n$  iterations?
  - ROI variance? (e.g., for Huesman’s WLS kinetics)

3.48

RBI (rescaled block iterative) [209].

Soares and Glick *et al.* [43] [42] have extended the work of Barrett *et al.* [35] to the OSEM case.

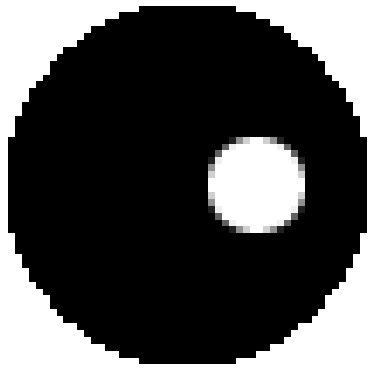
Wang *et al.* have extended it to the penalized case, for the OSL algorithm [41].

© J. Fessler, May 12, 2008

3.48

p3x

# OSEM vs Penalized Likelihood



- $64 \times 62$  image
- $66 \times 60$  sinogram
- $10^6$  counts
- 15% randoms/scatter
- uniform attenuation
- contrast in cold region
- within-region  $\sigma$  opposite side

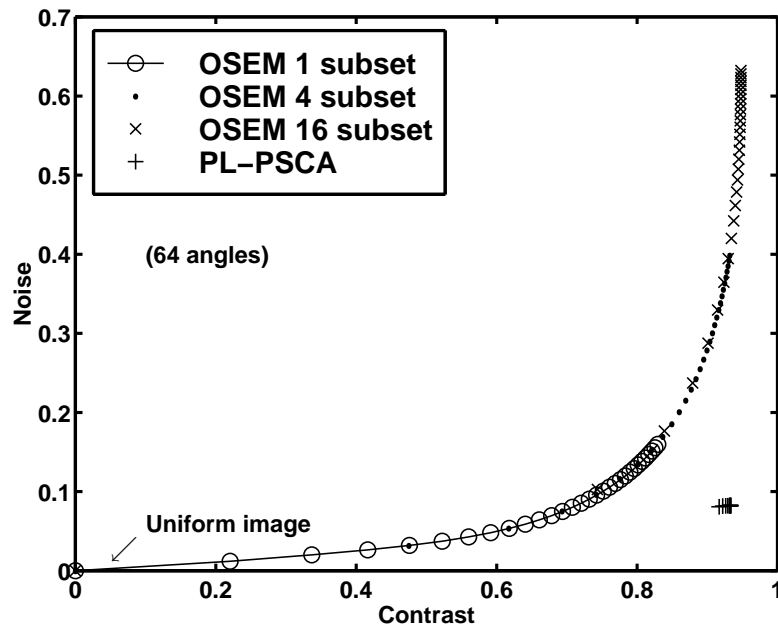
3.49

© J. Fessler, May 12, 2008

3.49

p3x

## Contrast-Noise Results

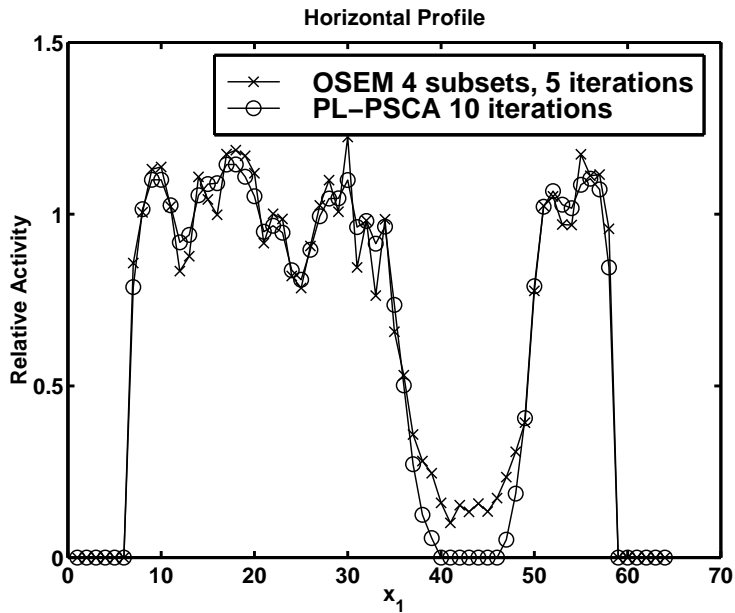


3.50

© J. Fessler, May 12, 2008

3.50

p3x



3.51

© J. Fessler, May 12, 2008

3.51

p3x

## Making OS Methods Converge

- Relaxation
- Incrementalism

### Relaxed block-iterative methods

$$\Psi(\mathbf{x}) = \sum_{m=1}^M \Psi_m(\mathbf{x})$$

$$\mathbf{x}^{(n+(m+1)/M)} = \mathbf{x}^{(n+m/M)} - \alpha_n D(\mathbf{x}^{(n+m/M)}) \nabla \Psi_m(\mathbf{x}^{(n+m/M)}), \quad m = 0, \dots, M-1$$

Relaxation of step sizes:

$$\alpha_n \rightarrow 0 \text{ as } n \rightarrow \infty, \quad \sum_n \alpha_n = \infty, \quad \sum_n \alpha_n^2 < \infty$$

- ART
- RAMLA, BSREM (De Pierro, T-MI, 1997, 2001)
- Ahn and Fessler, NSS/MIC 2001, T-MI 2003

### Considerations

- Proper relaxation can induce convergence, *but* still lacks monotonicity.
- Choice of relaxation schedule requires experimentation.
- $\Psi_m(\mathbf{x}) = \ell_m(\mathbf{x}) + \frac{1}{M} R(\mathbf{x})$ , so each  $\Psi_m$  includes part of the likelihood yet all of  $R$

3.52

© J. Fessler, May 12, 2008

3.52

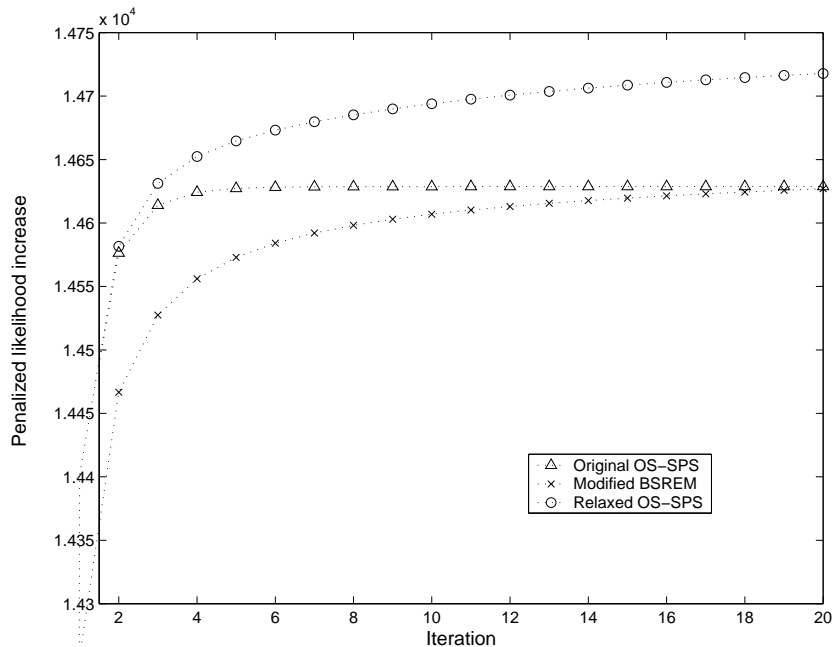
p3x

RAMLA [206] (for ML only)

Kudo [241] does not give convergence proof in English...

BSREM [242] convergence proof requires some "a posteriori" assumptions. These have been eliminated in [243].

## Relaxed OS-SPS



3.53

© J. Fessler, May 12, 2008

3.53

p3x

## Incremental Methods

Incremental EM applied to emission tomography by Hsiao *et al.* as C-OSEM

Incremental optimization transfer (Ahn & Fessler, MIC 2004)

Find majorizing surrogate for each sub-objective function:

$$\begin{aligned} \phi_m(\mathbf{x}; \mathbf{x}) &= \Psi_m(\mathbf{x}), & \forall \mathbf{x} \\ \phi_m(\mathbf{x}; \bar{\mathbf{x}}) &\geq \Psi_m(\mathbf{x}), & \forall \mathbf{x}, \bar{\mathbf{x}} \end{aligned}$$

Define the following augmented cost function:  $F(\mathbf{x}; \bar{\mathbf{x}}_1, \dots, \bar{\mathbf{x}}_M) = \sum_{m=1}^M \phi_m(\mathbf{x}; \bar{\mathbf{x}}_m)$ .

Fact: by construction  $\hat{\mathbf{x}} = \arg \min_{\mathbf{x}} \Psi(\mathbf{x}) = \arg \min_{\mathbf{x}} \min_{\bar{\mathbf{x}}_1, \dots, \bar{\mathbf{x}}_M} F(\mathbf{x}; \bar{\mathbf{x}}_1, \dots, \bar{\mathbf{x}}_M)$ .

Alternating minimization: for  $m = 1, \dots, M$ :

$$\begin{aligned} \mathbf{x}^{\text{new}} &= \arg \min_{\mathbf{x}} F(\mathbf{x}; \bar{\mathbf{x}}_1^{(n+1)}, \dots, \bar{\mathbf{x}}_{m-1}^{(n+1)}, \bar{\mathbf{x}}_m^{(n)}, \bar{\mathbf{x}}_{m+1}^{(n)}, \dots, \bar{\mathbf{x}}_M^{(n)}) \\ \bar{\mathbf{x}}_m^{(n+1)} &= \arg \min_{\bar{\mathbf{x}}_m} F(\mathbf{x}^{\text{new}}; \bar{\mathbf{x}}_1^{(n+1)}, \dots, \bar{\mathbf{x}}_{m-1}^{(n+1)}, \bar{\mathbf{x}}_m, \bar{\mathbf{x}}_{m+1}^{(n)}, \dots, \bar{\mathbf{x}}_M^{(n)}) = \mathbf{x}^{\text{new}}. \end{aligned}$$

- Use all current information, but increment the surrogate for only one subset.
- Monotone in  $F$ , converges under reasonable assumptions on  $\Psi$
- In contrast, OS-EM uses the information from *only* one subset at a time

3.54

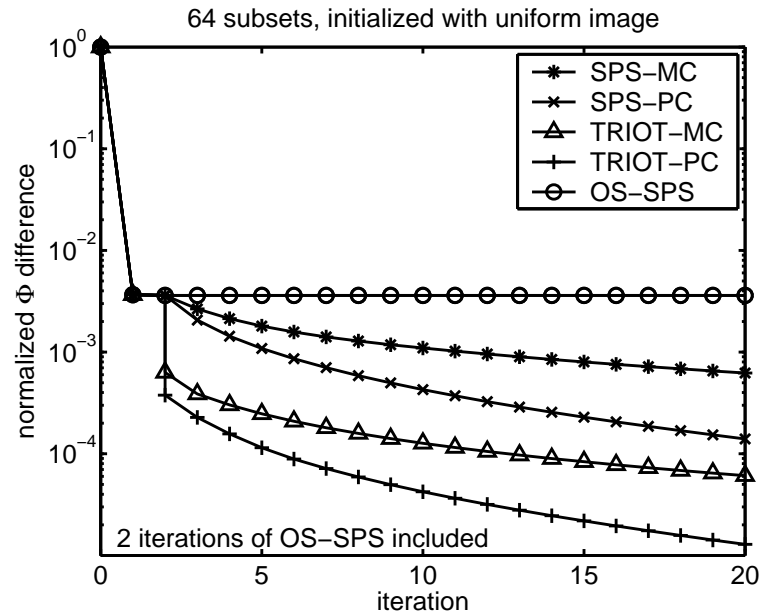
© J. Fessler, May 12, 2008

3.54

p3x

# TRIOT Example: Convergence Rate

Transmission incremental optimization transfer (TRIOT)



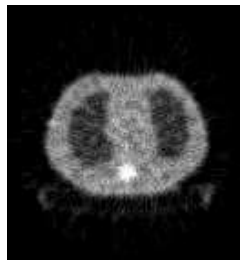
3.55

© J. Fessler, May 12, 2008

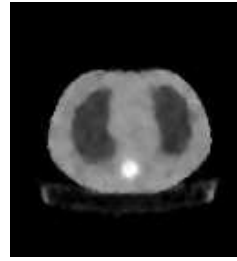
3.55

p3x

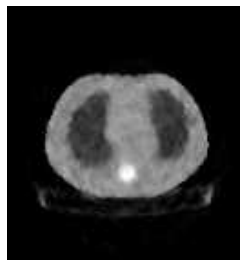
# TRIOT Example: Attenuation Map Images



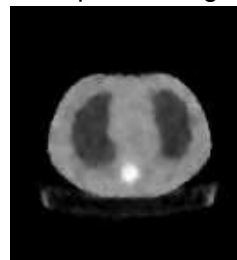
FBP



PL optimal image



OS-SPS



TRIOT-PC

OS-SPS: 64 subsets, 20 iterations, one point of the limit cycle

TRIOT-PC: 64 subsets, 20 iterations, after 2 iterations of OS-SPS

3.56

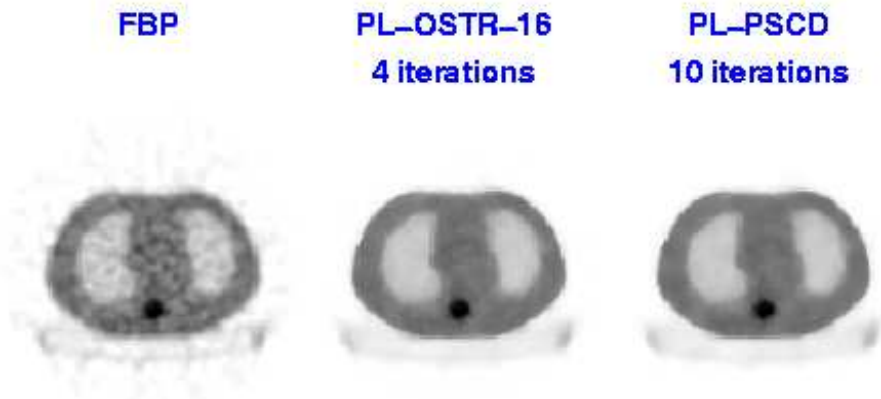
© J. Fessler, May 12, 2008

3.56

p3x

# OSTR aka Transmission OS-SPS

Ordered subsets for PET/SPECT transmission scans [248], and for X-ray CT [48].



Ordered subsets version of separable paraboloidal surrogates for PET transmission problem with nonquadratic convex regularization

Matlab m-file [http://www.eecs.umich.edu/~fessler/irt/irt/transmission/tpl\\_os\\_sps.m](http://www.eecs.umich.edu/~fessler/irt/irt/transmission/tpl_os_sps.m)

3.57

© J. Fessler, May 12, 2008

3.57

p3x

## Precomputed curvatures for OS-SPS

Separable Paraboloidal Surrogate (SPS) Algorithm:

$$x_j^{(n+1)} = \left[ x_j^{(n)} - \frac{\sum_{i=1}^{n_d} a_{ij} \dot{h}_i([\mathbf{A}\mathbf{x}^{(n)}]_i)}{\sum_{i=1}^{n_d} a_{ij} |a_i c_i^{(n)}} \right]_+, \quad j = 1, \dots, n_p$$

Ordered-subsets abandons monotonicity, so why use optimal curvatures  $c_i^{(n)}$ ?

Precomputed curvature:

$$c_i = \dot{h}_i(\hat{l}_i), \quad \hat{l}_i = \arg \min_l h_i(l)$$

Precomputed denominator (saves one backprojection each iteration!):

$$d_j = \sum_{i=1}^{n_d} a_{ij} |a_i c_i, \quad j = 1, \dots, n_p.$$

OS-SPS algorithm with  $M$  subsets:

$$x_j^{(n+1)} = \left[ x_j^{(n)} - \frac{\sum_{i \in S^{(n)}} a_{ij} \dot{h}_i([\mathbf{A}\mathbf{x}^{(n)}]_i)}{d_j / M} \right]_+, \quad j = 1, \dots, n_p$$

3.58

© J. Fessler, May 12, 2008

3.58

p3x

Precomputed parabola surrogate curvature for transmission problem and ordered subsets [220, 248].

For emission problem,  $c_i \approx 1/y_i$ .

For transmission problem,  $c_i \approx y_i$ .

Precomputed curvatures combined with suitable relaxation yields guaranteed convergence for convex problems [243].

## Summary of Algorithms

- General-purpose optimization algorithms
- Optimization transfer for image reconstruction algorithms
- Separable surrogates  $\implies$  high curvatures  $\implies$  slow convergence
- Ordered subsets accelerate *initial* convergence  
require relaxation or incrementalism for true convergence
- Principles apply to emission and transmission reconstruction
- Still work to be done...

Matlab/Freemat “image reconstruction toolbox” online:  
<http://www.eecs.umich.edu/~fessler/code>

### An Open Problem

Still no algorithm with all of the following properties:

- Nonnegativity easy
- Fast converging
- Intrinsically monotone global convergence
- Accepts any type of system matrix
- Parallelizable

3.59

---

Until an “ideal” algorithm is developed, OSEM will probably remain very popular...

---

© J. Fessler, May 12, 2008

3.59

p3x

## Part 4. Performance Characteristics

Easy case: MRI with quadratic regularization

- Spatial resolution properties
- Noise properties

General case

- Spatial resolution properties
- Noise properties
- Detection properties

4a.1

© J. Fessler, May 12, 2008

4a.1

p4mri

## Regularized Least-Squares Estimation

Estimate object by minimizing a *regularized* cost function:

$$\hat{\mathbf{x}} = \arg \min_{\mathbf{x} \in \mathbb{C}^{np}} \Psi(\mathbf{x}), \quad \Psi(\mathbf{x}) = \|\mathbf{y} - \mathbf{Ax}\|^2 + \alpha R(\mathbf{x})$$

- data fit term  $\|\mathbf{y} - \mathbf{Ax}\|^2$   
corresponds to negative log-likelihood of Gaussian distribution
- regularizing term  $R(\mathbf{x})$  controls noise by penalizing roughness,

$$\text{e.g. : } R(\mathbf{x}) \approx \int \|\nabla f\|^2 d\vec{r}$$

- regularization parameter  $\alpha > 0$   
controls tradeoff between spatial resolution and noise
- Equivalent to Bayesian MAP estimation with prior  $\propto e^{-\alpha R(\mathbf{x})}$

Complexities:

- choosing  $R(f)$
- choosing  $\alpha$
- computing minimizer rapidly.

4a.2

© J. Fessler, May 12, 2008

4a.2

p4mri

## Quadratic regularization

1D example: squared differences between neighboring pixel values:

$$R(f) = \sum_{j=2}^{n_p} \frac{1}{2} |f_j - f_{j-1}|^2.$$

In matrix-vector notation,  $R(\mathbf{x}) = \frac{1}{2} \|\mathbf{Cx}\|^2$  where

$$\mathbf{C} = \begin{bmatrix} -1 & 1 & 0 & 0 & \dots & 0 \\ 0 & -1 & 1 & 0 & \dots & 0 \\ & & & \ddots & \ddots & \\ 0 & \dots & 0 & 0 & -1 & 1 \end{bmatrix}, \text{ so } \mathbf{Cx} = \begin{bmatrix} x_2 - x_1 \\ \vdots \\ x_N - x_{N-1} \end{bmatrix}.$$

For 2D and higher-order differences, modify differencing matrix  $\mathbf{C}$ .

Leads to closed-form solution:

$$\begin{aligned} \hat{\mathbf{x}} &= \arg \min_{\mathbf{x}} \|\mathbf{y} - \mathbf{Ax}\|^2 + \alpha \|\mathbf{Cx}\|^2 \\ &= [\mathbf{A}'\mathbf{A} + \alpha \mathbf{C}'\mathbf{C}]^{-1} \mathbf{A}'\mathbf{y}. \end{aligned}$$

(a formula of limited practical use for computing  $\hat{\mathbf{x}}$ )

4a.3

© J. Fessler, May 12, 2008

4a.3

p4mri



# Choosing the Regularization Parameter

Spatial resolution analysis (Fessler & Rogers, IEEE T-IP, 1996):

$$\hat{x} = [A'A + \alpha C'C]^{-1} A'y$$

$$E[\hat{x}] = [A'A + \alpha C'C]^{-1} A'E[y]$$

$$E[\hat{x}] = \underbrace{[A'A + \alpha C'C]^{-1} A'A}_{\text{blur}} x$$

$A'A$  and  $C'C$  are Toeplitz  $\implies$  blur is approximately shift-invariant.

Frequency response of blur:

$$L(\omega) = \frac{H(\omega)}{H(\omega) + \alpha R(\omega)}$$

- $H(\omega_k) = \text{FFT}(A'A e_j)$  (lowpass)
- $R(\omega_k) = \text{FFT}(C'C e_j)$  (highpass)

Adjust  $\alpha$  to achieve desired spatial resolution.

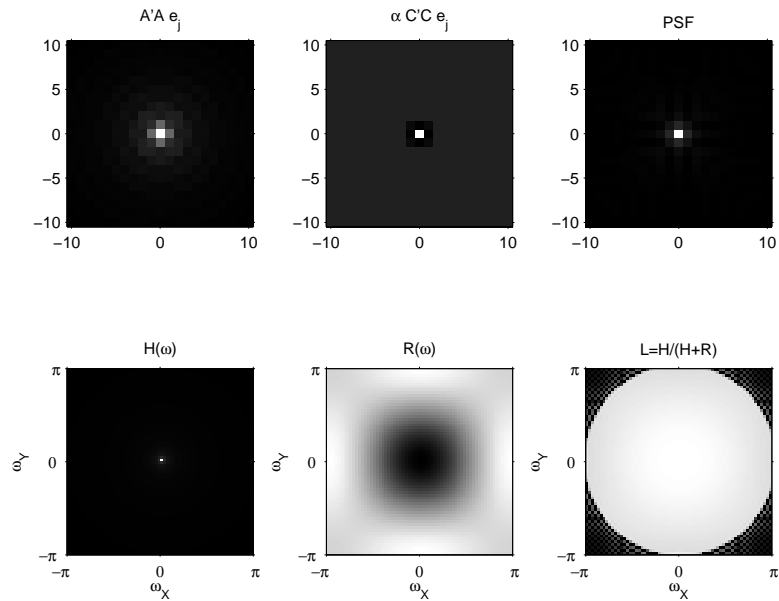
4a.4

© J. Fessler, May 12, 2008

4a.4

p4mri

## Spatial Resolution Example



Radial k-space trajectory, FWHM of PSF is 1.2 pixels

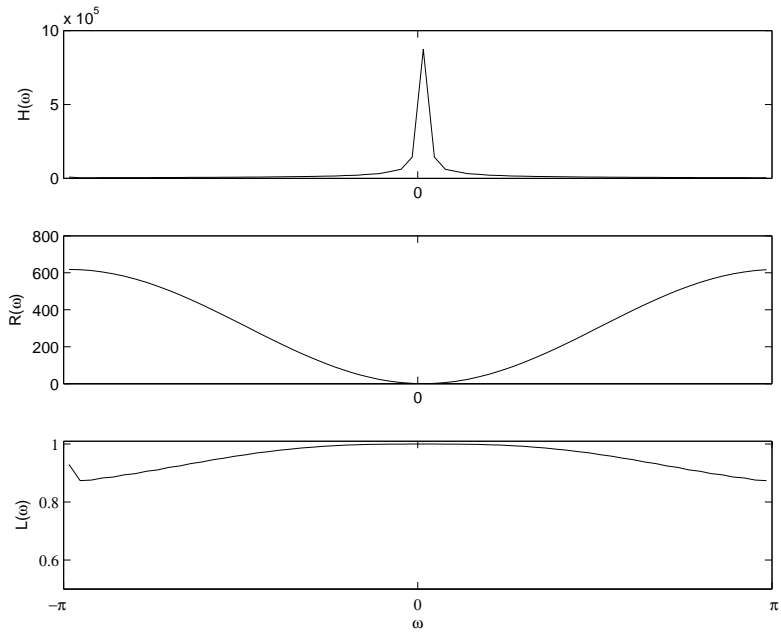
4a.5

© J. Fessler, May 12, 2008

4a.5

p4mri

### Spatial Resolution Example: Profiles



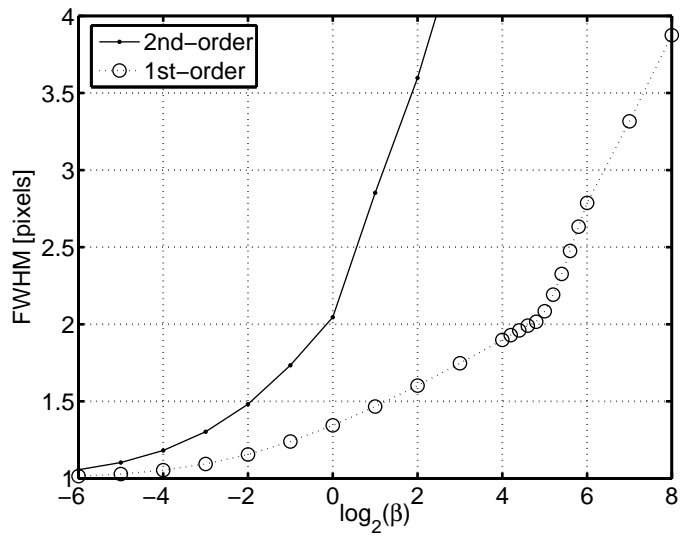
4a.6

© J. Fessler, May 12, 2008

4a.6

p4mri

### Tabulating Spatial Resolution vs Regularization



Trajectory specific, but easily computed using a few FFTs  
Works only for quadratic regularization

4a.7

© J. Fessler, May 12, 2008

4a.7

p4mri

## Resolution/noise tradeoffs

Noise analysis:

$$\text{Cov}\{\hat{\mathbf{x}}\} = [\mathbf{A}'\mathbf{A} + \alpha\mathbf{C}'\mathbf{C}]^{-1} \mathbf{A}' \text{Cov}\{\mathbf{y}\} \mathbf{A} [\mathbf{A}'\mathbf{A} + \alpha\mathbf{C}'\mathbf{C}]^{-1}$$

Using circulant approximations to  $\mathbf{A}'\mathbf{A}$  and  $\mathbf{C}'\mathbf{C}$  yields:

$$\text{Var}\{\hat{x}_j\} \approx \sigma_\varepsilon^2 \sum_k \frac{H(\omega_k)}{(H(\omega_k) + \alpha R(\omega_k))^2}$$

- $H(\omega_k) = \text{FFT}(\mathbf{A}'\mathbf{A} e_j)$  (lowpass)
- $R(\omega_k) = \text{FFT}(\mathbf{C}'\mathbf{C} e_j)$  (highpass)

⇒ Predicting reconstructed image noise requires just 2 FFTs.  
(cf. gridding approach?)

Adjust  $\alpha$  to achieve desired spatial resolution / noise tradeoff.

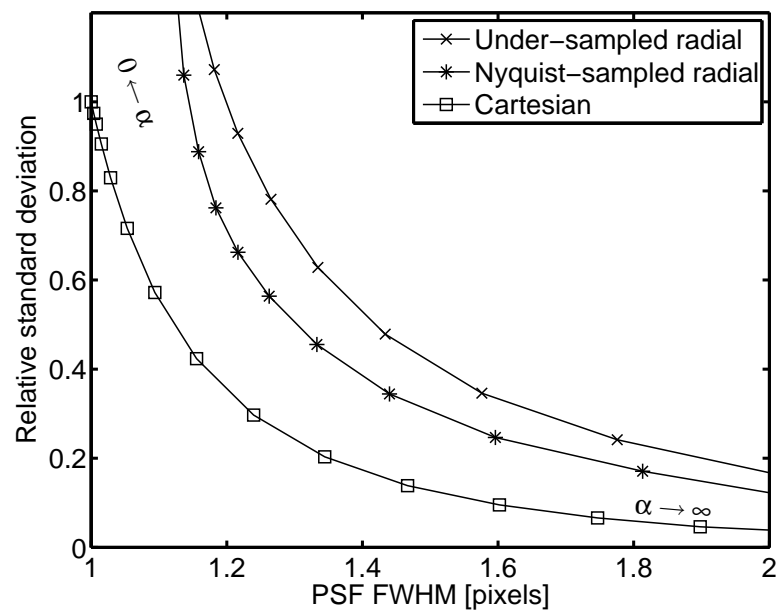
4a.8

© J. Fessler, May 12, 2008

4a.8

p4mri

### Resolution/Noise Tradeoff Example



In short: one can choose  $\alpha$  rapidly and predictably for quadratic regularization.

4a.9

© J. Fessler, May 12, 2008

4a.9

p4mri

## Part 4. Performance Characteristics

### (General case)

- Spatial resolution properties
- Noise properties
- Detection properties

4b.1

### Spatial Resolution Properties

Choosing  $\beta$  can be painful, so ...

For true minimization methods:

$$\hat{\mathbf{x}} = \arg \min_{\mathbf{x}} \Psi(\mathbf{x})$$

the *local impulse response* is approximately (Fessler and Rogers, T-MI, 1996):

$$\mathbf{l}_j(\mathbf{x}) = \lim_{\delta \rightarrow 0} \frac{E[\hat{\mathbf{x}}|\mathbf{x} + \delta \mathbf{e}_j] - E[\hat{\mathbf{x}}|\mathbf{x}]}{\delta} \approx [-\nabla^2 \Psi]^{-1} \nabla \Psi \frac{\partial}{\partial x_j} \bar{\mathbf{y}}(\mathbf{x}).$$

Depends only on chosen cost function and statistical model.

Independent of optimization algorithm (if iterated “to convergence”).

- Enables prediction of resolution properties (provided  $\Psi$  is minimized)
- Useful for designing regularization penalty functions with desired resolution properties. For penalized likelihood:

$$\mathbf{l}_j(\mathbf{x}) \approx [\mathbf{A}'\mathbf{W}\mathbf{A} + \beta\mathbf{R}]^{-1} \mathbf{A}'\mathbf{W}\mathbf{A}\mathbf{x}^{\text{true}}.$$

- Helps choose  $\beta$  for desired spatial resolution

4b.2

© J. Fessler, May 12, 2008

4b.1

p4prop

[38, 151, 249]

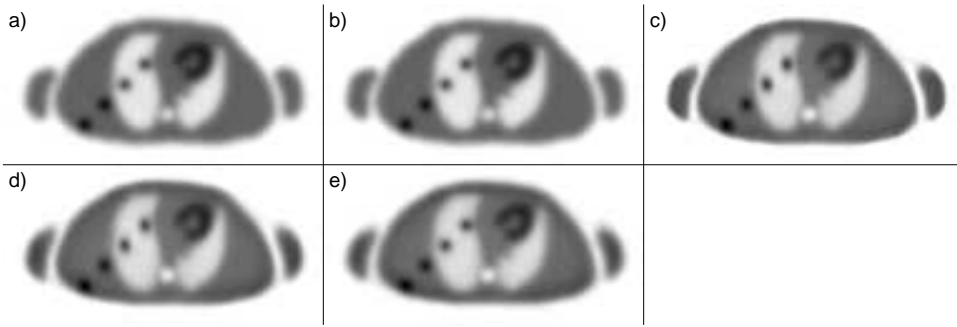
A commonly cited disadvantage of regularized methods is the need to select the regularization parameter  $\beta$ . One must also select the cutoff frequency for FBP, but at least that value is intuitive and works the same (resolution-wise) for all patients. Not so for stopping rules. The analysis in [38, 151, 249] brings some of the consistency of FBP-like resolution selection to statistical methods.

© J. Fessler, May 12, 2008

4b.2

p4prop

## Modified Penalty Example, PET



- a) filtered backprojection
- b) Penalized unweighted least-squares
- c) PWLS with conventional regularization
- d) PWLS with certainty-based penalty (Fessler & Rogers, 1996, T-MI)
- e) PWLS with modified penalty (Stayman & Fessler, 2000, T-MI)

4b.3

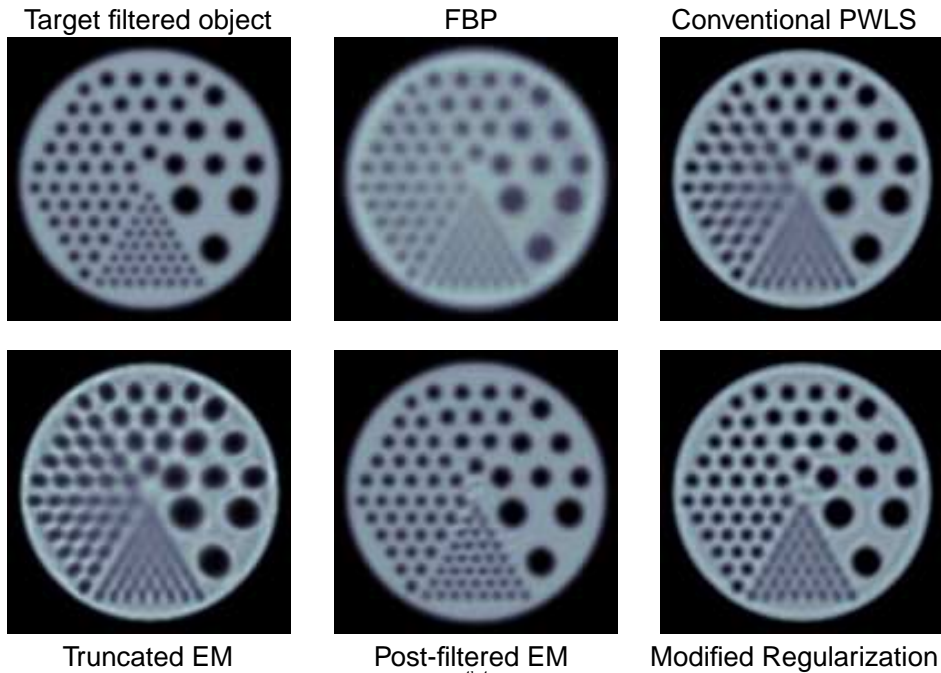
Figure from [151]. Certainty-based in [38].

4b.3

© J. Fessler, May 12, 2008

p4prop

## Modified Penalty Example, SPECT - Noiseless



4b.4

Figure from [152].

4b.4

© J. Fessler, May 12, 2008

p4prop

## Modified Penalty Example, SPECT - Noisy

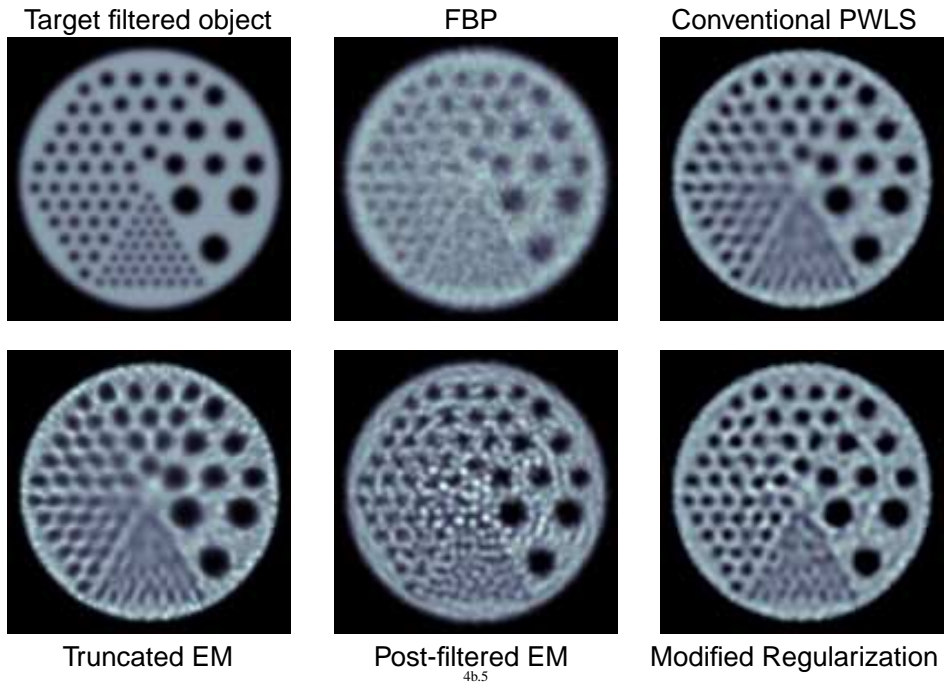


Figure from [152].

These were preliminary results, and they initially casted doubt on the claim sometimes made that post-filtered EM (or OSEM) is equivalent to truly regularized image reconstruction.

However, it turns out we had not matched spatial resolution as carefully as needed...

See [153, 250].

## Regularized vs Post-filtered, with Matched PSF

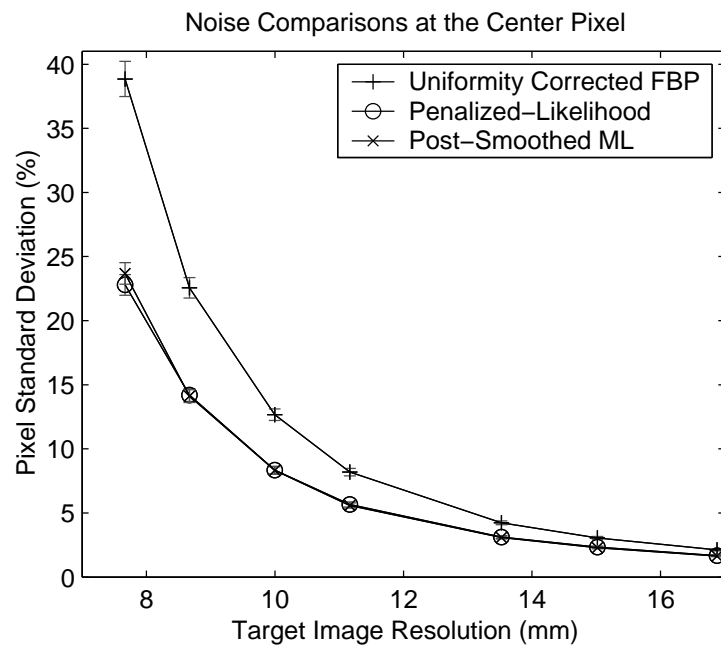


Figure from [153].

## Reconstruction Noise Properties

For unconstrained (converged) minimization methods, the estimator is *implicit*:

$$\hat{\mathbf{x}} = \hat{\mathbf{x}}(\mathbf{y}) = \arg \min_{\mathbf{x}} \Psi(\mathbf{x}, \mathbf{y}).$$

What is  $\text{Cov}\{\hat{\mathbf{x}}\}$ ?

New simpler derivation.

Denote the column gradient by  $g(\mathbf{x}, \mathbf{y}) \triangleq \nabla_{\mathbf{x}} \Psi(\mathbf{x}, \mathbf{y})$ .

Ignoring constraints, the gradient is zero at the minimizer:  $g(\hat{\mathbf{x}}(\mathbf{y}), \mathbf{y}) = \mathbf{0}$ .

First-order Taylor series expansion:

$$\begin{aligned} g(\hat{\mathbf{x}}, \mathbf{y}) &\approx g(\mathbf{x}^{\text{true}}, \mathbf{y}) + \nabla_{\mathbf{x}} g(\mathbf{x}^{\text{true}}, \mathbf{y})(\hat{\mathbf{x}} - \mathbf{x}^{\text{true}}) \\ &= g(\mathbf{x}^{\text{true}}, \mathbf{y}) + \nabla_{\mathbf{x}}^2 \Psi(\mathbf{x}^{\text{true}}, \mathbf{y})(\hat{\mathbf{x}} - \mathbf{x}^{\text{true}}). \end{aligned}$$

Equating to zero:

$$\hat{\mathbf{x}} \approx \mathbf{x}^{\text{true}} - [\nabla_{\mathbf{x}}^2 \Psi(\mathbf{x}^{\text{true}}, \mathbf{y})]^{-1} \nabla_{\mathbf{x}} \Psi(\mathbf{x}^{\text{true}}, \mathbf{y}).$$

If the Hessian  $\nabla^2 \Psi$  is weakly dependent on  $\mathbf{y}$ , then

$$\text{Cov}\{\hat{\mathbf{x}}\} \approx [\nabla_{\mathbf{x}}^2 \Psi(\mathbf{x}^{\text{true}}, \bar{\mathbf{y}})]^{-1} \text{Cov}\{\nabla_{\mathbf{x}} \Psi(\mathbf{x}^{\text{true}}, \mathbf{y})\} [\nabla_{\mathbf{x}}^2 \Psi(\mathbf{x}^{\text{true}}, \bar{\mathbf{y}})]^{-1}.$$

If we further linearize w.r.t. the data:  $g(\mathbf{x}, \mathbf{y}) \approx g(\mathbf{x}, \bar{\mathbf{y}}) + \nabla_{\mathbf{y}} g(\mathbf{x}, \bar{\mathbf{y}})(\mathbf{y} - \bar{\mathbf{y}})$ , then

$$\text{Cov}\{\hat{\mathbf{x}}\} \approx [\nabla_{\mathbf{x}}^2 \Psi]^{-1} (\nabla_{\mathbf{x}} \nabla_{\mathbf{y}} \Psi) \text{Cov}\{\mathbf{y}\} (\nabla_{\mathbf{x}} \nabla_{\mathbf{y}} \Psi)' [\nabla_{\mathbf{x}}^2 \Psi]^{-1}.$$

4b.7

© J. Fessler, May 12, 2008

4b.7

p4prop

## Covariance Continued

Covariance approximation:

$$\text{Cov}\{\hat{\mathbf{x}}\} \approx [\nabla_{\mathbf{x}}^2 \Psi(\mathbf{x}^{\text{true}}, \bar{\mathbf{y}})]^{-1} \text{Cov}\{\nabla_{\mathbf{x}} \Psi(\mathbf{x}^{\text{true}}, \mathbf{y})\} [\nabla_{\mathbf{x}}^2 \Psi(\mathbf{x}^{\text{true}}, \bar{\mathbf{y}})]^{-1}$$

Depends only on chosen cost function and statistical model.

Independent of optimization algorithm.

- Enables prediction of noise properties
- Can make variance images
- Useful for computing ROI variance (e.g., for weighted kinetic fitting)
- Good variance prediction for quadratic regularization in nonzero regions
- Inaccurate for nonquadratic penalties, or in nearly-zero regions

4b.8

© J. Fessler, May 12, 2008

4b.8

p4prop

---

The latter approximation was derived in [37].

---



---

Qi has developed an approximation that may help with the nonnegativity constraint [251].

---

# Detection Analysis

Qi and Huesman (IEEE T-MI, Aug. 2001) showed analytically:  
 SNR of MAP reconstruction > SNR of FBP reconstruction

- quadratic regularization
- SKE/BKE task
- prewhitened observer
- non-prewhitened observer

## Open issues

Choice of regularizer to optimize detectability?  
 Active work in several groups.

Qi's theoretical predictions are consistent with some empirical results, e.g., [252].

See recent detection analyses papers, e.g., [44, 253–258].

4b.9

© J. Fessler, May 12, 2008

4b.9

p4prop

## Choosing $\beta$ : Unknown location

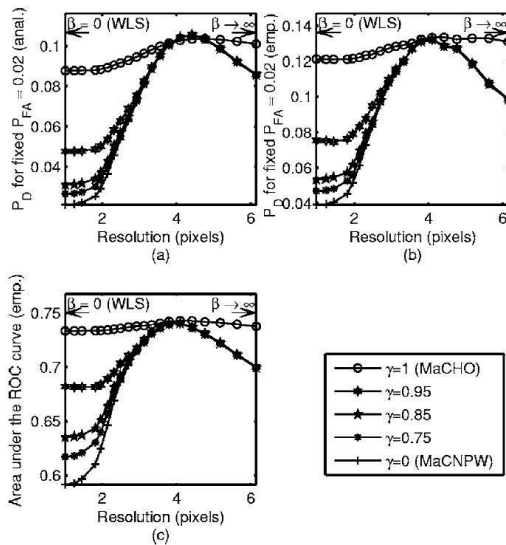


Fig. 2. Detection performance of MaCPPW observers versus QPWLS reconstruction resolution:  $P_D$  obtained analytically (a),  $P_D$  obtained empirically (b), and AUC obtained empirically (c). Results are shown for five different degrees of prewhitening accuracy. The search area is a disk with a diameter of 9 pixels.

4b.10

AUC for signal detection with unknown location task.  
 Yendiki & Fessler, JOSA-A 24(12):B199, Dec. 2007

© J. Fessler, May 12, 2008

4b.10

p4prop



## Summary of Performance Analysis

---

---

Spatial resolution / noise variance and covariance / AUC for signal detection:  
all (somewhat) predictable based on properties of *cost function*  $\Psi$ .  
(Provided an iterative algorithm is run “to convergence” to find minimizer of  $\Psi$ .)

This predictability also motivates regularized cost functions.  
(*cf.* unregularized cost function with a stopping rule.)

4b.11

© J. Fessler, May 12, 2008

4b.11

p4prop

## Part: Application examples

---

---

- X-ray CT
- MRI

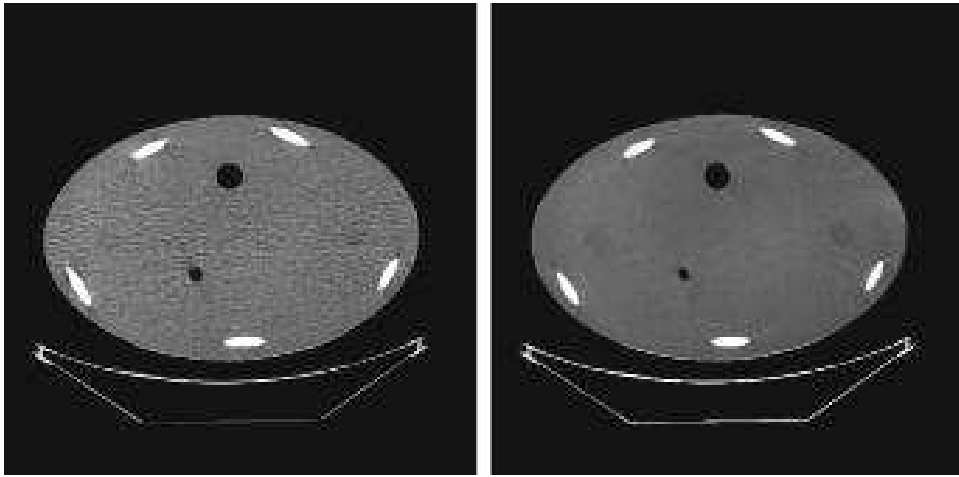
5.1

© J. Fessler, May 12, 2008

5.1

p6app

### Example: X-ray Helical CT



Left: FBP

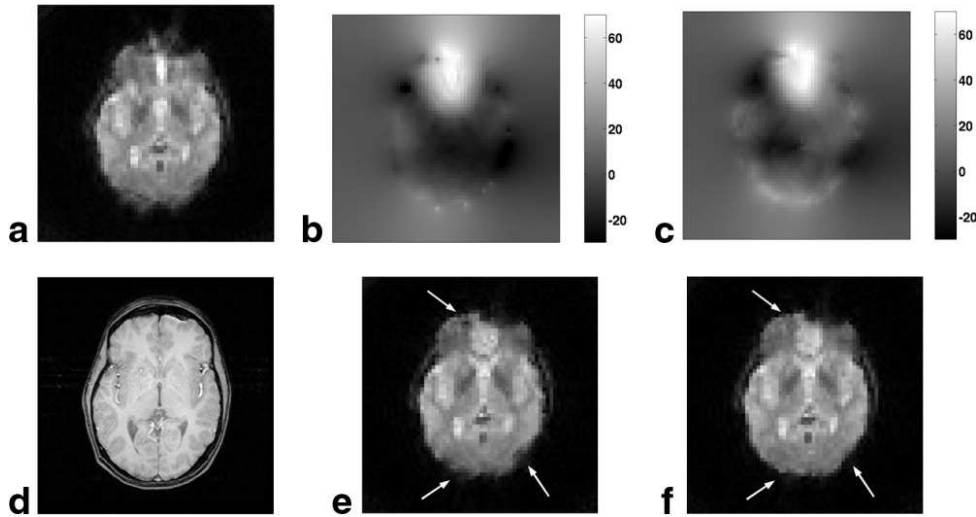
Right: PWLS-ICD, edge-preserving

Thibault *et al.*, Med Phys. 34(11):4526, Nov. 2007

5.2

[223]

### Example: fMRI with Joint Estimation of Fieldmap



(a) uncorr., (b) std. map, (c) joint map, (d) T1 ref, (e) using std, (f) using joint.

PWLS-CG with quadratic regularization.  $\beta$  chosen by PSF analysis.  
Sutton *et al.*, MRM 51(6):1194, Jun. 2004

5.3

© J. Fessler, May 12, 2008

5.2

p6app

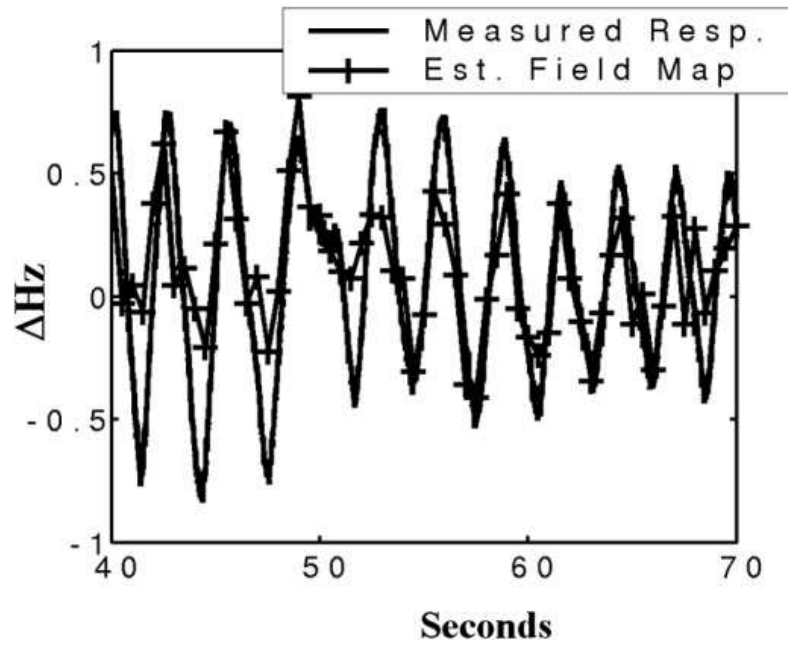
[53]

© J. Fessler, May 12, 2008

5.3

p6app

## Tracking Respiration-Induced Field Changes



5.4

© J. Fessler, May 12, 2008

5.4

p6app

## Other Topics

- Dynamic image sequence reconstruction / 4D regularization
- Motion and/or dynamic contrast changes

### Dynamic reconstruction

- nonlinear models [62, 65, 68, 259–271]
- linear models [272–281]
- KL-based approaches [282–288]
- Motion/gating [289]

5.5

© J. Fessler, May 12, 2008

5.5

p.other

# Summary

- Iterative reconstruction has had clinical impact in PET and SPECT
- MRI and X-ray CT may be next?
- todo: Still work to be done...



5.6

## References

- [1] S. Webb. *From the watching of shadows: the origins of radiological tomography*. A. Hilger, Bristol, 1990.
- [2] H. H. Barrett and K. J. Myers. *Foundations of image science*. Wiley, New York, 2003.
- [3] J. Kay. The EM algorithm in medical imaging. *Stat. Meth. Med. Res.*, 6(1):55–75, January 1997.
- [4] J. A. Fessler. Statistical image reconstruction methods for transmission tomography. In M. Sonka and J. Michael Fitzpatrick, editors, *Handbook of Medical Imaging, Volume 2. Medical Image Processing and Analysis*, pages 1–70. SPIE, Bellingham, 2000.
- [5] R. M. Leahy and J. Qi. Statistical approaches in quantitative positron emission tomography. *Statistics and Computing*, 10(2):147–65, April 2000.
- [6] M. Defrise. A short reader's guide to 3D tomographic reconstruction. *Computerized Medical Imaging and Graphics*, 25(2):113–6, March 2001.
- [7] S. Vandenberghe, Y. D'Asseler, R. V. Walle, T. Kauppinen, M. Koole, L. Bouwens, K. V. Laere, I. Lemahieu, and R. A. Dierckx. Iterative reconstruction algorithms in nuclear medicine. *Computerized Medical Imaging and Graphics*, 25(2):105–11, March 2001.
- [8] G. L. Zeng. Image reconstruction, a tutorial. *Computerized Medical Imaging and Graphics*, 25(2):97–103, March 2001.
- [9] R. M. Lewitt and S. Matej. Overview of methods for image reconstruction from projections in emission computed tomography. *Proc. IEEE*, 91(10):1588–611, October 2003.
- [10] R. N. Bracewell. Strip integration in radio astronomy. *Aust. J. Phys.*, 9:198–217, 1956.
- [11] D. E. Kuhl and R. Q. Edwards. Image separation radioisotope scanning. *Radiology*, 80:653–62, 1963.
- [12] G. Hounsfield. A method of apparatus for examination of a body by radiation such as x-ray or gamma radiation, 1972. US Patent 1283915. British patent 1283915, London.
- [13] D. C. Solmon. The X-ray transform. *J. Math. Anal. Applic.*, 56(1):61–83, October 1976.
- [14] G. Muehlethner and R. A. Wetzel. Section imaging by computer calculation. *J. Nuc. Med.*, 12(2):76–85, February 1971.
- [15] D. E. Kuhl, R. Q. Edwards, A. R. Ricci, and M. Reivich. Quantitative section scanning using orthogonal tangent correction. *J. Nuc. Med.*, 14(4):196–200, April 1973.
- [16] R. Gordon, R. Bender, and G. T. Herman. Algebraic reconstruction techniques (ART) for the three-dimensional electron microscopy and X-ray photography. *J. Theor. Biol.*, 29(3):471–81, December 1970.
- [17] R. Gordon and G. T. Herman. Reconstruction of pictures from their projections. *Comm. ACM*, 14(12):759–68, December 1971.
- [18] G. T. Herman, A. Lent, and S. W. Rowland. ART: mathematics and applications (a report on the mathematical foundations and on the applicability to real data of the algebraic reconstruction techniques). *J. Theor. Biol.*, 42(1):1–32, November 1973.
- [19] R. Gordon. A tutorial on ART (algebraic reconstruction techniques). *IEEE Trans. Nuc. Sci.*, 21(3):78–93, June 1974.
- [20] W. H. Richardson. Bayesian-based iterative method of image restoration. *J. Opt. Soc. Am.*, 62(1):55–9, January 1972.
- [21] L. Lucy. An iterative technique for the rectification of observed distributions. *The Astronomical Journal*, 79(6):745–54, June 1974.
- [22] A. J. Rockmore and A. Macovski. A maximum likelihood approach to emission image reconstruction from projections. *IEEE Trans. Nuc. Sci.*, 23:1428–32, 1976.
- [23] A. J. Rockmore and A. Macovski. A maximum likelihood approach to transmission image reconstruction from projections. *IEEE Trans. Nuc. Sci.*, 24(3):1929–35, June 1977.
- [24] A. P. Dempster, N. M. Laird, and D. B. Rubin. Maximum likelihood from incomplete data via the EM algorithm. *J. Royal Stat. Soc. Ser. B*, 39(1):1–38, 1977.
- [25] L. A. Shepp and Y. Vardi. Maximum likelihood reconstruction for emission tomography. *IEEE Trans. Med. Imag.*, 1(2):113–22, October 1982.
- [26] K. Lange and R. Carson. EM reconstruction algorithms for emission and transmission tomography. *J. Comp. Assisted Tomo.*, 8(2):306–16, April 1984.
- [27] S. Geman and D. E. McClure. Bayesian image analysis: an application to single photon emission tomography. In *Proc. of Stat. Comp. Sect. of Amer. Stat. Assoc.*, pages 12–8, 1985.
- [28] H. M. Hudson and R. S. Larkin. Accelerated image reconstruction using ordered subsets of projection data. *IEEE Trans. Med. Imag.*, 13(4):601–9, December 1994.
- [29] M. Goitein. Three-dimensional density reconstruction from a series of two-dimensional projections. *Nucl. Instr. Meth.*, 101(3):509–18, June 1972.
- [30] T. F. Budinger and G. T. Gulberg. Three dimensional reconstruction in nuclear medicine emission imaging. *IEEE Trans. Nuc. Sci.*, 21(3):2–20, June 1974.
- [31] R. H. Huesman, G. T. Gulberg, W. L. Greenberg, and T. F. Budinger. *RECLBL library users manual*. Lawrence Berkeley Laboratory, Berkeley, CA, 1977.
- [32] R. H. Huesman. A new fast algorithm for the evaluation of regions of interest and statistical uncertainty in computed tomography. *Phys. Med. Biol.*, 29(5):543–52,

B.1

© J. Fessler, May 12, 2008

- May 1984.
- [33] D. W. Wilson and B. M. W. Tsui. Noise properties of filtered-backprojection and ML-EM reconstructed emission tomographic images. *IEEE Trans. Nuc. Sci.*, 40(4):1198–1203, August 1993.
- [34] D. W. Wilson and B. M. W. Tsui. Spatial resolution properties of FB and ML-EM reconstruction methods. In *Proc. IEEE Nuc. Sci. Symp. Med. Im. Conf.*, volume 2, pages 1189–93, 1993.
- [35] H. H. Barrett, D. W. Wilson, and B. M. W. Tsui. Noise properties of the EM algorithm: I. Theory. *Phys. Med. Biol.*, 39(5):833–46, May 1994.
- [36] D. W. Wilson, B. M. W. Tsui, and H. H. Barrett. Noise properties of the EM algorithm: II. Monte Carlo simulations. *Phys. Med. Biol.*, 39(5):847–72, May 1994.
- [37] J. A. Fessler. Mean and variance of implicitly defined biased estimators (such as penalized maximum likelihood): Applications to tomography. *IEEE Trans. Im. Proc.*, 5(3):493–506, March 1996.
- [38] J. A. Fessler and W. L. Rogers. Spatial resolution properties of penalized-likelihood image reconstruction methods: Space-invariant tomographs. *IEEE Trans. Im. Proc.*, 5(9):1346–58, September 1996.
- [39] W. Wang and G. Gindi. Noise analysis of regularized EM SPECT reconstruction. In *Proc. IEEE Nuc. Sci. Symp. Med. Im. Conf.*, volume 3, pages 1933–7, 1996.
- [40] C. K. Abbey, E. Clarkson, H. H. Barrett, S. P. Mueller, and F. J. Rybicki. Approximate distributions for maximum likelihood and maximum a posteriori estimates under a Gaussian noise model. In J. Duncan and G. Gindi, editors, *Information Processing in Medical Im.*, pages 167–75. Springer-Verlag, Berlin, 1997.
- [41] W. Wang and G. Gindi. Noise analysis of MAP-EM algorithms for emission tomography. *Phys. Med. Biol.*, 42(11):2215–32, November 1997.
- [42] S. J. Glick and E. J. Soares. Noise characteristics of SPECT iterative reconstruction with a mis-matched projector-backprojector pair. *IEEE Trans. Nuc. Sci.*, 45(4):2183–8, August 1998.
- [43] E. J. Soares, C. L. Byrne, T.-S. Pan, S. J. Glick, and M. A. King. Modeling the population covariance matrices of block-iterative expectation-maximization reconstructed images. In *Proc. SPIE 3034, Med. Im. 1997: Im. Proc.*, pages 415–25, 1997.
- [44] J. Qi and R. H. Huesman. Theoretical study of lesion detectability of MAP reconstruction using computer observers. *IEEE Trans. Med. Imag.*, 20(8):815–22, August 2001.
- [45] D. Brasse, P. E. Kinahan, R. Clackdoyle, M. Defrise, C. Comtat, and D. W. Townsend. Fast fully 3-D image reconstruction in PET using planograms. *IEEE Trans. Med. Imag.*, 23(4):413–25, April 2004.
- [46] J. A. Fessler, I. Elbakri, P. Sukovic, and N. H. Clinthorne. Maximum-likelihood dual-energy tomographic image reconstruction. In *Proc. SPIE 4684, Medical Imaging 2002: Image Proc.*, volume 1, pages 38–49, 2002.
- [47] B. De Man, J. Nuyts, P. Dupont, G. Marchal, and P. Suetens. An iterative maximum-likelihood polychromatic algorithm for CT. *IEEE Trans. Med. Imag.*, 20(10):999–1008, October 2001.
- [48] I. A. Elbakri and J. A. Fessler. Statistical image reconstruction for polyenergetic X-ray computed tomography. *IEEE Trans. Med. Imag.*, 21(2):89–99, February 2002.
- [49] I. A. Elbakri and J. A. Fessler. Segmentation-free statistical image reconstruction for polyenergetic X-ray computed tomography with experimental validation. *Phys. Med. Biol.*, 48(15):2543–78, August 2003.
- [50] P. E. Kinahan, J. A. Fessler, and J. S. Karp. Statistical image reconstruction in PET with compensation for missing data. *IEEE Trans. Nuc. Sci.*, 44(4):1552–7, August 1997.
- [51] J. A. Fessler and B. P. Sutton. Nonuniform fast Fourier transforms using min-max interpolation. *IEEE Trans. Sig. Proc.*, 51(2):560–74, February 2003.
- [52] B. P. Sutton, D. C. Noll, and J. A. Fessler. Fast, iterative image reconstruction for MRI in the presence of field inhomogeneities. *IEEE Trans. Med. Imag.*, 22(2):178–88, February 2003.
- [53] B. P. Sutton, D. C. Noll, and J. A. Fessler. Dynamic field map estimation using a spiral-in / spiral-out acquisition. *Mag. Res. Med.*, 51(6):1194–204, June 2004.
- [54] R. Van de Walle, H. H. Barrett, K. J. Myers, M. I. Altbach, B. Desplanques, A. F. Gmitro, J. Cornelis, and I. Lemahieu. Reconstruction of MR images from data acquired on a general non-regular grid by pseudoinverse calculation. *IEEE Trans. Med. Imag.*, 19(12):1160–7, December 2000.
- [55] B. W. Silverman. Some aspects of the spline smoothing approach to non-parametric regression curve fitting. *J. Royal Stat. Soc. Ser. B*, 47(1):1–52, 1985.
- [56] M. Bertero, C. De Mol, and E. R. Pike. Linear inverse problems with discrete data. I: General formulation and singular system analysis. *Inverse Prob.*, 1(4):301–30, November 1985.
- [57] K. M. Hanson and G. W. Wecksung. Local basis-function approach to computed tomography. *Appl. Optics*, 24(23):4028–39, December 1985.
- [58] E. J. Mazur and R. Gordon. Interpolative algebraic reconstruction techniques without beam partitioning for computed tomography. *Med. Biol. Eng. Comput.*, 33(1):82–6, January 1995.

5.6

p.summ

B.2

- [59] Y. Censor. Finite series expansion reconstruction methods. *Proc. IEEE*, 71(3):409–19, March 1983.
- [60] D. L. Snyder. Utilizing side information in emission tomography. *IEEE Trans. Nuc. Sci.*, 31(1):533–7, February 1984.
- [61] R. E. Carson, M. V. Green, and S. M. Larson. A maximum likelihood method for calculation of tomographic region-of-interest (ROI) values. *J. Nuc. Med. (Abs. Book)*, 26:P20, 1985.
- [62] R. E. Carson and K. Lange. The EM parametric image reconstruction algorithm. *J. Am. Stat. Assoc.*, 80(389):20–2, March 1985.
- [63] R. E. Carson. A maximum likelihood method for region-of-interest evaluation in emission tomography. *J. Comp. Assisted Tomo.*, 10(4):654–63, July 1986.
- [64] A. R. Formiconi. Least squares algorithm for region-of-interest evaluation in emission tomography. *IEEE Trans. Med. Imag.*, 12(1):90–100, March 1993.
- [65] B. W. Reutter, G. T. Gulberg, and R. H. Huesman. Kinetic parameter estimation from attenuated SPECT projection measurements. *IEEE Trans. Nuc. Sci.*, 45(6):3007–13, December 1998.
- [66] D. J. Rossi and A. S. Willsky. Reconstruction from projections based on detection and estimation of objects—Parts I & II: Performance analysis and robustness analysis. *IEEE Trans. Acoust. Sp. Sig. Proc.*, 32(4):886–906, August 1984.
- [67] S. P. Müller, M. F. Kijewski, S. C. Moore, and B. L. Holman. Maximum-likelihood estimation: a mathematical model for quantitation in nuclear medicine. *J. Nuc. Med.*, 31(10):1693–701, October 1990.
- [68] P. C. Chiao, W. L. Rogers, N. H. Clinthorne, J. A. Fessler, and A. O. Hero. Model-based estimation for dynamic cardiac studies using ECT. *IEEE Trans. Med. Imag.*, 13(2):217–26, June 1994.
- [69] Z. P. Liang, F. E. Boada, R. T. Constable, E. M. Haacke, P. C. Lauterbur, and M. R. Smith. Constrained reconstruction methods in MR imaging. *Reviews of Magnetic Resonance in Medicine*, 4:67–185, 1992.
- [70] G. S. Cunningham and A. Lehovich. 4D reconstructions from low-count SPECT data using deformable models with smooth interior intensity variations. In *Proc. SPIE 3979: Medical Imaging 2000: Image Proc.*, pages 564–74, 2000.
- [71] A. Yendiki and J. A. Fessler. A comparison of rotation- and blob-based system models for 3D SPECT with depth-dependent detector response. *Phys. Med. Biol.*, 49(11):2157–68, June 2004.
- [72] R. M. Lewitt. Multidimensional digital image representations using generalized Kaiser-Bessel window functions. *J. Opt. Soc. Am. A*, 7(10):1834–46, October 1990.
- [73] R. M. Lewitt. Alternatives to voxels for image representation in iterative reconstruction algorithms. *Phys. Med. Biol.*, 37(3):705–16, March 1992.
- [74] G. L. Zeng and G. T. Gulberg. Unmatched projector/backprojector pairs in an iterative reconstruction algorithm. *IEEE Trans. Med. Imag.*, 19(5):548–55, May 2000.
- [75] C. Kamphuis, F. J. Beekman, P. P. van Rijk, and M. A. Viergever. Dual matrix ordered subsets reconstruction for accelerated 3D scatter compensation in single-photon emission tomography. *Eur. J. Nuc. Med.*, 25(1):8–18, January 1998.
- [76] F. J. Beekman, H. W. A. M. de Jong, and S. van Geloven. Efficient fully 3D iterative SPECT reconstruction with Monte Carlo based scatter compensation. *IEEE Trans. Med. Imag.*, 21(8):867–77, August 2002.
- [77] R. Griesse and A. Walther. Evaluating gradients in optimal control: continuous adjoints versus automatic differentiation. *J. Optim. Theory Appl.*, 122(1):63–86, July 2004.
- [78] C. W. Stearns and J. A. Fessler. 3D PET reconstruction with FORE and WLS-OS-EM. In *Proc. IEEE Nuc. Sci. Symp. Med. Im. Conf.*, volume 2, pages 912–5, 2002.
- [79] M. Yavuz and J. A. Fessler. Objective functions for tomographic reconstruction from randoms-precorrected PET scans. In *Proc. IEEE Nuc. Sci. Symp. Med. Im. Conf.*, volume 2, pages 1067–71, 1996.
- [80] M. Yavuz and J. A. Fessler. New statistical models for randoms-precorrected PET scans. In J. Duncan and G. Gindi, editors, *Information Processing in Medical Im.*, volume 1230 of *Lecture Notes in Computer Science*, pages 190–203. Springer-Verlag, Berlin, 1997.
- [81] M. Yavuz and J. A. Fessler. Statistical image reconstruction methods for randoms-precorrected PET scans. *Med. Im. Anal.*, 2(4):369–78, December 1998.
- [82] M. Yavuz and J. A. Fessler. Penalized-likelihood estimators and noise analysis for randoms-precorrected PET transmission scans. *IEEE Trans. Med. Imag.*, 18(8):665–74, August 1999.
- [83] D. L. Snyder, A. M. Hammoud, and R. L. White. Image recovery from data acquired with a charge-coupled-device camera. *J. Opt. Soc. Am. A*, 10(5):1014–23, May 1993.
- [84] D. L. Snyder, C. W. Helstrom, A. D. Lanterman, M. Faisal, and R. L. White. Compensation for readout noise in CCD images. *J. Opt. Soc. Am. A*, 12(2):272–83, February 1995.
- [85] U. Engeland, T. Striker, and H. Luig. Count-rate statistics of the gamma camera. *Phys. Med. Biol.*, 43(10):2939–47, October 1998.
- [86] J. A. Fessler. Penalized weighted least-squares image reconstruction for positron emission tomography. *IEEE Trans. Med. Imag.*, 13(2):290–300, June 1994.
- [87] C. Comtat, P. E. Kinahan, M. Deprise, C. Michel, and D. W. Townsend. Fast reconstruction of 3D PET data with accurate statistical modeling. *IEEE Trans. Nuc. Sci.*, 45(3):1083–9, June 1998.
- [88] B. R. Whiting. Signal statistics in x-ray computed tomography. In *Proc. SPIE 4682, Medical Imaging 2002: Med. Phys.*, pages 53–60, 2002.
- [89] B. R. Whiting, L. J. Montagnino, and D. G. Politte. Modeling X-ray computed tomography sinograms, 2001. submitted to mp.
- [90] I. A. Elbakri and J. A. Fessler. Efficient and accurate likelihood for iterative image reconstruction in X-ray computed tomography. In *Proc. SPIE 5032, Medical Imaging 2003: Image Proc.*, pages 1839–50, 2003.
- [91] A. O. Hero, J. A. Fessler, and M. Usman. Exploring estimator bias-variance tradeoffs using the uniform CR bound. *IEEE Trans. Sig. Proc.*, 44(8):2026–41, August 1996.
- [92] Y. C. Eldar. Minimum variance in biased estimation: bounds and asymptotically optimal estimators. *IEEE Trans. Sig. Proc.*, 52(7):1915–30, July 2004.
- [93] E. Mumcuoglu, R. Leahy, S. Cherry, and E. Hoffman. Accurate geometric and physical response modeling for statistical image reconstruction in high resolution PET scanners. In *Proc. IEEE Nuc. Sci. Symp. Med. Im. Conf.*, volume 3, pages 1569–73, 1996.
- [94] J. Qi, R. M. Leahy, S. R. Cherry, A. Chatzioannou, and T. H. Farquhar. High resolution 3D Bayesian image reconstruction using the microPET small-animal scanner. *Phys. Med. Biol.*, 43(4):1001–14, April 1998.
- [95] G. Christ. Exact treatment of the dual-energy method in CT using polyenergetic X-ray spectra. *Phys. Med. Biol.*, 29(12):151–25, December 1984.
- [96] Z. Liang. Compensation for attenuation, scatter, and detector response in SPECT reconstruction via iterative FBP methods. *Med. Phys.*, 20(4):1097–106, July 1993.
- [97] X. L. Xu, J. S. Liow, and S. C. Strother. Iterative algebraic reconstruction algorithms for emission computed tomography: a unified framework and its application to positron emission tomography. *Med. Phys.*, 20(6):1675–84, November 1993.
- [98] J. W. Wallis and T. R. Miller. Rapidly converging iterative reconstruction algorithms in single-photon emission computed tomography. *J. Nuc. Med.*, 34(10):1793–800, October 1993.
- [99] P. J. Green. Iteratively reweighted least squares for maximum likelihood estimation, and some robust and resistant alternatives. *J. Royal Stat. Soc. Ser. B*, 46(2):143–92, 1984.
- [100] J. M. M. Anderson, B. A. Mair, M. Rao, and C. H. Wu. A weighted least-squares method for PET. In *Proc. IEEE Nuc. Sci. Symp. Med. Im. Conf.*, volume 2, pages 1292–6, 1995.
- [101] J. M. M. Anderson, B. A. Mair, M. Rao, and C. H. Wu. Weighted least-squares reconstruction methods for positron emission tomography. *IEEE Trans. Med. Imag.*, 16(2):159–65, April 1997.
- [102] P. J. Huber. *Robust statistics*. Wiley, New York, 1981.
- [103] C. Bouman and K. Sauer. A generalized Gaussian image model for edge-preserving MAP estimation. *IEEE Trans. Im. Proc.*, 2(3):296–310, July 1993.
- [104] E. Tanaka. Improved iterative image reconstruction with automatic noise artifact suppression. *IEEE Trans. Med. Imag.*, 11(1):21–7, March 1992.
- [105] B. W. Silverman, M. C. Jones, J. D. Wilson, and D. W. Nychka. A smoothed EM approach to indirect estimation problems, with particular reference to stereology and emission tomography. *J. Royal Stat. Soc. Ser. B*, 52(2):271–324, 1990.
- [106] T. R. Miller, J. W. Wallis, C. S. Butler, M. I. Miller, and D. L. Snyder. Improved brain SPECT by maximum-likelihood reconstruction. *J. Nuc. Med. (Abs. Book)*, 33(5):964, May 1992.
- [107] F. J. Beekman, E. T. P. Slijpen, and W. J. Niessen. Selection of task-dependent diffusion filters for the post-processing of SPECT images. *Phys. Med. Biol.*, 43(6):1713–30, June 1998.
- [108] D. S. Lalush and B. M. W. Tsui. Performance of ordered subset reconstruction algorithms under conditions of extreme attenuation and truncation in myocardial SPECT. *J. Nuc. Med.*, 41(4):737–44, April 2000.
- [109] E. T. P. Slijpen and F. J. Beekman. Comparison of post-filtering and filtering between iterations for SPECT reconstruction. *IEEE Trans. Nuc. Sci.*, 46(6):2233–8, December 1999.
- [110] R. H. Huesman. The effects of a finite number of projection angles and finite lateral sampling of projections on the propagation of statistical errors in transverse section reconstruction. *Phys. Med. Biol.*, 22(3):511–21, May 1977.
- [111] D. L. Snyder and M. I. Miller. The use of sieves to stabilize images produced with the EM algorithm for emission tomography. *IEEE Trans. Nuc. Sci.*, 32(5):3864–71, October 1985.
- [112] D. L. Snyder, M. I. Miller, L. J. Thomas, and D. G. Politte. Noise and edge artifacts in maximum-likelihood reconstructions for emission tomography. *IEEE Trans.*

B.3

B.4

- [113] T. R. Miller and J. W. Wallis. Clinically important characteristics of maximum-likelihood reconstruction. *J. Nuc. Med.*, 33(9):1678–84, September 1992.
- [114] A. Tikhonov and V. Arsenin. *Solution of ill-posed problems*. Wiley, New York, 1977.
- [115] I. Csizsar. Why least squares and maximum entropy? An axiomatic approach to inference for linear inverse problems. *Ann. Stat.*, 19(4):2032–66, 1991.
- [116] D. L. Donoho, I. M. Johnstone, A. S. Stern, and J. C. Hoch. Does the maximum entropy method improve sensitivity. *Proc. Natl. Acad. Sci.*, 87(13):5066–8, July 1990.
- [117] D. L. Donoho, I. M. Johnstone, J. C. Hoch, and A. S. Stern. Maximum entropy and the nearly black object. *J. Royal Stat. Soc. Ser. B*, 54(1):41–81, 1992.
- [118] R. T. Constable and R. M. Henkelman. Why MEM does not work in MR image reconstruction. *Mag. Res. Med.*, 14(1):12–25, April 1990.
- [119] A. R. De Pierro. A modified expectation maximization algorithm for penalized likelihood estimation in emission tomography. *IEEE Trans. Med. Imag.*, 14(1):132–7, March 1995.
- [120] A. H. Delaney and Y. Bresler. A fast and accurate Fourier algorithm for iterative parallel-beam tomography. *IEEE Trans. Im. Proc.*, 5(5):740–53, May 1996.
- [121] S. J. Lee, A. Rangarajan, and G. Gindi. A comparative study of the effects of using higher order mechanical priors in SPECT reconstruction. In *Proc. IEEE Nuc. Sci. Symp. Med. Im. Conf.*, volume 4, pages 1696–1700, 1994.
- [122] S.-J. Lee, A. Rangarajan, and G. Gindi. Bayesian image reconstruction in SPECT using higher order mechanical models as priors. *IEEE Trans. Med. Imag.*, 14(4):669–80, December 1995.
- [123] S. Geman and D. Geman. Stochastic relaxation, Gibbs distributions, and Bayesian restoration of images. *IEEE Trans. Patt. Anal. Mach. Int.*, 6(6):721–41, November 1984.
- [124] B. W. Silverman, C. Jennison, J. Stander, and T. C. Brown. The specification of edge penalties for regular and irregular pixel images. *IEEE Trans. Patt. Anal. Mach. Int.*, 12(10):1017–24, October 1990.
- [125] V. E. Johnson, W. H. Wong, X. Hu, and C. T. Chen. Image restoration using Gibbs priors: Boundary modeling, treatment of blurring, and selection of hyperparameter. *IEEE Trans. Patt. Anal. Mach. Int.*, 13(5):413–25, May 1991.
- [126] V. E. Johnson. A model for segmentation and analysis of noisy images. *J. Am. Stat. Assoc.*, 89(425):230–41, March 1994.
- [127] S. Alenius and U. Ruotsalainen. Bayesian image reconstruction for emission tomography based on median root prior. *Eur. J. Nuc. Med.*, 24(3):258–65, March 1997.
- [128] S. Alenius, U. Ruotsalainen, and J. Astola. Using local median as the location of the prior distribution in iterative emission tomography image reconstruction. *IEEE Trans. Nuc. Sci.*, 45(6):3097–104, December 1998.
- [129] W. Cholewicki, F. Hermansen, and S. B. Hansen. Noise reduction and convergence of Bayesian algorithms with blobs based on the huber function and median root prior. *Phys. Med. Biol.*, 49(20):4717–30, October 2004.
- [130] V. Y. Panin, G. L. Zeng, and G. T. Gulberg. Total variation regulated EM algorithm. *IEEE Trans. Nuc. Sci.*, 46(6):2202–10, December 1999.
- [131] P. Kisilev, M. Zibulevsky, and Y. Zeevi. Wavelet representation and total variation regularization in emission tomography. In *Proc. IEEE Intl. Conf. on Image Processing*, volume 1, pages 702–5, 2001.
- [132] C. R. Vogel and M. E. Oman. Fast numerical methods for total variation minimization in image reconstruction. In *Proc. SPIE 2563, Adv. Signal Proc. Alg.*, pages 359–67, 1995.
- [133] M. Lassas and S. Siltanen. Can one use total variation prior for edge-preserving Bayesian inversion? *Inverse Prob.*, 20(5):1537–1564, October 2004.
- [134] D. Donoho. Superresolution via sparsity constraints. *SIAM J. Math. Anal.*, 23(5):1309–31, 1993.
- [135] G. Hari Kumar and Y. Bresler. A new algorithm for computing sparse solutions to linear inverse problems. In *Proc. IEEE Conf. Acoust. Speech Sig. Proc.*, volume 3, pages 1331–4, 1996.
- [136] I. F. Gorodnitsky and B. D. Rao. Sparse signal reconstruction from limited data using FOCUSS: a re-weighted minimum norm algorithm. *IEEE Trans. Sig. Proc.*, 45(3):600–16, March 1997.
- [137] D. Donoho. For most large underdetermined systems of linear equations, the minimal  $\ell_1$  norm solution is also the sparsest solution. *Comm. Pure Appl. Math.*, 59(6):797–829, June 2006.
- [138] E. J. Candès, J. Romberg, and T. Tao. Robust uncertainty principles: exact signal reconstruction from highly incomplete frequency information. *IEEE Trans. Info. Theory*, 52(2):489–509, February 2006.
- [139] D. L. Donoho. Compressed sensing. *IEEE Trans. Info. Theory*, 52(4):1289–1306, April 2006.
- [140] D. L. Donoho, M. Elad, and V. N. Temlyakov. Stable recovery of sparse overcomplete representations in the presence of noise. *IEEE Trans. Info. Theory*,
- 52(1):6–18, January 2006.
- [141] M. Figueiredo, R. Nowak, and S. J. Wright. Gradient projection for sparse reconstruction: Application to compressed sensing and other inverse problems. *IEEE J. Sel. Top. Sig. Proc.*, 1(4):586–97, December 2007.
- [142] E. Candès and J. Romberg. Sparsity and incoherence in compressive sampling. *Inverse Prob.*, 23(3):969–86, June 2007.
- [143] R. G. Baraniuk. Compressive sensing. *IEEE Sig. Proc. Mag.*, 24(4):118–21, 2007.
- [144] I.-T. Hsiao, A. Rangarajan, and G. Gindi. A new convex edge-preserving median prior with applications to tomography. *IEEE Trans. Med. Imag.*, 22(5):580–5, May 2003.
- [145] M. Nikolova. Thresholding implied by truncated quadratic regularization. *IEEE Trans. Sig. Proc.*, 48(12):3437–50, December 2000.
- [146] A. Antoniadis and J. Fan. Regularization and wavelet approximations. *J. Am. Stat. Assoc.*, 96(455):939–55, September 2001.
- [147] D. F. Yu and J. A. Fessler. Edge-preserving tomographic reconstruction with nonlocal regularization. In *Proc. IEEE Intl. Conf. on Image Processing*, volume 1, pages 29–33, 1998.
- [148] D. F. Yu and J. A. Fessler. Edge-preserving tomographic reconstruction with nonlocal regularization. *IEEE Trans. Med. Imag.*, 21(2):159–73, February 2002.
- [149] J. Ye, Y. Bresler, and P. Moulin. A self-referencing level-set method for image reconstruction from sparse Fourier samples. In *Proc. IEEE Intl. Conf. on Image Processing*, volume 2, pages 33–6, 2001.
- [150] M. J. Black and A. Rangarajan. On the unification of line processes, outlier rejection, and robust statistics with applications in early vision. *Intl. J. Comp. Vision*, 19(1):57–91, July 1996.
- [151] J. W. Stayman and J. A. Fessler. Regularization for uniform spatial resolution properties in penalized-likelihood image reconstruction. *IEEE Trans. Med. Imag.*, 19(6):601–15, June 2000.
- [152] J. W. Stayman and J. A. Fessler. Nonnegative definite quadratic penalty design for penalized-likelihood reconstruction. In *Proc. IEEE Nuc. Sci. Symp. Med. Im. Conf.*, volume 2, pages 1060–3, 2001.
- [153] J. W. Stayman and J. A. Fessler. Compensation for nonuniform resolution using penalized-likelihood reconstruction in space-variant imaging systems. *IEEE Trans. Med. Imag.*, 23(3):269–84, March 2004.
- [154] C. T. Chen, X. Ouyang, W. H. Wong, and X. Hu. Improvement of PET image reconstruction using high-resolution anatomical images. In *Proc. IEEE Nuc. Sci. Symp. Med. Im. Conf.*, volume 3, page 2062, 1991. (Abstract).
- [155] R. Leahy and X. H. Yan. Statistical models and methods for PET image reconstruction. In *Proc. of Stat. Comp. Sect. of Amer. Stat. Assoc.*, pages 1–10, 1991.
- [156] J. A. Fessler, N. H. Clinthorne, and W. L. Rogers. Regularized emission image reconstruction using imperfect side information. *IEEE Trans. Nuc. Sci.*, 39(5):1464–71, October 1992.
- [157] I. G. Zubal, M. Lee, A. Rangarajan, C. R. Harrell, and G. Gindi. Bayesian reconstruction of SPECT images using registered anatomical images as priors. *J. Nuc. Med. (Abs. Book)*, 33(5):963, May 1992.
- [158] G. Gindi, M. Lee, A. Rangarajan, and I. G. Zubal. Bayesian reconstruction of functional images using anatomical information as priors. *IEEE Trans. Med. Imag.*, 12(4):670–80, December 1993.
- [159] X. Ouyang, W. H. Wong, V. E. Johnson, X. Hu, and C.-T. Chen. Incorporation of correlated structural images in PET image reconstruction. *IEEE Trans. Med. Imag.*, 13(4):627–40, December 1994.
- [160] S. J. Lee, G. R. Gindi, I. G. Zubal, and A. Rangarajan. Using ground-truth data to design priors in Bayesian SPECT reconstruction. In Y. Bizais, C. Barillot, and R. D. Paola, editors, *Information Processing in Medical Im.* Kluwer, 1995.
- [161] J. E. Bowsher, V. E. Johnson, T. G. Turkington, R. J. Jaszczyk, C. E. Floyd, and R. E. Coleman. Bayesian reconstruction and use of anatomical a priori information for emission tomography. *IEEE Trans. Med. Imag.*, 15(5):673–86, October 1996.
- [162] S. Sastry and R. E. Carson. Multimodality Bayesian algorithm for image reconstruction in positron emission tomography: a tissue composition model. *IEEE Trans. Med. Imag.*, 16(6):750–61, December 1997.
- [163] R. Piramuthu and A. O. Hero. Side information averaging method for PML emission tomography. In *Proc. IEEE Intl. Conf. on Image Processing*, volume 2, pages 671–5, 1998.
- [164] C. Comtat, P. E. Kinahan, J. A. Fessler, T. Beyer, D. W. Townsend, M. Deprise, and C. Michel. Reconstruction of 3d whole-body PET data using blurred anatomical labels. In *Proc. IEEE Nuc. Sci. Symp. Med. Im. Conf.*, volume 3, pages 1651–5, 1998.
- [165] A. O. Hero, R. Piramuthu, S. R. Titus, and J. A. Fessler. Minimax emission computed tomography using high resolution anatomical side information and B-spline models. *IEEE Trans. Info. Theory*, 45(3):920–38, April 1999.

B.6

[166] D. F. Yu and J. A. Fessler. Mean and variance of singles photon counting with deadline. *Phys. Med. Biol.*, 45(7):2043–56, July 2000.

[167] D. F. Yu and J. A. Fessler. Mean and variance of coincidence photon counting with deadline. *Nucl. Instr. Meth. Phys. Res. A*, 488(1-2):362–74, August 2002.

[168] J. Qi and R. H. Huesman. Propagation of errors from the sensitivity image in list mode reconstruction. *IEEE Trans. Med. Imag.*, 23(9):1094–9, September 2004.

[169] J. Qi and R. H. Huesman. Effect of errors in the system matrix on iterative image reconstruction. In *Proc. IEEE Nuc. Sci. Symp. Med. Im. Conf.*, volume 5, pages 2854–8, 2004.

[170] Y. S. Shim and Z. H. Cho. SVD pseudoinversion image reconstruction. *IEEE Trans. Acoust. Sp. Sig. Proc.*, 29(4):904–9, August 1981.

[171] U. Raffi, D. N. Stroud, and W. R. Hendee. Improvement of lesion detection in scintigraphic images by SVD techniques for resolution recovery. *IEEE Trans. Med. Imag.*, 5(1):35–44, March 1986.

[172] D. A. Fish, J. Grochmalicki, and E. R. Pike. Scanning SVD method for restoration of images with space-variant blur. *J. Opt. Soc. Am. A*, 13(3):464–9, March 1996.

[173] A. Caponnetto and M. Bertero. Tomography with a finite set of projections: singular value decomposition and re solution. *Inverse Prob.*, 13(5):1191–1205, October 1997.

[174] A. K. Louis. Incomplete data problems in x-ray computerized tomography. I. Singular value decomposition of the limited angle transform. *Numerische Mathematik*, 48(3):251–62, May 1986.

[175] F. Natterer. Numerical treatment of ill-posed problems. In G Talenti, editor, *Inverse Prob.*, volume 1225, pages 142–67. Berlin, Springer, 1986. Lecture Notes in Math.

[176] R. C. Liu and L. D. Brown. Nonexistence of informative unbiased estimators in singular problems. *Ann. Stat.*, 21(1):1–13, March 1993.

[177] J. Ory and R. G. Pratt. Are our parameter estimators biased? The significance of finite-different regularization operators. *Inverse Prob.*, 11(2):397–424, April 1995.

[178] I. M. Johnstone. On singular value decompositions for the Radon Transform and smoothness classes of functions. Technical Report 310, Dept. of Statistics, Stanford, January 1989.

[179] M. F. Smith, C. E. Floyd, R. J. Jaszczyk, and R. E. Coleman. Reconstruction of SPECT images using generalized matrix inverses. *IEEE Trans. Med. Imag.*, 11(2):165–75, June 1992.

[180] M. Lavielle. A stochastic algorithm for parametric and non-parametric estimation in the case of incomplete data. *Signal Processing*, 42(1):3–17, 1995.

[181] W. H. Press, B. P. Flannery, S. A. Teukolsky, and W. T. Vetterling. *Numerical recipes in C*. Cambridge Univ. Press, New York, 1988.

[182] K. Sauer and C. Bouman. Bayesian estimation of transmission tomograms using local optimization operations. In *Proc. IEEE Nuc. Sci. Symp. Med. Im. Conf.*, volume 3, pages 2089–93, 1991.

[183] K. Sauer and C. Bouman. Bayesian estimation of transmission tomograms using segmentation based optimization. *IEEE Trans. Nuc. Sci.*, 39(4):1144–52, August 1992.

[184] D. P. Bertsekas and S. K. Mitter. A descent numerical method for optimization problems with nondifferentiable cost functionals. *SIAM J. Control*, 11(4):637–52, 1973.

[185] W. C. Davidson. Variable metric methods for minimization. Technical Report ANL-5990, AEC Research and Development Report, Argonne National Laboratory, USA, 1959.

[186] H. F. Khalfan, R. H. Byrd, and R. B. Schnabel. A theoretical and experimental study of the symmetric rank-one update. *SIAM J. Optim.*, 3(1):1–24, February 1993.

[187] C. Zhu, R. H. Byrd, P. Lu, and J. Nocedal. Algorithm 778: L-BFGS-B: Fortran subroutines for large-scale bound-constrained optimization. *ACM Trans. Math. Software*, 23(4):550–60, December 1997.

[188] T. G. Kolda, D. P. O’Leary, and L. Nazareth. BFGS with update skipping and varying memory. *SIAM J. Optim.*, 8(4):1060–83, 1998.

[189] K. Lange. *Numerical analysis for statisticians*. Springer-Verlag, New York, 1999.

[190] B. T. Polyak. *Introduction to optimization*. Optimization Software Inc, New York, 1987.

[191] D. P. Bertsekas. *Constrained optimization and Lagrange multiplier methods*. Academic-Press, New York, 1982.

[192] R. H. Byrd, P. Lu, J. Nocedal, and C. Zhu. A limited memory algorithm for bound constrained optimization. *SIAM J. Sci. Comp.*, 16(5):1190–208, 1995.

[193] L. Kaufman. Reduced storage, Quasi-Newton trust region approaches to function optimization. *SIAM J. Optim.*, 10(1):56–69, 1999.

[194] M. Hanke, J. G. Nagy, and C. Vogel. Quasi-Newton approach to nonnegative image restorations. *Linear Algebra and its Applications*, 316(1):223–36, September 2000.

[195] J. L. Morales and J. Nocedal. Automatic preconditioning by limited memory Quasi-Newton updating. *SIAM J. Optim.*, 10(4):1079–96, 2000.

[196] R. R. Meyer. Sufficient conditions for the convergence of monotonic mathematical programming algorithms. *J. Comput. System. Sci.*, 12(1):108–21, 1976.

B.7

[226] J. A. Fessler, N. H. Clinthorne, and W. L. Rogers. On complete data spaces for PET reconstruction algorithms. *IEEE Trans. Nuc. Sci.*, 40(4):1055–61, August 1993.

[227] J. A. Fessler and H. Erdog an. A paraboloidal surrogates algorithm for convergent penalized-likelihood emission image reconstruction. In *Proc. IEEE Nuc. Sci. Symp. Med. Im. Conf.*, volume 2, pages 1132–5, 1998.

[228] T. Hebert and R. Leahy. A Bayesian reconstruction algorithm for emission tomography using a Markov random field prior. In *Proc. SPIE 1092, Med. Im. Ill: Im. Proc.*, pages 458–66, 1989.

[229] T. Hebert and R. Leahy. A generalized EM algorithm for 3-D Bayesian reconstruction from Poisson data using Gibbs priors. *IEEE Trans. Med. Imag.*, 8(2):194–202, June 1989.

[230] T. J. Hebert and R. Leahy. Statistic-based MAP image reconstruction from Poisson data using Gibbs priors. *IEEE Trans. Sig. Proc.*, 40(9):2290–303, September 1992.

[231] E. Tanaka. Utilization of non-negativity constraints in reconstruction of emission tomograms. In S L Bacharach, editor, *Information Processing in Medical Im.*, pages 379–93. Martinus-Nijhoff, Boston, 1985.

[232] R. M. Lewitt and G. Muehlelehner. Accelerated iterative reconstruction for positron emission tomography based on the EM algorithm for maximum likelihood estimation. *IEEE Trans. Med. Imag.*, 5(1):16–22, March 1986.

[233] T. Hebert, R. Leahy, and M. Singh. Three-dimensional maximum-likelihood reconstruction for an electronically collimated single-photon-emission imaging system. *J. Opt. Soc. Am. A*, 7(7):1305–13, July 1990.

[234] S. Holte, P. Schmidlin, A. Lind en, G. Rosenqvist, and L. Eriksson. Iterative image reconstruction for emission tomography: A study of convergence and quantitation problems. *IEEE Trans. Nuc. Sci.*, 37(2):629–35, April 1990.

[235] D. P. Bertsekas. A new class of incremental gradient methods for least squares problems. *SIAM J. Optim.*, 7(4):913–26, November 1997.

[236] R. Neal and G. E. Hinton. A view of the EM algorithm that justifies incremental, sparse and other variants. In M. I. Jordan, editor, *Learning in Graphical Models*, pages 255–68. Kluwer, Dordrecht, 1998.

[237] A. Nedic and D. Bertsekas. Convergence rate of incremental subgradient algorithms. In S. Uryasev and P. M. Pardalos, editors, *Stochastic Optimization: Algorithms and Applications*, pages 263–304. Kluwer, New York, 2000.

[238] A. Nedic, D. Bertsekas, and V. Borkar. Distributed asynchronous incremental subgradient methods. In D. Butnariu, Y. Censor, and S. Reich, editors, *Inherently Parallel Algorithms in Feasibility and Optimization and Their Applications*. Elsevier, Amsterdam, 2000.

[239] A. Nedic and D. P. Bertsekas. Incremental subgradient methods for nondifferentiable optimization. *SIAM J. Optim.*, 12(1):109–38, 2001.

[240] V. M. Kibardin. Decomposition into functions in the minimization problem. *Avtomatika i Telemekhanika*, 9:66–79, September 1979. Translation: p. 1311–23 in Plenum Publishing Co. “Adaptive Systems”.

[241] H. Kudo, H. Nakazawa, and T. Saito. Convergent block-iterative method for general convex cost functions. In *Proc. Intl. Mtg. on Fully 3D Image Recon. in Rad. and Nuc. Med. pages* 247–250, 1999.

[242] A. R. De Pierro and M. E. B. Yamagishi. Fast EM-like methods for maximum ‘a posteriori’ estimates in emission tomography. *IEEE Trans. Med. Imag.*, 20(4):280–8, April 2001.

[243] S. Ahn and J. A. Fessler. Globally convergent image reconstruction for emission tomography using relaxed ordered subsets algorithms. *IEEE Trans. Med. Imag.*, 22(5):613–26, May 2003.

[244] S. Ahn and J. A. Fessler. Globally convergent ordered subsets algorithms: Application to tomography. In *Proc. IEEE Nuc. Sci. Symp. Med. Im. Conf.*, volume 2, pages 1064–8, 2001.

[245] P. Khurd, I.-T. Hsiao, A. Rangarajan, and G. Gindi. A globally convergent regularized ordered-subset EM algorithm for list-mode reconstruction. *IEEE Trans. Nuc. Sci.*, 51(3):719–25, June 2004.

[246] S. Ahn, J. A. Fessler, D. Blatt, and A. O. Hero. Convergent incremental optimization transfer algorithms: Application to tomography. *IEEE Trans. Med. Imag.*, 25(3):283–96, March 2006.

[247] S. Ahn, J. A. Fessler, D. Blatt, and A. O. Hero. Incremental surrogates algorithms: Application to transmission tomography. In *Proc. IEEE Nuc. Sci. Symp. Med. Im. Conf.*, volume 5, pages 2835–9, 2004.

[248] H. Erdog an and J. A. Fessler. Ordered subsets algorithms for transmission tomography. *Phys. Med. Biol.*, 44(11):2835–51, November 1999.

[249] J. W. Stayman and J. A. Fessler. Spatially-variant roughness penalty design for uniform resolution in penalized-likelihood image reconstruction. In *Proc. IEEE Intl. Conf. on Image Processing*, volume 2, pages 685–9, 1998.

B.9

[197] L. Kaufman. Implementing and accelerating the EM algorithm for positron emission tomography. *IEEE Trans. Med. Imag.*, 6(1):37–51, March 1987.

[198] N. H. Clinthorne, T. S. Pan, P. C. Chiao, W. L. Rogers, and J. A. Stamos. Preconditioning methods for improved convergence rates in iterative reconstructions. *IEEE Trans. Med. Imag.*, 12(1):78–83, March 1993.

[199] J. A. Fessler and S. D. Booth. Conjugate-gradient preconditioning methods for shift-variant PET image reconstruction. *IEEE Trans. Im. Proc.*, 8(5):688–99, May 1999.

[200] E. U. Mumcuoglu, R. Leahy, S. R. Cherry, and Z. Zhou. Fast gradient-based methods for Bayesian reconstruction of transmission and emission PET images. *IEEE Trans. Med. Imag.*, 13(3):687–701, December 1994.

[201] E. U. Mumcuoglu, R. M. Leahy, and S. R. Cherry. Bayesian reconstruction of PET images: methodology and performance analysis. *Phys. Med. Biol.*, 41(9):1777–1807, September 1996.

[202] J. A. Fessler and A. O. Hero. Space-alternating generalized expectation-maximization algorithm. *IEEE Trans. Sig. Proc.*, 42(10):2664–77, October 1994.

[203] J. A. Fessler and A. O. Hero. Penalized maximum-likelihood image reconstruction using space-alternating generalized EM algorithms. *IEEE Trans. Im. Proc.*, 4(10):1417–29, October 1995.

[204] J. A. Fessler, E. P. Ficarino, N. H. Clinthorne, and K. Lange. Grouped-coordinate ascent algorithms for penalized-likelihood transmission image reconstruction. *IEEE Trans. Med. Imag.*, 16(2):166–75, April 1997.

[205] J. A. Fessler and A. O. Hero. Space-alternating generalized EM algorithms for penalized maximum-likelihood image reconstruction. Technical Report 286, Comm. and Sign. Proc. Lab., Dept. of EECES, Univ. of Michigan, Ann Arbor, MI, 48109-2122, February 1994.

[206] J. A. Browne and A. R. De Pierro. A row-action alternative to the EM algorithm for maximizing likelihoods in emission tomography. *IEEE Trans. Med. Imag.*, 15(5):687–99, October 1996.

[207] C. L. Byrne. Block-iterative methods for image reconstruction from projections. *IEEE Trans. Im. Proc.*, 5(5):792–3, May 1996.

[208] C. L. Byrne. Convergent block-iterative algorithms for image reconstruction from inconsistent data. *IEEE Trans. Im. Proc.*, 6(9):1296–304, September 1997.

[209] C. L. Byrne. Accelerating the EMML algorithm and related iterative algorithms by rescaled block-iterative methods. *IEEE Trans. Im. Proc.*, 7(1):100–9, January 1998.

[210] M. E. Daube-Witherspoon and G. Muehlelehner. An iterative image space reconstruction algorithm suitable for volume ECT. *IEEE Trans. Med. Imag.*, 5(2):61–66, June 1986.

[211] J. M. Ollinger. Iterative reconstruction-reprojection and the expectation-maximization algorithm. *IEEE Trans. Med. Imag.*, 9(1):94–8, March 1990.

[212] A. R. De Pierro. On the relation between the ISRA and the EM algorithm for positron emission tomography. *IEEE Trans. Med. Imag.*, 12(2):328–33, June 1993.

[213] P. J. Green. Bayesian reconstructions from emission tomography data using a modified EM algorithm. *IEEE Trans. Med. Imag.*, 9(1):84–93, March 1990.

[214] P. J. Green. On the use of the EM algorithm for penalized likelihood estimation. *J. Royal Stat. Soc. Ser. B*, 52(3):443–452, 1990.

[215] K. Sauer and C. Bouman. A local update strategy for iterative reconstruction from projections. *IEEE Trans. Sig. Proc.*, 41(2):534–48, February 1993.

[216] K. G. Murty. *Linear complementarity, linear and nonlinear programming*. Heldermann Verlag, Berlin, 1988.

[217] C. A. Bouman, K. Sauer, and S. S. Saquib. Tractable models and efficient algorithms for Bayesian tomography. In *Proc. IEEE Conf. Acoust. Speech Sig. Proc.*, volume 5, pages 2907–10, 1995.

[218] C. A. Bouman and K. Sauer. A unified approach to statistical tomography using coordinate descent optimization. *IEEE Trans. Im. Proc.*, 5(3):480–92, March 1996.

[219] J. A. Fessler. Hybrid Poisson/polynomial objective functions for tomographic image reconstruction from transmission scans. *IEEE Trans. Im. Proc.*, 4(10):1439–50, October 1995.

[220] H. Erdog an and J. A. Fessler. Monotonic algorithms for transmission tomography. *IEEE Trans. Med. Imag.*, 18(9):801–14, September 1999.

[221] E. P. Ficarino, J. A. Fessler, R. J. Ackerman, W. L. Rogers, J. R. Corbett, and M. Schwaiger. Simultaneous transmission-emission TI-201 cardiac SPECT: Effect of attenuation correction on myocardial tracer distribution. *J. Nuc. Med.*, 36(6):921–31, June 1995.

[222] E. P. Ficarino, J. A. Fessler, P. D. Shreve, J. N. Kritzman, P. A. Rose, and J. R. Corbett. Simultaneous transmission/emission myocardial perfusion tomography: Diagnostic accuracy of attenuation-corrected 99m-Tc-Sestamibi SPECT. *Circulation*, 93(3):463–73, February 1996.

[223] J.-B. Thibault, K. Sauer, C. Bouman, and J. Hsieh. A three-dimensional statistical approach to improved image quality for multi-slice helical CT. *Med. Phys.*, 34(11):4526–44, November 2007.

[224] C. A. Johnson, J. Seidel, and A. Sofer. Interior point methodology for 3-D PET reconstruction. *IEEE Trans. Med. Imag.*, 19(4):271–85, April 2000.

[225] K. Lange and J. A. Fessler. Globally convergent algorithms for maximum a posteriori transmission tomography. *IEEE Trans. Im. Proc.*, 4(10):1430–8, October 1995.

B.8

[250] J. Nuys and J. A. Fessler. A penalized-likelihood image reconstruction method for emission tomography, compared to post-smoothed maximum-likelihood with matched spatial resolution. *IEEE Trans. Med. Imag.*, 22(9):1042–52, September 2003.

[251] J. Qi and R. M. Leahy. Resolution and noise properties of SMAP reconstruction for fully 3D PET. In *Proc. Intl. Mtg. on Fully 3D Image Recon. in Rad. and Nuc. Med.*, pages 35–9, 1999.

[252] T. H. Farquhar, J. Dlacer, C. K. Hoh, J. Czernin, S. S. Gambhir, M. A. Seltzer, D. H. Silverman, J. Qi, C. Hsu, and E. J. Hoffman. ROC and localization ROC analyses of lesion detection in whole-body FDG PET: effects of acquisition mode, attenuation correction and reconstruction algorithm. *J. Nuc. Med.*, 40(12):2043–52, December 1999.

[253] P. Bonetto, J. Qi, and R. M. Leahy. Covariance approximation for fast and accurate computation of channelized Hotelling observer statistics. *IEEE Trans. Nuc. Sci.*, 47(4):1567–72, August 2000.

[254] J. Qi. Theoretical evaluation of the detectability of random lesions in Bayesian emission reconstruction. In *Information Processing in Medical Im.*, pages 354–65, 2003.

[255] P. K. Khurd and G. R. Gindi. LROC model observers for emission tomographic reconstruction. In *Proc. SPIE 5372, Medical Imaging 2004: Image Perception, Observer Performance, and Technology Assessment*, pages 509–20, 2004.

[256] J. Qi and R. H. Huesman. Fast approach to evaluate MAP reconstruction for lesion detection and localization. In *Proc. SPIE 5372, Medical Imaging 2004: Image Perception, Observer Performance, and Technology Assessment*, pages 273–82, 2004.

[257] J. Qi. Analysis of lesion detectability in Bayesian emission reconstruction with nonstationary object variability. *IEEE Trans. Med. Imag.*, 23(3):321–9, March 2004.

[258] A. Yendiki and J. A. Fessler. Analysis of observer performance in unknown-location tasks for tomographic image reconstruction. *J. Opt. Soc. Am. A*, 24(12):B99–109, December 2007. Special issue on Image Quality.

[259] D. L. Snyder. Parameter estimation for dynamic studies in emission-tomography systems having list-mode data. *IEEE Trans. Nuc. Sci.*, 31(2):925–31, April 1984.

[260] J. M. Ollinger and D. L. Snyder. A preliminary evaluation of the use of the EM algorithm for estimating parameters in dynamic tracer-studies. *IEEE Trans. Nuc. Sci.*, 32(1):848–54, February 1985.

[261] J. M. Ollinger and D. L. Snyder. An evaluation of an improved method for computing histograms in dynamic tracer studies using positron-emission tomography. *IEEE Trans. Nuc. Sci.*, 33(1):435–8, February 1986.

[262] J. M. Ollinger. Estimation algorithms for dynamic tracer studies using positron-emission tomography. *IEEE Trans. Med. Imag.*, 6(2):115–25, June 1987.

[263] J. M. Ollinger. An evaluation of a practical algorithm for estimating histograms in dynamic tracer studies using positron-emission tomography. *IEEE Trans. Nuc. Sci.*, 34(1):349–53, February 1987.

[264] F. O’Sullivan. Imaging radiotracer model parameters in PET: a mixture approach. *IEEE Trans. Med. Imag.*, 12(3):399–412, September 1993.

[265] P. C. Chiao, W. L. Rogers, J. A. Fessler, N. H. Clinthorne, and A. O. Hero. Model-based estimation with boundary side information or boundary regularization. *IEEE Trans. Med. Imag.*, 13(2):227–34, June 1994.

[266] M. A. Limber, M. N. Limber, A. Celler, J. S. Barney, and J. M. Borwein. Direct reconstruction of functional parameters for dynamic SPECT. *IEEE Trans. Nuc. Sci.*, 42(4):1249–56, August 1995.

[267] G. L. Zeng, G. T. Gullberg, and R. H. Huesman. Using linear time-invariant system theory to estimate kinetic parameters directly from projection measurements. *IEEE Trans. Nuc. Sci.*, 42(6-2):2339–46, December 1995.

[268] J. M. Borwein and W. Sun. The stability analysis of dynamic SPECT systems. *Numerische Mathematik*, 77(3):283–98, September 1997.

[269] R. H. Huesman, B. W. Reutter, G. L. Zeng, and G. T. Gullberg. Kinetic parameter estimation from SPECT cone-beam projection measurements. *Phys. Med. Biol.*, 43(4):973–82, April 1998.

[270] J. S. Maltz, E. Polak, and T. F. Budinger. Multistart optimization algorithm for joint spatial and kinetic parameter estimation from dynamic ECT projection data. In *Proc. IEEE Nuc. Sci. Symp. Med. Im. Conf.*, volume 3, pages 1567–73, 1998.

[271] J. S. Maltz. Direct recovery of regional tracer kinetics from temporally inconsistent dynamic ECT projections using dimension-reduced time-activity basis. *Phys. Med. Biol.*, 45(11):3413–29, November 2000.

[272] E. Hebbner, D. Oldenburg, T. Farncombe, and A. Celler. Direct estimation of dynamic parameters in SPECT tomography. *IEEE Trans. Nuc. Sci.*, 44(6-2):2425–30, December 1997.

[273] D. S. Lalush and B. M. W. Tsui. Block-iterative techniques for fast 4D reconstruction using a priori motion models in gated cardiac SPECT. *Phys. Med. Biol.*, 43(4):875–86, April 1998.

[274] H. H. Bauschke, D. Noll, A. Celler, and J. M. Borwein. An EM algorithm for dynamic SPECT. *IEEE Trans. Med. Imag.*, 18(3):252–61, March 1999.

B.10

- [275] T. Farncombe, A. Celler, D. Noll, J. Maeght, and R. Harrop. Dynamic SPECT imaging using a single camera rotation (dSPECT). *IEEE Trans. Nuc. Sci.*, 46(4-2):1055–61, August 1999.
- [276] T. E. Nichols, J. Qi, and R. M. Leahy. Continuous time dynamic PET imaging using list mode data. In A. Todd-Pokropek A. Kuba, M. Smal, editor, *Information Processing in Medical Im.*, pages 98–111. Springer, Berlin, 1999.
- [277] E. Asma, T. E. Nichols, J. Qi, and R. M. Leahy. 4D PET image reconstruction from list mode data. In *Proc. IEEE Nuc. Sci. Symp. Med. Im. Conf.*, volume 2, pages 15/57–65, 2000.
- [278] B. W. Reutter, G. T. Gullberg, and R. H. Huesman. Direct least squares estimation of spatiotemporal distributions from dynamic SPECT projections using a spatial segmentation and temporal B-splines. *IEEE Trans. Med. Imag.*, 19(5):434–50, May 2000.
- [279] T. E. Nichols, J. Qi, E. Asma, and R. M. Leahy. Spatiotemporal reconstruction of list mode PET data. *IEEE Trans. Med. Imag.*, 21(4):396–404, April 2002.
- [280] U. Schmitt and A. K. Louis. Efficient algorithms for the regularization of dynamic inverse problems: I. Theory. *Inverse Prob.*, 18(3):645–58, June 2002.
- [281] U. Schmitt, A. K. Louis, C. Wolters, and M. Vauhkonen. Efficient algorithms for the regularization of dynamic inverse problems: II. Applications. *Inverse Prob.*, 18(3):659–76, June 2002.
- [282] C-M. Kao, J. T. Yap, J. Mukherjee, and M. N. Wernick. Image reconstruction for dynamic PET based on low-order approximation and restoration of the sinogram. *IEEE Trans. Med. Imag.*, 16(6):727–37, December 1997.
- [283] J. Matthews, D. Bailey, P. Price, and V. Cunningham. The direct calculation of parametric images from dynamic PET data using maximum-likelihood iterative reconstruction. *Phys. Med. Biol.*, 42(6):1155–73, June 1997.
- [284] S. R. Meikle, J. C. Matthews, V. J. Cunningham, D. L. Bailey, L. Livieratos, T. Jones, and P. Price. Parametric image reconstruction using spectral analysis of PET projection data. *Phys. Med. Biol.*, 43(3):651–66, March 1998.
- [285] M. V. Narayanan, M. A. King, E. J. Soares, C. L. Byrne, P. H. Pretorius, and M. N. Wernick. Application of the Karhunen-Loeve transform to 4D reconstruction of cardiac gated SPECT images. *IEEE Trans. Nuc. Sci.*, 46(4-2):1001–8, August 1999.
- [286] M. N. Wernick, E. J. Infusino, and M. Milosevic. Fast spatio-temporal image reconstruction for dynamic PET. *IEEE Trans. Med. Imag.*, 18(3):185–95, March 1999.
- [287] M. V. Narayanan, M. A. King, M. N. Wernick, C. L. Byrne, E. J. Soares, and P. H. Pretorius. Improved image quality and computation reduction in 4-D reconstruction of cardiac-gated SPECT images. *IEEE Trans. Med. Imag.*, 19(5):423–33, May 2000.
- [288] J. S. Maltz. Optimal time-activity basis selection for exponential spectral analysis: application to the solution of large dynamic emission tomographic reconstruction problems. *IEEE Trans. Nuc. Sci.*, 48(4-2):1452–64, August 2001.
- [289] J. E. Koss, D. L. Kirch, E. P. Little, T. K. Johnson, and P. P. Steele. Advantages of list-mode acquisition of dynamic cardiac data. *IEEE Trans. Nuc. Sci.*, 44(6-2):2431–8, December 1997.

The literature on image reconstruction is enormous and growing. Many valuable publications are not included in this list, which is not intended to be comprehensive.

Slides and lecture notes available from:

<http://www.eecs.umich.edu/~fessler>  
B.11